Chapter 7

VUV Thin Films

Muamer Zukic and Douglas G. Torr

University of Alabama in Huntsville

Physics Department

Research Institute Room C-10

Huntsville, AL 35899

The application of thin film technology to the vacuum ultraviolet (VUV) wavelength region from 120 nm to 230 nm has not been fully exploited in the past because of absorption effects which complicate the accurate determination of the optical functions of dielectric materials. The problem therefore reduces to that of determining the real and imaginary parts of a complex optical function, namely the frequency dependent refractive index n and extinction coefficient k. We discuss technique for the inverse retrieval of n and k for dielectric materials at VUV wavelengths from measurements of their reflectance and transmittance. Suitable substrate and film materials are identified for application in the VUV. Such applications include coatings for the fabrication of narrow and broadband filters and beamsplitters. The availability of such devices open the VUV regime to high resolution photometry, interferometry and polarimetry both for space based and laboratory applications. This chapter deals with the optics of absorbing multilayers, the determination of the optical functions for several useful materials, the design of VUV multilayer stacks as applied to the design of narrow and broadband reflection and transmission filters and beamsplitters. Experimental techniques are discussed briefly, and several examples of the optical functions derived for selected materials are presented.

TABLE OF CONTENTS

7.1 Introduction

The topic of this chapter is the theory, design and fabrication of all-dielectric interference filters for the vacuum ultraviolet (VUV) wavelength region from 120 nm - 230 nm. The development of thin film technology for the VUV has not progressed as rapidly as that for the visible and infrared because substrate and thin film materials exhibit absorption characteristics in this wavelength range. As a result of absorption, the optical function (referred as complex refractive index or optical constant) becomes a complex number. Not only does this complicate the theoretical treatment of the propagation of light across layered media, but it introduces problems in the determination of the optical functions of thin film and substrate materials. The latter now comprises a refractive index and extinction coefficient, which renders it a complex quantity.

This chapter deals with these issues in the following way. First we rework the optical theory of thin films taking absorption of film materials into account and derive expressions for the transmittance, reflectance, and absorptance of a multilayer stack as a function of complex reflection and transmission coefficients. Expressions for the latter are obtained using Maxwell's theory for the propagation of light across layered media, taking into account energy loss. We then discuss the experimental determination of the optical functions of weakly absorbing substrates and absorbing but transparent thin films. An approach that utilizes inverse problem theory is developed to retrieve the refractive index and extinction coefficient

of substrate and film materials from measurements of their transmittance and reflectance. Results obtained for several materials that exhibit useful properties for VUV applications are presented. We find that only MgF_2 and LiF are suitable as a substrates, but that LiF proved not be suitable for application in a high energy radiation environment [7.1]. Suitable film materials identified include BaF_2, CaF_2, LaF_3, MgF_2, Al_2O_3 and SiO_2. The theory of tuned multilayers with absorbing films is presented together with development of some useful approximating relations. With the knowledge acquired of the optical functions of these materials in hand, we describe designs developed for coatings suitable for VUV devices such as beamsplitters, narrow and broadband filters, and high reflective coatings.

A comparison of the theoretically predicted performance of some of these devices is compared with their measured performance. We focus on narrowband and broadband filters with special transmission characteristics to validate the theory and the method developed for the experimental determination of optical functions. We demonstrate that not only is relatively good agreement obtained between the predicted and measured responses, but the theoretical knowledge gained allows the limits of the approach to be evaluated so that optimum performance can be realized. Thus this chapter should provide a better understanding of the behavior of the optical functions of dielectric film materials in the vacuum ultraviolet wavelength regime. It also includes a brief discussion on some of the experimental procedures such as sample preparation and handling, and the procedure used for the photometric measurements.

7.2 Optical Properties of an Absorbing Layered Medium

7.2.1 Physical Factors Neglected

Before proceeding with the theoretical development, we discuss the limitations of the approach and assumptions made. Optical thin film theory is essentially Maxwell's macroscopic theory of electromagnetic waves applied to the propagation of light across a layered medium. We assume that the film is an optically isotropic medium characterized by its optical function which is usually referred to as the optical constant or complex refractive index, and defined in space by two parallel dividing planes with lateral dimensions being infinite. The incident light is considered as being plane, monochromatic and linearly polarized in one of two orthogonal states, *s* and *p*, with respect to the plane of incidence. The *s* polarized state has the electric vector of the incident wave perpendicular to the plane of incidence, while the *p* polarized wave has the magnetic vector perpendicular to the plane of incidence.

The physical factors which are neglected in the usual theoretical calculations of the spectral performances of the multilayers are surface and volume scattering of the incident light, anisotropy and inhomogeneity of film materials, and diffusion between adjacent materials forming a multilayer.

Surface scattering is caused by the roughness of the planes bounding the film, while volume scattering is caused by the internal structure of the film material. The papers by *Elson* [7.2], *Guenther* [7.3] and *Macleod* [7.4] may be mentioned as illustrations of efforts which consider the scattering effects from the films of

the multilayer. Apart from some attempts to consider the volume and surface scattering as a perturbation, neither surface nor volume scattering have been incorporated into a complete multilayer theory. The reason for this becomes very obvious when the random nature of the scattering inside a multilayer is considered; scattered light from a point within the layered structure can further be subjected to scattering or interference with other scattered, reflected or transmitted parts of the incident light.

The anisotropy of film materials is usually caused by the internal stress of the film material. It is mostly induced during the process of the film deposition. Although anisotropic media have their own matrix calculus, it can only be used to compute the transformation of the amplitudes upon a single pass through the medium. The multiple reflections within multilayer cannot be taken into account within the frame of this theory. The multilayer theory may include anisotropy within its own frame through the tensor nature of the optical function [7.5].

Variations in the deposition conditions such as the deposition rate, pressure, and substrate temperature may induce inhomogeneites in the optical function of the film. Diffusion either between adjacent films or between a film and a substrate is always present in a stratified medium. The process of diffusion forms a transition layer which is in general inhomogeneous and is sometimes considered as the film that makes continuous connection of the optical functions of adjacent media. The inhomogeneity and diffusion may be taken into account by the present theory if the actual optical parameters and profiles of the optical functions of the films are known [7.6-9].

7.2.2 VUV Absorption of Dielectrics

The absorption of dielectrics in the VUV can be treated classically or quantum mechanically. Because of the present accuracy of the reflectance and transmittance measurements there is no advantage to using the quantum approach; thus the classical model for the optical functions is used in this chapter. In this model, bound electrons in a dielectric which is illuminated with electromagnetic radiation are treated as charged particles subjected to damped harmonic motion [7.10].

In order to determine the optical functions of metals, the classical theory uses the free electron gas model. The absorption effects in dielectrics and in metals are two different physical phenomena (bound electrons in dielectrics and free electrons in metals) but the final result is the same, i.e. loss of the energy of the incident electromagnetic radiation.

Fortunately, both phenomena can be described in terms of a complex optical function. However, the transition from the real optical function of a loss-less medium (dielectrics in the visible part of spectrum) to the complex one of an absorbing medium requires redefinition of the physical quantities such as the phase velocity v and the wave number k_λ such that

$$v = \frac{c}{N}, \tag{7.1}$$

and

$$k_\lambda = \frac{\omega}{c} N \tag{7.2}$$

(where N is the complex optical function) are now the complex quantities.

The complex velocity is used to describe light propagation through absorbing anisotropic media [7.10]. In addition, the angles between the direction of the light propagation and the normal to the film plane must be the complex quantities and they no longer represent just the refraction of the propagating light. They are mathematical quantities introduced in order to preserve generality of the Snell's law. Since thin film materials and substrates (within the scope of this chapter) are assumed to be isotropic media, calculations of the reflectance, transmittance, and absorptance are done in terms of complex optical functions and complex angles.

7.2.3 Theoretical Development

A medium whose optical properties are constant throughout each plane perpendicular to a fixed direction is called a stratified or layered medium. We shall now consider the propagation of a plane, time-harmonic electromagnetic wave through such a medium assuming that all films forming a layered medium are absorbing. The incident medium (vacuum) and substrate will be considered as non-absorbing. In the standard optics textbooks [7.10-13] multilayers are usually treated as a non-absorbing systems. In the VUV, apart from bulk MgF_2 and LiF, no other material can be treated as non or low-absorbing. Therefore the theoretical analysis which follows takes into account absorption of thin films.

The intensity reflection and transmission coefficients for a plane electromagnetic wave incident on a multilayer are

$$r = \frac{(M_{11} + M_{12}\eta_S)\eta_0 - (M_{21} + M_{22}\eta_S)}{(M_{11} + M_{12}\eta_S)\eta_0 + (M_{21} + M_{22}\eta_S)}, \tag{7.3}$$

$$t = \frac{2\eta_0}{(M_{11} + M_{12}\eta_S)\eta_0 + (M_{21} + M_{22}\eta_S)}. \tag{7.4}$$

η_0 and η_S which are the effective optical functions of the incident medium and the substrate, are defined as

$$\eta_0 = n_0 \cos\theta_0, \tag{7.5}$$

$$\eta_S = n_S \cos\theta_S \tag{7.6}$$

for s polarization, and as

$$\eta_0 = \frac{\cos\theta_0}{n_0}, \tag{7.7}$$

$$\eta_S = \frac{\cos\theta_S}{n_S}, \tag{7.8}$$

for p polarization. Angles, θ_0 and θ_s, for light propagation through the incident medium and the substrate are measured relative to the normal to the film plane. n_0 and n_S are the refractive indices of the incident medium and the substrate, respectively. It is assumed that both the substrate and incident medium have negligible values of the extinction coefficients and therefore real optical functions. The terms $M_{i,j}, i,j = 1,2$ are the elements of the multilayer characteristic matrix M which is defined as the product of the matrices of the individual layers $\mathbf{M_l}$ $(l = 1,2,\ldots P)$,

$$\mathbf{M} = \mathbf{M_1} \times \mathbf{M_2} \times \cdots \times \mathbf{M_P}, \tag{7.9}$$

where P is the total number of layers. Matrices $\mathbf{M_l}$ are given by

$$\mathbf{M_l} = \begin{pmatrix} \cos\delta_l & \frac{i}{\eta_l}\sin\delta_l \\ i\eta_l \sin\delta_l & \cos\delta_l \end{pmatrix}. \tag{7.10}$$

The phase thicknesses of the films δ_l are

$$\delta_l = \frac{2\pi}{\lambda_0} N_l d_l \cos\Theta_l, \tag{7.11}$$

where λ_0 is the vacuum wavelength of the incident light. N_l is the optical function of the *l-th* layer defined as

$$N_l = n_l(1 + i\kappa_l) = n_l + in_l\kappa_l = n_l + ik_l, \tag{7.12}$$

with $\kappa_l = k_l/n_l$, and where n_l is the refractive index, k_l is the extinction coefficient, d_l is the physical thickness, and Θ_l is the complex angle of the light within the *l-th* film. If the complex angle Θ_l is written as

$$\sin\Theta_l = q_l e^{i\gamma_l} = q_l\cos\gamma_l + iq_l\sin\gamma_l, \tag{7.13}$$

then the generalized Snell's law applied at the interface between non-absorbing *(l-1)-th* medium and absorbing *l-th* medium is given by

$$N_l\sin\Theta_l = (n_l + ik_l)q_l e^{i\gamma_l} = n_{l-1}\sin\theta_{l-1}. \tag{7.14}$$

The right hand side of Equation (7.14) is real, thus

$$n_l q_l\cos\gamma_l - k_l q_l\sin\gamma_l = n_{l-1}\sin\theta_{l-1}, \tag{7.15}$$

$$n_l q_l\sin\gamma_l + k_l q_l\cos\gamma_l = 0. \tag{7.16}$$

From Equations (7.15) and (7.16) it follows that q_l and γ_l are given by

$$q_l = \frac{n_{l-1}\sin\theta_{l-1}}{\sqrt{n_l^2 + k_l^2}}, \tag{7.17}$$

$$\gamma_l = \cos^{-1}\left(\frac{n_l}{\sqrt{n_l^2 + k_l^2}}\right). \tag{7.18}$$

If $k_l = 0$ then

$$q_l = \frac{n_{l-1}\sin\theta_{l-1}}{n_l}, \tag{7.19}$$

$$\gamma_l = 0 \tag{7.20}$$

and the generalized Snell's law (Equation 7.14) reduces to the well known law of refraction. The transition from a real to a complex optical function necessitated the introduction of complex angles. In order to avoid possible confusion that arises in trying to understand the physical meaning of complex angles, it is simpler to regard them merely as mathematical quantities. They are introduced in order to preserve the generality of the Snell's law.

The reflection and transmission coefficients r and t are complex numbers of the form

$$r = |r|e^{i\phi_r}, \tag{7.20}$$

$$t = |t|e^{i\phi_t}, \tag{7.21}$$

where ϕ_r and ϕ_t are the phase changes on reflection and transmission given by,

$$\phi_r = tan^{-1}\left(\frac{Im(r)}{Re(r)}\right) \tag{7.22}$$

$$\phi_t = tan^{-1}\left(\frac{Im(t)}{Re(t)}\right). \tag{7.23}$$

The phase change of the reflected light ϕ_r is referred to the plane boundary between the semi-infinite incident medium and the front surface of the multilayer, while the phase change of the transmitted light ϕ_t is referred to the plane boundary between the multilayer and the semi-infinite medium of the substrate.

The intensity reflectance R, transmittance T, and absorptance A of a multilayer are given by

$$R = rr^*, \tag{7.24}$$

$$T = \frac{\eta_S}{\eta_0} tt^*, \tag{7.25}$$

$$A = 1 - (R + T). \tag{7.26}$$

If the incident light is randomly polarized, usually referred to as unpolarized light, then the reflectance is the average of the s and p intensity reflectances,

$$R_{av} = \frac{1}{2}(R_s + R_p), \tag{7.27}$$

and similarly the overall transmittance of randomly polarized incident light is given by

$$T_{av} = \frac{1}{2}(T_s + T_p). \tag{7.28}$$

The s and p components of the reflectance and transmittance are calculated when the effective optical functions defined in Equations (7.5), (7.6), (7.7), and (7.8) are inserted into the matrix Equation (7.9) and into Equations (7.3), (7.4), (7.24), and (7.25).

7.3 Determination of Optical Functions

7.3.1 Experimental and Numerical Method

The optical function of an isotropic material - the refractive index n and the extinction coefficient k - can be inferred from photometric or polarimetric measurements. Since compensators or transmission polarizers are not generally available in the VUV, photometric methods are almost exclusively used for obtaining n and k. A number of methods exist for extracting optical functions from reflectance (R) and transmittance (T) measurements at both normal and oblique angles of incidence. Because R and T are complicated functions of optical functions it is generally impossible to express the refractive index n and extinction coefficient k as explicit functions of R and T. Most approaches to solving this complicated dependence involve either graphical or numerical techniques [7.14-21]. The expressions are nonlinear so the problem may be considered as a numerical exercise in which n and k are found through an iteration process of matching calculated and measured values of reflectance and transmittance. The numerical method employed here is based on the use of a damped least squares fitting approach incorporated into a thin film design computer program [7.22, 23].

Beam diagrams for the measurements and calculations of the optical functions of the substrate and substrate with a single thin film are shown in Figures 7.1a, and 7.1b. The reflectance, R_1, from the semi-infinite media is measured by means of the wedged substrate, and transmittance, T_M, is measured using a plane parallel substrate as it is shown in Figure 7.1a. From the beam diagram for theoretical

derivation of transmittance of the non-absorbing slab, T_0, shown in Figure 7.1a, it follows that

$$T_0 = T_1(1 - R_1) + T_1R_1^2(1 - R_1) + T_1R_1^4(1 - R_1) + T_1R_1^6(1 - R_1) + \ldots, \tag{7.29}$$

and after multiplying we get

$$T_0 = T_1(1 - R_1 + R_1^2 - R_1^3 + R_1^4 - R_1^5 + R_1^6 + \ldots). \tag{7.30}$$

Using the binomial expansion the transmittance of a thick non-absorbing slab can be written as

$$T_0 = \frac{T_1}{1 + R_1} = \frac{1 - R_1}{1 + R_1}, \tag{7.31}$$

where R_1 is the measured reflectance from the single side of the substrate. If absorption is present in the slab, then the measured transmittance is smaller than that calculated theoretically using Equation (7.31). If the measured transmittance is denoted as T_M, then the total loss due to the substrate absorption is given by

$$A = 1 - \frac{T_M}{T_0}, \tag{7.32}$$

and the correction factor for any other transmittance measurement on this substrate at the particular wavelength by

$$C = \frac{T_M}{T_0}. \tag{7.33}$$

Since the imaginary part of the refractive index of the MgF_2 substrate is very low (of the order of 10^{-7}), it does not affect significantly the measured reflectance R_1 on the wedged substrate. Thus, R_1 can be used in the calculation of the refractive index n of the substrate i.e.

$$R_1 = \frac{(n - 1)^2}{(n + 1)^2}, \tag{7.34}$$

and

$$n = \frac{1 + \sqrt{R_1}}{1 - \sqrt{R_1}}. \tag{7.35}$$

The correction factor given in Equation (7.33) can be considered as the intrinsic transmission of the substrate material. Using the known intensity relation for light propagating through the absorbing media

$$I(z) = I(z = 0)e^{-\alpha z}, \tag{7.36}$$

where $I(z)$ is the light intensity at point z and the coefficient of absorption α is given by

$$\alpha = \frac{4\pi}{\lambda}k \tag{7.37}$$

we get

$$k = -\frac{\lambda}{4\pi z} ln\left(\frac{I(z)}{I(0)}\right). \tag{7.38}$$

The ratio $I(z)/I(z=0)$ is the so-called intrinsic transmission of the medium (no reflection occurs). Using the correction factor C defined in (7.33) we have

$$k = -\frac{\lambda}{4\pi D} ln\left(\frac{T_M}{T_0}\right), \tag{7.39}$$

where D is the thickness of the substrate. Thus, from measured values R_1 and T_M using Equations (7.35) and (7.39), optical functions of the weakly absorbing substrate (MgF_2 in our measurements) can be obtained. As an example consider measurements done at λ=135 nm on the MgF_2 substrate with thickness D =2mm. The measured reflectance on the wedged substrate is R_1=5.5% and measured transmittance T_M=77.4% giving n =1.61 and k =6.2 10^{-7} which agrees with known values for bulk MgF_2 in the VUV [7.24].

From the beam diagrams for reflectance and transmittance measurements shown in Figure 7.1b, it follows that the transmittance of a single film deposited onto a non-absorbing dielectric slab, T_0^F, is

$$T_0^F = T_F T_1[1 + R_1 R_2^F + (R_1 R_2^F)^2 + (R_1 R_2^F)^3 + (R_1 R_2^F)^4 \ldots] \tag{7.40}$$

and again using the binomial expansion we obtain

$$T_0^F = \frac{T_F T_1}{1 - R_1 R_2^F} = \frac{T_F(1 - R_1)}{1 - R_1 R_2^F} \tag{7.41}$$

where R_2^F is the calculated reflectance of the single film with the substrate as an incident medium and vacuum as an emerging medium (substrate), and T_F is the calculated transmittance of the film. Equation (7.41) gives the transmittance of the single absorbing film on the non-absorbing substrate. Using the correction factor defined in Equation (7.33) we represent the calculated transmittance of the substrate with a single film by

$$T_C^F = C\frac{T_F(1 - R_1)}{1 - R_1 R_2^F}, \tag{7.42}$$

and calculating R_C^F from the initial values of n and k, we form the merit function F defined as

$$F = W_1(R_1^F - R_C^F)^2 + W_2(T_M^F - T_C^F)^2 \tag{7.43}$$

where R_1^F and R_C^F are the measured and calculated reflectances of the film on the wedged (semi-infinite) substrate; T_M^F and T_C^F are measured and calculated values of transmittance through the plane parallel substrate with single film; W_1 and W_2 are the weighting factors chosen according to the relative accuracy of the R and T measurements for each wavelength.

The merit function F is then minimized using a damped least squares approach. This is implemented as a subroutine in a computer program for thin film design. The reflectances R_1^F, R_C^F and transmittance T_C^F are calculated using values of n and k at the particular wavelength. The merit function

$$F = F(R_1^F, R_C^F, T_M^F, T_C^F(R_2^F)) \tag{7.44}$$

depends on five variables of which three are dependent on n and k of the film. Thus, the minimum value of F has a high probability of providing accurate values for optical functions of the thin film. In order to minimize uncertainties of the optical function determination, several single films of the same film material but with different thicknesses, are deposited on separate substrates. The total merit function F_T is then given by

$$F_T = \sum_{n=1}^{L} F_n \tag{7.45}$$

where F_n is the merit function of the n-th film defined in Equation (7.43) and L is the total number of single films with different thicknesses deposited on the same type of the substrate material.

7.3.2 Sample Preparation and Handling

All depositions were made on 12.7 mm diameter by 2 mm thick magnesium fluoride substrates with rms $\leq$ 2.5 nm. To eliminate the contribution of the back side reflection to the reflectance measurements, some of the substrates have a 3 degree bias. The substrates are cleaned by the supplier (Acton Research Corp., Acton, Massachusetts) using the following procedure: optical soap wash, water

rinse, ethanol soak then ultrasonic bath, fresh ethanol rinse, and finally a Freon rinse.

The substrates are shipped in Delrin holders wrapped with lens paper and are only removed immediately prior to deposition. After deposition, the substrates are transported in a stainless steel container purged with dry nitrogen or helium to prevent contamination due to exposure. All depositions were made at the University of Alabama in Huntsville Optical Aeronomy Laboratory and the transmittance and reflectance measurements were made at the Atomic Physics Branch of the NASA/Marshall Space Flight Center.

7.3.3 Deposition of Thin Films

The vacuum system consists of a cryo-pump and a sorption pump giving an oil-free environment for all depositions and therefore providing a very low probability for hydrocarbon contamination of the films. The film materials BaF_2, CaF_2, and LaF_3 are prepared for vacuum deposition by CERAC with a typical purity of 99.9%. Al_2O_3 (99.5%), SiO_2 (99.98%), and MgF_2 (99.95%) are standard BALZERS coating materials while HfO_2 with a purity of 99.5% is prepared by EM Chemicals.

The fluoride films are deposited with low deposition rates on heated substrates. In order to reoxidize dissociated molecules of the oxides Al_2O_3, HfO_2 and SiO_2, films are deposited with a low deposition rate on heated substrates in an oxygen residual atmosphere. The depositions are made with an electron gun. The gun has fixed voltage of 10 KV and low power depositions are maintained by supplying low current to the gun. The source to substrate distance is 50 cm and the source to the

thickness monitor distance is 35 cm. The thickness control and rate measurements during film depositions are done with the Kronos Digital Film Thickness Monitor QM-300 series and the Kronos Deposition Rate/Thickness Output Accessory RI-100/RO-200 series with FFT-300 transducer. Further details about the conditions of depositions are given in Table 7.1.

The vacuum chamber geometry provides excellent calibration constants C_c for all film materials. The calibration constant C_c is defined as the ratio of the film thickness expressed in the transducer counts (Hz) and the measured thickness in nanometers, i.e. the number of counts (Hz) in order to obtain a 1 nm thick film. The values of C_c vary from 44.09 Hz/nm for MgF_2 up to 72.23 Hz/nm for LaF_3. The physical thickness measurements of the films are made with a Talystep stylus profilometer. The stylus radius is 2μm and the stylus loading is 1 mg.

7.3.4 Photometric Measurements

Transmittance and reflectance measurements are performed in a hydrocarbon free vacuum system at pressures below 10^{-5} torr. A sealed deuterium lamp with a MgF_2 window is used in tandem with a 0.2 meter monochromator producing a beam with 1 nm FWHM spectral resolution. Folding and collimating optics are used to produce a 1 cm by 0.75 cm reference beam which is incident on an eight position filter wheel containing the substrates. Different detectors are used for transmittance and reflectance measurements. Each detector is comprised of a sodium salycilate coated pyrex window placed in front of a bialkali photometer. A schematic diagram of the system optics is shown in Figure 7.2.

Absolute transmittance and reflectance are measured by determining the ratio of the transmitted or reflected beam intensity and the unattenuated incident beam intensity. For reflectance measurements, the unattenuated beam intensity is determined by the measured reflectance of a calibrated VUV enhanced aluminum mirror located in one of the filter wheel positions. The reflectance measurements are made at a 6° angle of incidence. The uncertainties associated with the thin film thickness, reflectance and transmittance measurements resulted in the total uncertainty for the optical constants determination of the order of ±5%. The uncertainty is derived from the discrepancies between the theoretically and experimentally obtained spectral performance of multilayers.

7.3.5 Optical Functions of Films and MgF_2 Substrate

The reflectance and transmittance measurements shown in Figure 7.3a were done on wedged and 2 mm thick parallel substrates, respectively. The optical constants n and k shown in Figure 7.3b are determined using Equations (7.35) and (7.39). They agree with known n and k values of bulk MgF_2 in the VUV. The temperature of the MgF_2 substrate during the deposition of the fluoride films is 250°C. The pressure before (P_0) and during deposition (P) as well as the deposition rates (D_R) and physical thicknesses of the films (d) are listed in Table 7.1. A single set of the R and T measurements of BaF_2, CaF_2, LaF_3, and MgF_2 films deposited on the MgF_2 substrates are given in Figures 7.4a, 7.5a, 7.6a, and 7.7a respectively. The corresponding optical constants determined from at least two independent R and T measurements (Equation 7.26) are given in Figures 7.4b, 7.5b, 7.6b, and 7.7b.

From the reflectance and transmittance curves of a 53 nm single film of BaF_2, it follows that this coating material can be used for the wavelengths longer than 135 nm. Even a single film of BaF_2 could be used as the cut-on filter if the wavelengths shorter than 130 nm are not desired. The refractive index n has values between 1.87 and 2 for wavelengths from 125 - 135 nm and it is higher than 1.7 throughout the region from 140 - 210 nm, increasing up to 1.98 at 230 nm. The extinction coefficient k has values of the order of 10^{-2} for the wavelengths from 140 - 230 nm. The measured reflectance and transmittance of a 99 nm thick CaF_2 film indicate low values of the refractive index n and relatively small extinction coefficient k for the wavelengths longer than 135 nm. The values of the refractive index n of CaF_2 are lower than 1.4 for $\lambda \geq 170$ nm, and k values are of the order of 10^{-2} for the same wavelength region. Low values of the refractive index make CaF_2 suitable for use as the alternative low index material for the longer wavelengths of the VUV. The material with highest values of the refractive index among all fluorides $n \geq 1.85$ within the range of the VUV wavelengths from 135 - 230 nm is LaF_3. The extinction coefficient has values lower then 2.2×10^{-2} for $\lambda \geq 145$ nm (Figure 7.6b). Compared to other fluoride and oxide coating materials the LaF_3 seems to be the best choice for the high index material in the considered spectral region. The reflectance and transmittance of a 51 nm thick LaF_3 film are shown in Figure 7.6a. Magnesium Fluoride films have values of the extinction coefficient lower than 5×10^{-4} throughout the entire wavelength region from 120 - 230 nm. This makes MgF_2 the most attractive low index material for the VUV. The reflectance and transmittance of a 68 nm thick MgF_2 film are shown in Figure

7.7a, while its optical constants are shown in Figure 7.7b.

The temperature of the MgF_2 substrate during the deposition of oxide films is 300°C. The deposition conditions P_0, P, and D_R as well as the physical thicknesses of the films d are listed in Table 7.1. The measured spectral curves of R and T for Al_2O_3, HfO_2, and SIO_2 films deposited on the MgF_2 substrates are shown in Figures 7.8a, 7.9a, and 7.10a while the corresponding optical constants are given in Figures 7.8b, 7.9b, and 7.10b, respectively. The transmittance curve of a 112 nm thick Al_2O_3 single film suggests that this material could possibly be used for design of absorption edge filters with cut-on wavelength between 160 and 180 nm depending on the thickness of the Al_2O_3 film. The values of the refractive index n are higher than 1.85 for almost entire region from 120 nm - 230 nm while k values are higher than 10^{-1} for 120 nm $\leq \lambda \leq$ 175 nm. The HfO_2 film has the highest value of the extinction coefficient (shown in Figure 7.9b) and it does not seem that this material could be useful for the vacuum ultraviolet wavelength region, particularly for the wavelengths below 200 nm. The measured reflectance and transmittance of a 30 nm thick HfO_2 film are shown in Figure 7.9a. The values of the refractive index n of SiO_2 films are very close to the values of the bulk SiO_2, while k values are of the order of magnitude higher [7.25]. The refractive index $n \geq 1.8$ for 125 nm $\leq \lambda \leq$ 150 nm decreases gradually down to 1.6 at 200 nm. The extinction coefficient k is if the order of 10^{-1} for 120 nm $\leq \lambda \leq$ 135 nm which makes SiO_2 useful material for the design of a single layer absorption edge filter with cut-on wavelength within the interval from 125 - 135 nm depending on the relative thickness of the SiO_2 film. The measured reflectance and transmittance of

a 51 nm thick SiO_2 film are shown in Figure 7.10a.

The fluoride film materials have generally lower extinction coefficients than the oxides. High values of the refractive index n make LaF_3 and BaF_2 useful materials for the VUV particularly for constructing a High-Low index pair with MgF_2 being the most useful low index material. The designs of the VUV coatings such as narrowband transmission, and narrowband reflection filters are possible with these materials. The SiO_2 coating material, among other oxides measured in the VUV, seems to be the most applicable for design of multilayer stacks such as the narrowband reflection filters. The Al_2O_3 coating material may be used for the design of absorption edge filters for $\lambda \geq 160$ nm, while HfO_2 becomes a useful high index material for wavelengths longer than 230 nm.

7.4 Tuned Multilayers as High Reflective Coatings

7.4.1 Quarterwave Multilayers

Multilayers formed by high and low index materials alternating throughout the stack are by the analogy with electrical networks called tuned filters or tuned multilayers. Because of their importance in the design of the VUV coatings presented in this chapter, we shall investigate the properties of tuned multilayers with absorbing film materials in more detail here. The basic design of such a multilayer is given in either symmetric $[(HL)^pH]$ or asymmetric form $[(HL)^p]$. The symmetric $[(LH)^pL]$ and asymmetric $[(LH)^p]$ tuned multilayers represent another form of the basic design. The H and L stand for the high and low index materials, respectively. The optical thicknesses of the films may be quarterwave, thirdwave, or they may have some other values usually derived from the optimization procedure. If the optical thickness of the film is equal to the quarter of some reference wavelength then this film is referred to as a quarterwave. The optical thickness of the film is defined as the product of the physical thickness of the film and its refractive index.

Most applications of QW multilayers are based on the fact that for the incident wavelength $\lambda_0 = \lambda_r$ (where λ_r is the wavelength relative to which films are quarterwave) the beams reflected from the various interfaces will all be in phase, so the reflectance obtained is a maximum. Consider the multilayer $(HL)^p$ with a total number of films P = 2p. Let the angle of incidence be zero, i.e. $\theta_0 = 0$. By

denoting the angle within the low index material as Θ_L and the angle within the high index material as Θ_H we may write

$$\Theta_H = \Theta_L = 0. \tag{7.46}$$

Thus, the phase thicknesses δ_H and δ_L are now given by

$$\delta_H = \frac{2\pi}{\lambda_0}(n_H + ik_H)d_H, \tag{7.47}$$

for the high index material, and for the low index material

$$\delta_L = \frac{2\pi}{\lambda_0}(n_L + ik_L)d_L. \tag{7.48}$$

If the optical thicknesses of both H and L materials are quarterwave relative to the some reference wavelength λ_r then

$$n_L d_L = \frac{\lambda_r}{4}, \tag{7.49}$$

$$n_H d_H = \frac{\lambda_r}{4}, \tag{7.50}$$

and the phase thicknesses δ_H and δ_L are given respectively by

$$\delta_H = \frac{\pi}{2}\frac{\lambda_r}{\lambda_0}(1 + i\frac{k_H}{n_H}), \tag{7.51}$$

$$\delta_L = \frac{\pi}{2}\frac{\lambda_r}{\lambda_0}(1 + i\frac{k_L}{n_L}). \tag{7.52}$$

Using the definition of the ratio κ,

$$\kappa_H = \frac{k_H}{n_H}, \tag{7.53}$$

$$\kappa_L = \frac{k_L}{n_L}, \tag{7.54}$$

Equations (7.51) and (7.52) can be written as

$$\delta_H = \frac{\pi}{2}\frac{\lambda_r}{\lambda_0}(1 + i\kappa_H), \tag{7.55}$$

$$\delta_L = \frac{\pi}{2}\frac{\lambda_r}{\lambda_0}(1 + i\kappa_L). \tag{7.56}$$

The matrices of such quarterwave films at $\lambda_r = \lambda_0$ become

$$\mathbf{M_H} = \begin{pmatrix} -i\sinh\alpha_H & \frac{i}{N_H}\cosh\alpha_H \\ iN_H\cosh\alpha_H & -i\sinh\alpha_H \end{pmatrix}, \tag{7.57}$$

$$\mathbf{M_L} = \begin{pmatrix} -i\sinh\alpha_L & \frac{i}{N_L}\cosh\alpha_L \\ iN_L\cosh\alpha_L & -i\sinh\alpha_L \end{pmatrix}, \tag{7.58}$$

where

$$\alpha_H = \frac{\pi}{2}\frac{k_H}{n_H} = \frac{\pi}{2}\kappa_H, \tag{7.59}$$

$$\alpha_L = \frac{\pi}{2}\frac{k_L}{n_L} = \frac{\pi}{2}\kappa_L. \tag{7.60}$$

At this point, we shall assume (just for purpose of discussion of tuned multilayers with absorbing films and not for the exact calculation), that the hyperbolic functions in Equations (7.57) and (7.58) may be approximated by their values at the origin, i.e. $\sinh x \to 0$ and $\cosh x \to 1$ for $x \to 0$. The matrices $\mathbf{M}_H$ and $\mathbf{M}_L$ within this approximation and for $\lambda_0 = \lambda_r$ can be written as

$$\mathbf{M_H} = \begin{pmatrix} 0 & \frac{i}{N_H} \\ iN_H & 0 \end{pmatrix}, \tag{7.61}$$

$$\mathbf{M_L} = \begin{pmatrix} 0 & \frac{i}{N_L} \\ iN_L & 0 \end{pmatrix} \tag{7.62}$$

giving the matrix $\mathbf{M}_1$ of the basic sequence (HL),

$$\mathbf{M_1} = \mathbf{M_H} \times \mathbf{M_L} = \begin{pmatrix} \frac{-N_L}{N_H} & 0 \\ 0 & \frac{-N_H}{N_L} \end{pmatrix}. \tag{7.63}$$

The characteristic matrix of the multilayer $(HL)^p$ is then given by

$$\mathbf{M_p} = (\mathbf{M_H} \times \mathbf{M_L})^p = \begin{pmatrix} (\frac{-N_L}{N_H})^p & 0 \\ 0 & (\frac{-N_H}{N_L})^p \end{pmatrix}, \tag{7.64}$$

and from Equation (2.3) it follows that the reflection coefficient is given by

$$r = \frac{1 - \frac{n_s}{n_0}\left(\frac{N_H}{N_L}\right)^{2p}}{1 + \frac{n_s}{n_0}\left(\frac{N_H}{N_L}\right)^{2p}}. \tag{7.65}$$

The ratio of the optical constants N_H and N_L can be written as

$$\frac{N_H}{N_L} = \frac{n_H}{n_L}\frac{(1 + i\kappa_H)}{(1 + i\kappa_L)} = \frac{n_H}{n_L}(a^2 + b^2)^{1/2}e^{i\beta}, \tag{7.66}$$

where

$$a = \frac{1 + \kappa_H\kappa_L}{1 + \kappa_L^2}, \tag{7.67}$$

$$b = \frac{\kappa_H - \kappa_L}{1 + \kappa_L^2}, \tag{7.68}$$

and

$$\beta = tan^{-1}(\frac{b}{a}). \tag{7.69}$$

Thus, $(\frac{N_H}{N_L})$ can be written as

$$(\frac{N_H}{N_L})^p = F(p)e^{i\psi(p)}, \tag{7.70}$$

where

$$F(p) = (\frac{n_H}{n_L})^p(a^2 + b^2)^{p/2}, \tag{7.71}$$

$$\psi(p) = p\beta. \tag{7.72}$$

Now, Equation (7.65) for r becomes

$$r(p) = \frac{1 - \left(\frac{n_s}{n_0}\right) F(2p) e^{i\psi(2p)}}{1 + \left(\frac{n_s}{n_0}\right) F(2p) e^{i\psi(2p)}} \tag{7.73}$$

giving for the reflectance $R(p)$ of the $(HL)^p$ multilayer at $\lambda_0 = \lambda_r$

$$R(p) = \frac{1 + \left(\frac{n_s}{n_0}\right)^2 F^2(2p) - 2\left(\frac{n_s}{n_0}\right) F(2p) \cos\psi(2p)}{1 + \left(\frac{n_s}{n_0}\right)^2 F^2(2p) + 2\left(\frac{n_s}{n_0}\right) F(2p) \cos\psi(2p)}. \tag{7.74}$$

If $p = 0$, i.e. if no films are present on the substrate then the Equation (7.74) must reduce to the well known formula for the reflectance at the boundary between two semi-infinite media with indices n_0 and n_S. It is easy to prove that this is true by inserting $p = 0$ into Equation (7.74),

$$R(0) = \frac{\left(1 - \frac{n_s}{n_0}\right)^2}{\left(1 + \frac{n_s}{n_0}\right)^2}. \tag{7.75}.$$

From Equation (7.74) it follows that the reflectance of the $(HL)^p$ stack has its maximum value if for $l = 0, 1, 2...$,

$$\psi(2p) = (l + \frac{1}{2})\pi, \tag{7.76}$$

Thus, for $l = 0$, from Equations (7.67), (7.68), (7.69), (7.71), (7.72), and (7.76) it follows that the maximum reflectance is achieved if

$$p = p_0 = \frac{\pi}{4}\left(\tan^{-1}\left(\frac{\kappa_H - \kappa_L}{1 + \kappa_H \kappa_L}\right)\right)^{-1}. \tag{7.77}$$

Furthermore, Equation (7.74) indicates that $R(p_0) = 1$ if p satisfies Equation (7.77). This relationship is caused by the high level of approximation at the beginning of

our derivation. Equation (7.77) relates the number of (HL) pairs p_0 required to achieve the maximum reflectance to the optical constants N_H and N_L, i.e. for $p \geq p_0$

$$R_{max} = R(p_0) \rightarrow constant. \tag{7.78}$$

Thus, the value of $p = p_0$ corresponds to the number of (HL) pairs for which both the absorptance and reflectance of the stack are constant (R+A $\rightarrow$ 1) resulting in the value of the stack transmittance practically equal to zero [7.26].

The exact calculations of how the reflectance $R(p)$ and absorptance $A(p)$ depend on the number of the (HL) pairs p of the multilayer formed by BaF_2, LaF_3, and SiO_2 as the high index materials and MgF_2 as the low index material are shown in Figures 7.11a, 7.12a, and 7.13a, respectively. The optical film thicknesses of all films are quarterwave relative to the wavelength $\lambda_0 = \lambda_r = 135$ nm. At this wavelength the ratio κ for the SiO_2 film is $\kappa_H = 0.05759$, and for the MgF_2 $\kappa_L = 0.00025$, giving $p_0 = 13.7$, i.e $p_0 \mapsto 14$ which agrees with the exact calculation shown in Figure 7.11a. Since the extinction coefficients of BaF_2 and LaF_3 are about an order of magnitude lower than the extinction coefficient of SiO_2, p_0 is much higher if these fluorides are used as the high index material. From the reflectance $R(p)$ and absorptance $A(p)$ curves shown in Figures 7.11a, 7.12a, and 7.13a, it follows that BaF_2 has the greatest potential as the high index material at $\lambda_0 = 135$ nm. At the longer wavelengths $\lambda_0 \geq 150$ nm, the extinction coefficients of LaF_3 and BaF_2 become very similar while the refractive index of LaF_3 remains higher.

7.4.2 Thirdwave Tuned Multilayers

The definition of the thirdwave (TW) multilayers is not standardized as that of the quarterwave (QW). We define TW multilayers as tuned multilayers which have one material with optical thickness equal to one third of some reference wavelength, while the optical thickness of the other material is equal to one sixth of the reference wavelength. The two H and L films in the QW multilayer form an (HL) pair with total optical thickness equal to $\lambda_r/2$ which corresponds to the total phase thickness of the pair $\delta = \pi$. Similarly, the (HL) pair of the TW multilayer has the overall optical thickness equal to $\lambda_r/2$ which again corresponds to the total phase thickness of the pair equal to π. Thus, the principle of the high reflectance at the reference wavelength of the TW tuned multilayer is similar to that of the QW stack.

The $R(p)$ and $A(p)$ curves shown in Figures 7.11b, 7.12b, and 7.13b correspond to the TW multilayers with BaF_2, LaF_3, and SiO_2 as the high index materials and with optical thicknesses given by

$$n_H d_H = \frac{\lambda_r}{6}, \tag{7.79}$$

$$n_L d_L = \frac{\lambda_r}{3}, \tag{7.80}$$

where n_L is the refractive index of MgF_2, and $\lambda_0 = \lambda_r = 135$ nm. The overall thickness of the high index materials is larger in the QW than in the TW multilayers, thus one may expect that the TW designs will have lower absorptance and therefore the higher reflectance. That this expectation is justified follows from

the comparison of the $R(p)$ and $A(p)$ curves for the QW multilayers shown in Figures 7.11a, 7.12a, 7.13a and $R(p)$ and $A(p)$ curves for the TW multilayers shown in Figures 7.11b, 7.12b, and 7.13b. The maximum reflectance of the QW stack with BaF_2 is $R = 85.4\%$ (Figure 7.11a) while the TW multilayer with the same high index material has the maximum reflectance $R = 87.6\%$ (Figure 7.11b). The largest difference between the maximum reflectances of the TW, relative to the QW stacks is for a multilayer with SiO_2 as the high index material. The maximum reflectance of the QW stack is $R = 60.9\%$ (Figure 7.13a) while for the TW stack $R = 66.3\%$ (Figure 7.13b).

7.4.3 Π Multilayers

We define the Π multilayer as one whose basic (HL) pair has a total optical thickness of $\frac{\lambda_r}{2}$. Optical thicknesses of the individual H and L films forming a pair satisfy the following condition

$$H + L = \frac{\lambda_r}{2},$$

where λ_r is the reference wavelength of the multilayer. The total phase thickness of the pair is equal to π, i.e. $\delta_H + \delta_L = \pi$.

Thus, the quarterwave and thirdwave stacks are the special cases of Π multilayers. In the quarterwave stack light reflected from all interfaces is in phase, while in thirdwave and other Π multilayers light reflected from each (HL) pair is in phase. Obviously, quarterwave stacks with low-absorbing film materials (available in the visible and infrared parts of spectrum) provide higher reflectance with fewer layers than other Π stacks. However, in the VUV where low-absorbing high index

film materials do not exist, the Π multilayer with much smaller thickness of H relative to L can provide lower absorptance and therefore higher reflectance of the stack.

The increase of reflectance obtained by transition from quarterwave to third-wave stacks was demonstrated in the previous section of this chapter. Further increase of the reflection of the stacks may be obtained by decreasing the optical thickness of the high index material. Shown in Figure 7.14 is the maximum reflectance of the Π multilayer plotted against the ratio of optical thicknesses of high and low index material H/L. The reference wavelength is 145 nm, with MgF_2 as the low and LaF_3 as high index material, and bulk MgF_2 as the substrate. The angle of incidence is 0°.

7.4.4 Width of High Reflectance Zone and Higher Order Π Multilayers

The QW stacks generally have a wider high reflection zone than other Π multilayers. The width of the high reflection zone $(\Delta\lambda)_{H.R.}$ of a QW multilayer with non-absorbing film materials is given by [7.5]

$$(\Delta\lambda)_{H.R.} = \frac{1}{2(m-1)+1}\frac{4\lambda_r}{\pi}\sin^{-1}\left(\frac{n_H - n_L}{n_H + n_L}\right) \tag{7.81}$$

where m is the order of Π multilayer, n_H and n_L are the refractive indices of the high and low index materials, respectively. For absorbing film materials the width of high reflection zone is smaller than that calculated using Equation (7.82). Thus, Equation (7.82) gives the maximum width for the high reflectance zone obtainable for materials with refractive indices n_H and n_L, and for low absorbing materials ($k \leq 10^{-3}$) it can predict reasonably well the value of $(\Delta\lambda)_{H.R.}$.

The width of the high reflection zone decreases if the order of the Π multilayer is increased (Eq. 7.82). A narrow high reflection zone is desired for the design of narrowband reflection filters. An increase of the order of the Π stack from 1 to, say m, changes the total phase thickness of an (HL) pair from $\pi \rightarrow m\pi$. The total optical thickness of an (HL) pair is increased by $\lambda_r/2$ when the order of the Π stack is increased by unity. The increase of the order of the QW multilayers by unity is achieved by adding $\lambda_r/2$ to the optical thicknesses of one of the film materials, which corresponds to changing the total phase thickness of the (HL) pair by π. In order to increase the total phase thickness of an (HL) pair of the TW multilayer by π we add a total of $\lambda_r/2$ by adding $\lambda_r/6$ to the high index material and $\lambda_r/3$ to the low index material. The optical thicknesses are doubled in the second order filter relative to the optical thicknesses of the first order filter. If the first order TW stack has optical thicknesses given by Equations (7.79) and (7.80) then m-*th* order has optical thicknesses given by

$$n_H d_H = 2(m-1)\frac{\lambda_r}{6}, \tag{7.82}$$

$$n_L d_L = 2(m-1)\frac{\lambda_r}{3}. \tag{7.83}$$

where $m = 2, 3, \ldots$. The calculated reflectances of the first, second, and third order TW multilayers are shown in Figure 7.15. The bandwidth of the high reflectance zone and the value of peak reflectance decreases with increasing of the order of the filter. The decrease of the peak values of the reflectance is caused by the increased absorptance of the higher order multilayers. The increased absorptance is attributed to the thicker films of the higher order filters.

7.5 Narrowband Transmission Filters

A filter which transmits a narrow spectral band of the incident light is known as a narrowband transmission filter. The width of the pass zone is small compared to the central wavelength of the filter. The central wavelength is defined as the wavelength at which filter has a maximum transmittance. The bandwidth $(\Delta\lambda)_b$ of the pass zone is measured at half of the transmittance maximum and it is usually referred to as the full width at half maximum (FWHM).

Transmission or bandpass filters are frequently designed using the basic structure of the Fabry-Perot (FP) interferometer (the multilayer in which one of the layers, spacing layer or spacer, is bounded by two partial reflectors). The transmittance T of such a Fabry-Perot interference filter is given by [7.11]

$$T = \frac{T_{max}}{1 + F\sin^2\Psi}, \tag{7.84}$$

where

$$T_{max} = \frac{T_1 T_2}{(1 - \sqrt{R_1 R_2})^2}, \tag{7.85}$$

$$F = \frac{4\sqrt{R_1 R_2}}{(1 - \sqrt{R_1 R_2})^2}, \tag{7.86}$$

$$\Psi = \delta - \frac{\phi_1 + \phi_2}{2}. \tag{7.87}$$

T_{max} is the peak transmittance and F is the ratio of FWHM to the free spectral range (finesse). R_1 and R_2 are the reflectances and T_1 and T_2 are the transmittances of the partial reflectors bounding a spacing layer, calculated with a spacer taken as the incident medium (seen from the inside of the spacer). The emerging medium for the reflector R_1 is vacuum and for the partial reflector R_2 the emerging medium

is the substrate. δ is the phase thickness of the spacing layer defined in Equation (7.11), ϕ_1 and ϕ_2 are the phase changes (Equation 7.22) associated with reflections on the partial reflectors R_1 and R_2. The maxima of transmission, according to Equation (7.84) are given by

$$\Psi = \delta - \phi = m\pi, \tag{7.88}$$

where

$$\phi = \frac{\phi_1 + \phi_2}{2}, \tag{7.89}$$

and the bandwidth of the pass zone $(\Delta\lambda)_b$ is given by

$$(\Delta\lambda)_b = 2\lambda_0^{(m)} \left[\pi\sqrt{F} \left| m - \frac{1}{\pi} \left(\frac{d}{d\lambda_0}(\lambda_0\phi) \right)_{\lambda_0=\lambda^{(m)}} \right| \right]^{-1}, \tag{7.90}$$

of the m-*th* order filter (m = 1,2,...). λ_0 is the central wavelength of the filter.

For BaF_2, LaF_3, and SiO_2 the values of the extinction coefficient are too high in the VUV to be used as the film materials for the spacing layer. Thus, in all our designs MgF_2 will be exclusively used as the film material of the spacer. Possible designs D_1 and D_2 of the FP type interference filter are then given by

$$D_1 = Vacuum[H(LH)^p 2L(HL)^p H]Substrate,$$

$$D_2 = Vacuum[(LH)^p 2L(HL)^p]Substrate,$$

where L denotes the quarterwave optical thickness of the MgF_2, and H the quarterwave optical thickness of one of the high index materials (BaF_2, LaF_3, or SiO_2), and the substrate is bulk MgF_2. The optical thicknesses are a quarterwave relative to the central pass wavelength λ_0 of the FP filter. The partial reflectors in both

designs D_1 and D_2 consist of $(HL)^p$ QW tuned multilayers with an additional outer H layer in the design D_1.

The dependance of the reflectances R_1, and R_2 on the number p of (HL) pairs for BaF_2, LaF_3, and SiO_2 are shown in Figures (7.16a), (7.17a), and (7.18a), respectively. The maximum values of the transmittance T_{max} calculated using Equation (7.85) and the corresponding bandwidths $(\Delta\lambda)_b$ calculated according to Equation (7.90) for the first order filter (m=1) are plotted versus p (for the high index materials listed above) in Figures (7.16b), (7.17b), and (7.18b), respectively. The D_2 design is used for all calculations of $R_1, R_2, (\Delta\lambda)_b$, and T_{max}. The differentiation of the function

$$\Phi(\lambda_0) = \lambda_0\phi(\lambda_0), \tag{7.91}$$

in Equation (7.90) is done numerically, according to

$$\left(\frac{d}{d\lambda_0}\Phi(\lambda_0)\right)_{\lambda_0=\lambda^{(1)}} = (\phi(\lambda_0))_{\lambda_0=\lambda^{(1)}} + \left(\lambda_0\frac{d}{d\lambda_0}\phi(\lambda_0)\right)_{\lambda_0=\lambda^{(1)}}, \tag{7.92}$$

$$\left(\frac{d}{d\lambda_0}\Phi(\lambda_0)\right)_{\lambda_0=\lambda^{(1)}} = \left(\frac{\Phi(\lambda_0+\Delta\lambda)-\Phi(\lambda_0)}{\Delta\lambda}\right)_{\lambda_0=\lambda^{(1)}}, \tag{7.93}$$

where $\Delta\lambda \leq \lambda_0 \times 10^{-6}$ and the central pass wavelength of the FP filter $\lambda_0 = 135$ nm.

From Figure 7.16b, it follows that the FP filter centered at $\lambda_0 = 135$ nm should have $T_{max} \geq 30\%$ and $(\Delta\lambda_0)_b \leq 10$ nm, for H = BaF_2 and $p = 6$. The design (D_3) of the FP filter becomes

$$D_3 = Vacuum[(LH)^6 2L(HL)^6]Substrate,$$

where the substrate is bulk MgF_2. The experimentally obtained and theoretically calculated spectral performance of such a filter are shown in Figure 7.19. The experimentally obtained bandwidth is smaller than one predicted in Figure 7.16b. This can be explained by the fact that BaF_2 has much higher values of the extinction coefficient for wavelengths below 131 nm than for $\lambda_0 \geq 135$ nm ($k = 0.1$ at $\lambda = 130$ nm compared to $k = 0.026$ at $\lambda = 135$ nm).

The fact that the extinction coefficient of a BaF_2 film is almost four times larger at 130 nm than at 135 nm can be used for the design of a narrowband filter centered at 135 nm. The design of such a filter is a simple QW tuned stack with the high reflection zone centered at 140 nm. The theoretical and experimental spectral curves of the 25-layer QW tuned filter is shown in Figure 7.20. The interference effects are predominant in the wavelength region above 135 nm, while the absorption of the BaF_2 dominates for the wavelengths shorter than 135 nm. The peak value of the transmittance is $T_{max} = 39\%$ at $\lambda_0 = 135$ nm. The filter shown in Figure 7.20 combines absorption effects of the film material (BaF_2) to reject shorter wavelengths and interference effects to reject longer wavelengths relative to the central wavelength $\lambda_0 = 135$ nm. It has a much higher peak transmittance and at the same time provides a much better rejection of the longer wavelengths. Another possible design centered at 141 nm with a 25-layer TW tuned multilayer is shown in Figure 7.21. The rapid variation of the extinction coefficient k of SiO_2 film within 135 nm $\leq \lambda \leq$ 145 nm is utilized.

All these filters suffer from pass windows at the longer wavelengths. An edge filter is needed which will reject longer wavelengths. When the edge filter is combined

with the narrowband transmission filter, they should provide useful transmittance at λ_0. For the filter centered at 135 nm, an edge filter might be required (for some applications) to reject the longer wavelengths up to at least 170 nm to better than 95%, and at the same time provide $T \geq 50\%$ at $\lambda_0 = 135$ nm. The basic design of such a filter is again a tuned multilayer. The QW stack with H = LaF_3 and L = MgF_2 has a maximum width for the high reflectance zone of 21.6 nm at $\lambda_0 = 160$ nm, while the rejection zone of the measured spectral curve, shown in Figure 7.22, is less than 15 nm. Because of the transmission requirements at 135 nm, the idea of coupling QW or other Π multilayers centered at several wavelengths within the wavelength interval from 140 nm - 170 nm cannot be used. Thus, dielectric edge filters which would have a useful range of transmittance ($T \geq 50\%$ for $\lambda_0 \leq 145$ nm) and reject the longer wavelengths ($T \leq 5\%$ for 145 nm $\leq \lambda_0 \leq 230$ nm) do not seem to be feasible. Another possibility is to try to design a reflection pre-filter at an incident angle θ_0, which would pass a narrow spectral band with a reflectance of 50% or more at the desired wavelength. If this type of the filter is then combined with one of the previously presented transmission filters the combination could provide excellent rejection at shorter wavelengths, high peak transmittance, and reasonably good blocking of the longer wavelengths.

7.6 Narrowband Reflection Filters

The analysis of the Π multilayers showed that values of the reflectances as high as 90% can be realized, compared to 40% maximum transmittances obtained with bandpass filters. Useful dielectric film materials with high values of the refractive index n are BaF_2, LaF_3 and SiO_2. Again, an (HL) pair made either with BaF_2 - MgF_2, LaF_3 - MgF_2 or SiO_2 - MgF_2 forms the basic sequence of the multilayer that is used for the design of the narrowband reflection filter.

The design of the reflection filter is a tuned Π multilayer with optical thicknesses of the films corrected for the oblique incidence. The first order QW stack generally has a wider high reflection zone and suffers from high side reflection ripples. The ripples can be reduced by introducing films with optical thicknesses $H'/2$ and $L'/2$ (prime denotes correction of the quarterwave optical thicknesses for oblique incidence) at the first and last positions in the stack. An example of significant ripple reduction of the QW multilayer is shown in Figure 7.23 (theoretical curves). This is obtained by placing $L'/2$ films at the first and last position in the stack.

The width of the high reflection zone decreases if the order of the QW multilayer is increased. Because of its low extinction coefficient in the VUV range, MgF_2 is the material whose optical thickness can be increased to higher order without adversely affecting the maximum value of the reflectance using a first order QW. Experimental and theoretical spectral curves of a second order QW stack at an angle of incidence $\theta_0 = 45^0$ is shown in Figure 7.24. The design (D_4) of the filter

is given by

$$D_4 = Vacuum[\frac{3L'}{2}(H'3L')^{11}H'\frac{3L'}{2}]Substrate,$$

where $H' = BaF_2$ and $L' = MgF_2$, $\lambda_0 = 135$ nm, and primes denote the correction of the optical thicknesses of the films for oblique incidence. The width of the high reflection zone $(\Delta\lambda)_{H.R.} \leq 5$ nm and the reflectance at the central wavelength is 60%. The difference between the theory and experiment may be explained by the error made in film thickness monitoring during the deposition, film thickness non-uniformities, and possible scattering effects.

It follows from Figure 7.14 that narrowband reflection filters with higher reflectance compared to that of QW stacks can be obtained if the Π multilayers with smaller ratio $(n_H d_H)/(n_L d_L)$ are utilized . Figures 7.25 and 7.26 show theoretical and experimental spectral curves for 29-layer and 35-layer filters, respectively. The 29-layer filter has BaF_2 as the high index material and optical thicknesses

$$n_H d_H = \frac{\lambda}{8}$$

$$n_L d_L = \frac{3\lambda}{8}$$

for the high and low index film materials. The 35-layer filter has LaF_3 as the high index material and optical thicknesses are given by

$$n_H d_H = \frac{\lambda}{10}$$

$$n_L d_L = \frac{4\lambda}{10}$$

The substrate material is fused silica for both filters. The value of the peak reflectance is 85.6% for the 29-layer, and 88.3% for the 35-layer filter at an angle of incidence of 45°.

7.7 Combination Filters

7.7.1 Combination of Reflection and Transmission Filters

A combination of the reflection filter upon which light is incident at an angle different from zero and the transmission filter upon which light is incident at zero angle of incidence can be utilized in order to improve rejection of shorter wavelengths and reduce the bandwidth. By comparing the spectral curves of the transmission and reflection filters filter shown in Figures 7.20 and 7.24, respectively it is evident that the desired spectral performance for a narrowband filter centered at 135 nm, can be realized from the combination.

The measured spectral performance of the filter is shown in Figure 7.27. The peak value of the transmittance is $T_{max} = 24\%$, and the bandwidth $(\Delta\lambda)_b = 4$ nm. The average transmittance for the longer wavelengths is less than 3% while for the wavelengths shorter than 130 nm, the transmittance is less than 0.1%. An angular spread of the incident light of $\pm 5^0$ causes the bandwidth to increase to 7 nm. The spectral transmittance curve shown in Figure 7.28 is obtained when the transmission filter shown in Figure 7.21 is combined with a reflection filter centered at 141 nm. The peak transmittance is 25% and the bandwidth of the filter is 3.5 nm.

The spectral performances of the combined transmission and reflection filters centered at $\lambda_0 = 135$ nm are superior to the performances of commercially available Fabry-Perot filters made with aluminium and centered either at 130 nm or 135

nm. FP filters centered even at the longer wavelengths such as 180 nm have a transmittance of the order of 25% and bandwidths wider than 10 nm [7.29-31]. By using other film materials such as Al_2O_3 and HfO_2 or suitable bulk materials combined with reflection multilayers, narrowband filters with bandwidths smaller than 5 nm and overall transmittances higher than 25% are possible for the whole VUV region from 120 nm - 230 nm.

7.7.2 Multiple Reflection Filters

The reflection filters shown in Figures 7.25 and 7.26 have reflectance at the central wavelength of 85.6% and 88.3%, respectively. They both have relatively high reflectance in the shorter wavelength region and average reflectance of the order of 5% for the longer wavelengths. The reflectance outside the filters "pass" zone can be reduced by means of multiple reflections from two or more reflection filters upon which light is incident at an angle of 45°. The overall transmission of the combination of four and six 29-layer filters is shown in Figure 7.29.

The combination of 4 reflection filters does not change an optical axis and has a value of transmittance outside the pass zone of lower than 10^{-2}% for the wavelength region from 140 nm - 260 nm. The transmittance at the central wavelength is 53.6% and the bandwidth is less than 5 nm. If further improvement of the rejection outside the pass zone is required then 6 or more filters can be combined. However, adding more filters will reduce the overall transmittance of the combination. The peak transmittance for 6-reflector combination is 39.3% while the rejection outside the pass zone is better than 10^{-4}% for longer and better than 0.07% for shorter

wavelengths. If the MgF_2 window is placed at the entrance of the combination than the transmittance of shorter wavelengths may be less than $10^{-4}\%$. Figure 7.30 schematically illustartes combinations of four and six reflection filters.

7.8 Broadband Filters

The transmittance curves of currently available VUV broad bandpass filters have the shape of a Fabry-Perot filter with extended bandwidths [7.27-29]. The transmittance in the pass zone varies from 35% for wavelengths below 140 nm to 45% for wavelengths above 170 nm. For most applications a more rectangular shape and higher average transmittance in the pass zone are desired. The pass zone of a broadband filter is bounded by a lower and upper wavelength. Ideally, the spectral components of the incident light, with wavelengths shorter than the lower and longer than the upper wavelength of the filter, are rejected. In the design examples that follow, the rejection of the shorter wavelengths is achieved by the suitable choice of the substrate, i.e. the natural absorption of the substrate material is utilized. The measured transmittances of BaF_2, CaF_2, and fused silica substrates are shown in Figure 7.31. BaF_2 and CaF_2 substrates reject wavelengths below 135 nm, and 125 nm respectively, while fused silica may be used for broad bandpass filters with a lower pass limit above 145 nm.

In the broadband filters discussed here, wavelengths longer than upper limit of the pass zone are rejected by means of a high reflectance multilayer. The basic design of this reflector is the QW multilayer with quarterwave optical thicknesses relative to one or more wavelengths within the rejection zone. The width of the high reflectance zone has a maximum value of a 32 nm when LaF_3 is used as the high index material for the central wavelength $\lambda_0 = 210$ nm. The design D_s of the

filter with the QW multilayer centered at 210 nm is given by

$$D_5 = Vacuum \left[\frac{L}{2} (HL)^{11} H \frac{L}{2} \right] Substrate,$$

where H = LaF_3, L = MgF_2, and the substrate is fused silica. In order to reduce reflection ripples in the pass zone of the filter, films with optical thickness $L/2$ are placed at the first and last positions in the stack. Figure 7.32 shows the calculated and experimentally obtained optical properties of a filter with requirements $T \leq$ 0.1% for $\lambda_0 \leq$ 160 nm, $T_{av} \geq$ 75% for 170 nm $\leq \lambda_0 \leq$ 190 nm, and $T_{av} \leq$ 10% for 200 nm $\leq \lambda_0 \leq$ 220 nm. An improved design of the filter is obtained by computerized optimization using the TFD-V13 code [7.22]. The number of films is increased to 31 and film thicknesses are not quarterwave. The substrate is fused silica with H = LaF_3 and L = MgF_2 as high and low index film materials, respectively. Figure 7.33 presents the theoretical spectral performance of the optimized design.

Figure 7.34 shows the calculated optical properties of the initial and final design of a filter with pass zone 140 nm $\leq \lambda_0 \leq$ 170 nm. The initial design is a 35-layer QW stack with LaF_3 as the high index material and bulk BaF_2 as the substrate. The natural absorption of the BaF_2 substrate is utilized for the rejection of the shorter wavelengths. If the requirements for the transmittance in the pass zone of the filter are not very high, say 40%, than two QW stacks may be combined and the rejection zone of the longer wavelengths extended up to 60 nm. The optical properties of the filters shown in Figures 7.33 and 7.34 coupled into a single stack with BaF_2 as the substrate are given in Figure 7.35. This filter has an extended rejection zone with a width of 60 nm and average transmittance in the pass zone

of 40%. The pass zone of this filter may be extended down to 130 nm, as it is shown in Figure 7.36, if CaF_2 is used as the substrate material.

The design and fabrication of all-dielectric broadband filters is possible with average transmittances as high as 75% in the pass zone if the width of the rejection zone in the longer wavelengths is 30 nm or less. To increase the width of the rejection zone, two or more QW stacks can be coupled. Wavelengths below a lower limit of the pass zone are rejected (absorbed) by the suitable choice of the substrate material. The rejection of wavelengths longer than the upper limit of a pass zone is achieved by means of either a QW stack or its optimized version. Optimization can improve the shape of the spectral curve by reducing, for example, ripples in the pass and rejection zones. Because of the absorption due to the film materials, the transmittance of the filter in the pass zone is mainly limited by the number of the films and their thicknesses.

7.9 Beamsplitters

A multilayer which reflects part of the light at non-zero angle of incidence and transmits the other part is generally known as a beamsplitter. The splitting can be achromatic, dichroic, polarizing, or non-polarizing. A beamsplitter which splits only the intensity of the incident light is referred to as neutral or achromatic, while a filter which splits incident light according to its wavelength is known as a dichroic beamsplitter. Additional requirements related to the polarization states of the incident light may be imposed on both achromatic and dichroic beamsplitters. These filters are generally known as polarizing and non-polarizing beamsplitters.

Achromatic beamsplitters may be employed in VUV interferometry, imaging systems, and in any other instrument or experiment where intensity division of the incident light from a single source is required. In the longer wavelength regions (visible or infrared) where low absorbing materials are available it suffices to specify either the reflectance or transmittance of the beamsplitter and to use it as the optimization parameter. In the VUV the absorptance must be considered as an additional optimization parameter. The initial design of the achromatic beamsplitter is a 6-layer QW stack with LaF_3 as the high index material. The calculated spectral performance of the initial and optimized design obtained through the optimization procedure employing the TFD-V13 code is shown in Figures 7.37 and 7.38, respectively. The initial and optimized designs are given in Table 7.2. The spectral requirements are: $R = T = 40\%$ for 150 nm $\leq \lambda \leq$ 180 nm at the angle of incidence $\theta_0 = 45^\circ$. The calculated transmittance of the filter is 52% - 54% to compensate for the loss from substrate absorption and back side reflection.

Narrowband reflection filters can be considered as one type of dichroic beamsplitter. The design of the reflection filters is not constrained by the transmittance requirements outside the high reflection zone. The dichroic beamsplitter should provide the required transmittance in the pass zone in order to accomplish directional splitting of two different spectral parts of the incident light. Figure 7.39 shows the calculated spectral performance of the initial and optimized design of a beamsplitter which transmits wavelengths shorter than 170 nm and reflects the part of incident spectrum between 175 nm and 200 nm. The initial and optimized designs are given in Table 7.3.

In order to assess the possibility of designing polarizing and non-polarizing beamsplitters in the VUV, we consider the reflectances for the s and p states of polarization, R_s and R_p respectively, of a single absorbing film having a physical thickness d on a non-absorbing substrate. In this case it is more convenient to use the Airy summation technique [7.10] than the matrix formalism. The reflectance of a single absorbing film having optical constant $N_2 = n_2 + ik_2 = n_2(1 + \kappa_2)$ and sandwiched between two semi-infinite non-absorbing media with refractive indices n_1 and n_3 is given by

$$R = \frac{\rho_{12}^2 e^{2v\xi} + \rho_{23}^2 e^{-2v\xi} + 2\rho_{12}\rho_{23}cos[\phi_{23} - \phi_{12} + 2u\xi]}{e^{2v\xi} + \rho_{12}^2\rho_{23}^2 e^{-2v\xi} + 2\rho_{12}\rho_{23}cos[\phi_{23} + \phi_{12} + 2u\xi]}, \tag{7.94}$$

where

$$\xi = \frac{2\pi}{\lambda_0} d.$$

For the s state of polarization, the generalized Fresnel's amplitude reflection co-

efficients are defined as

$$\rho_{12}^2 = \frac{(n_1 cos\theta_1 - u)^2 + v^2}{(n_1 cos\theta_1 + u)^2 + v^2},$$

(7.95)

$$\rho_{23}^2 = \frac{(n_3 cos\theta_3 - u)^2 + v^2}{(n_3 cos\theta_3 + u)^2 + v^2},$$

and the phase changes on reflection ϕ_{12} and ϕ_{23} as

$$\phi_{12} = tan^{-1}\left(\frac{2v_2 n_1 \cos\theta_1}{u_2^2 + v_2^2 - n_1^2 \cos^2\theta_1}\right),$$

$$\phi_{23} = tan^{-1}\left(\frac{2v_2 n_3 \cos\theta_3}{u_2^2 + v_2^2 - n_3^2 \cos^2\theta_3}\right).$$

For the p state of polarization we have

$$\rho_{12}^2 = \frac{[n_2^2(1-\kappa_2^2)cos\theta_1 - n_1 u]^2 + [2n_2^2\kappa_2 cos\theta_1 - n_1 v]^2}{[n_2^2(1-\kappa_2^2)cos\theta_1 + n_1 u]^2 + [2n_2^2\kappa_2 cos\theta_1 + n_1 v]^2},$$

(7.96)

$$\rho_{23}^2 = \frac{[n_2^2(1-\kappa_2^2)cos\theta_3 - n_3 u]^2 + [2n_2^2\kappa_2 cos\theta_3 - n_3 v]^2}{[n_2^2(1-\kappa_2^2)cos\theta_3 + n_3 u]^2 + [2n_2^2\kappa_2 cos\theta_3 + n_3 v]^2}.$$

and the phase changes on reflection, ϕ_{12} and ϕ_{23}, are given by

$$\phi_{12} = tan^{-1}\left(2n_1 n_2^2 \cos\theta_1 \frac{2\kappa_2 u_2 - (1-\kappa_2^2)v_2}{n_2^4(1+\kappa_2^2)^2\cos^2\theta_1 - n_1^2(u_2^2+v_2^2)}\right),$$

$$\phi_{23} = tan^{-1}\left(2n_3 n_2^2 \cos\theta_3 \frac{2\kappa_2 u_2 - (1-\kappa_2^2)v_2}{n_2^4(1+\kappa_2^2)^2\cos^2\theta_3 - n_3^2(u_2^2+v_2^2)}\right).$$

The exponential terms u and v are defined as

$$u^2 = \frac{1}{2}\left(n_2^2(1-\kappa_2^2) - n_1^2 sin^2\theta_1 + \sqrt{[n_2^2(1-\kappa_2^2) - n_1^2 sin^2\theta_1]^2 + 4n_2^4\kappa_2^2}\right),$$

(7.97)

$$v^2 = \frac{1}{2}\left(-[n_2^2(1-\kappa_2^2) - n_1^2 sin^2\theta_1] + \sqrt{[n_2^2(1-\kappa_2^2) - n_1^2 sin^2\theta_1]^2 + 4n_2^4\kappa_2^2}\right).$$

R_s and R_p are complicated functions of the optical constants of the absorbing films. In order to obtain a polarizing beamsplitter with a single absorbing film deposited onto a non-absorbing substrate, the requirement $R_p = 0$ with $R_s \neq 0$ at an angle of incidence θ_0 needs to be inserted into Equation (7.94) and solved for n_2 and k_2. The indices of surrounding media n_1, and n_3 and the physical thickness of the film are assumed to be known. Similarly, for a non-polarizing beamsplitter the requirement $R_s = R_p$ may be inserted into Equation (7.94) and solved for n_2 and k_2.

Another approach is to employ a numerical fitting technique which would give values of the optical constants of the film as well as the optimum value of the physical thickness of the film. A QW multilayer is then designed to enhance the reflection of the s polarization component without altering the minimum reflectance of the p component. Figure 7.40 shows the calculated reflectance of such a filter. The design (D_6) is

$$D_6 = Vacuum[(H'L')^{12}H']Substrate,$$

where $H' = LaF_3$, $L' = MgF_2$, and substrate is MgF_2. The primes denote correction of the quarterwave optical thicknesses for oblique incidence. The angle of incidence is 45^0 and the p state has a minimum at $\lambda_0 = 160$ nm and $\lambda_0 = 173$ nm. The s state has a much higher value of reflectance (71%) than the p state at 160 nm.

This polarization beamsplitter polarizes a very narrow band of light centered at 160 nm. For some applications it might have to be combined with a narrowband transmission filter.

In order to obtain a non-polarizing beamsplitter, the refractive index of the incident medium should be much higher [7.8,12] than that of vacuum or bulk MgF_2. Since no dielectrics are available with both high values of the refractive index and low values of the extinction coefficient, the design of VUV broadband non-polarizing beamsplitters is an exciting challenge for future research. A possible solution may be found if graded index films with acceptable k values are designed and used at the interface between an incident medium (vacuum) and a QW multilayer.

7.10 Applications

Currently the vacuum ultraviolet wavelength regime lacks high performance optical devices for interferometric, polarimetric, photometric, and laser applications. The reasons for this have been the topic of this chapter. The designs and fabrication capability that we have described can be utilized to produce multilayer stacks that in turn can be used to build optical components that are considered fundamental in optics in the visible and infrared, but which are essentially nonexistent at this time for the VUV.

Optical coatings such as narrowband filters, achromatic and polarizing beamsplitters, Fabry-Perot etalons and high reflective mirrors, will open up the VUV to standard high resolution instrumentation such as high resolution Fabry-Perot, Michelson and Mach-Zender interferometers. The capability to produce high reflective coatings will facilitate the development of high performance VUV lasers.

In addition to basic laboratory applications, the need for such devices in space applications is significant from both the civilian and military perspective. Areas relevant to NASA, for example, where VUV optical technology could be exploited include environmental monitoring, astrophysics and astronomy, plasma physics and aeronomy, and space engineering.

References

[7.1] D. F. Heath and P. A Sacher, "Effects of a simulated high-energy space environment on the ultraviolet transmittance of optical materials", Appl. Opt. **5**, 937-943 (1966)

[7.2] J. M. Elson, J. P. Rahn, and J. M. Bennett, "Relationship of the total integrated scattering from multilayer-coated optics to angle of incidence, polarization, correlation length, and roughness cross-correlation properties", Appl. Opt. **22**, 3207-3214 (1983)

[7.3] K. H. Guenther, H. L. Gruber, and H. K. Pulker, "Morphology and light scattering of dielectric multilayer systems", Thin Solid Films, **34**, 363-381 (1976)

[7.4] H. A. Macleod, "Structure-related optical properties of thin films", J. Vac. Sci. Technol. **A 3**, 2089-2095 (1985)

[7.5] P. Yeh, **Optical Waves in Layered Media,** (John Wiley and Sons, 1988) chapters 5, 6, 9 and 10

[7.6] R. Jacobson, "Inhomogeneous and coevaporated homogeneous thin films for optical applications", in **Physics of Thin Films,** Vol. 8, (Academic Press, New York 1975)

[7.7] L. M. Brekhovskih, **Waves in Layered Media,** (Academic Press, New York 1960).

[7.8] M. Zukic and K. H. Guenther, "Design of nonpolarizing achromatic beamsplitters with dielectric multilayer coatings", Opt. Eng. **28**, 165-171 (1989)

[7.9] M. Zukic and K. H. Guenther, "Optical coatings with graded index films for high power laser applications: design", in **Laser Optics for Intracavity and Extracavity Applications,** P. M. Faucet and K. H. Guenther, eds. Proc. SPIE **895**, 271-277 (1988).

[7.10] M. Born and E. Wolf, **Principles of Optics,** (Pergamon Press, Oxford 1983) chapters 1, 2, 13 and 14

[7.11] H. A. Macleod, **Thin-Film Optical Filters,** (Adam Hilger Ltd, Bristol 1986) chapters 2, 5, and 7

[7.12] Z. Knittl, **Optics of Thin Films,** (John Wiley and Sons, London 1976)

[7.13] A. Thelen, **Design of Optical Interference Coatings,** (McGraw-Hill, New York 1989) chapters 2, 3 and 10

[7.14] D. P. Arndt *et al,* "Multiple determination of the optical constants of thin-film coating materials", Appl. Opt. **23**, 3571-3595 (1984)

[7.15] J. M. Bennett and M. J. Booty, "Computational method for determining n and k for a thin film from the measured reflectance, transmittance, and film thickness", Appl. Opt. **5**, 41-43 (1966)

[7.16] J. M. Bennett and M. J. Booty, "Computer program for determining optical constants of a film on an opaque substrate", Appl. Opt. **8**, 2366-2368 (1969)

[7.17] W. N. Hansen, "Optical characterization of thin films: theory", J. Opt. Soc. Amer. **63**, 793-802 (1973)

[7.18] L. Ward, "A survey of the accuracies of some methods for the determination of the optical constants of thin films", Opt. Acta **32**, 155-164 (1985)

[7.19] M. C. Gupta, "Optical constant determination of thin films", Appl. Opt. **27**, 954-959 (1988)

[7.20] F. Abelès, "Methods for determinig optical parameters of thin films" in **Progress in Optics**, E. Wolf, ed. Vol II, 268 (Wiley, New York, 1963)

[7.21] P. O. Nilsson, "Determination of optical constants from intensity measurements at normal incidence", Appl. Opt. **7**, 435-442 (1968)

[7.22] M. Zukic, "Damped Least Squares Technique for the Design of Optical Multilayer Filters", MS thesis, Imperial College, University of London (1984)

[7.23] M. Zukic, D.G. Torr, J.F. Spann and M.R. Torr, "VUV Thin Films, Part I: Optical constants of BaF_2, CaF_2, LaF_3, MgF_2, Al_2O_3, HfO_2 and SiO_2 thin films in the VUV", paper submited for publication in Applied Optics

[7.24] O. R. Wood II, H. G. Craighead, J. E. Sweeney, and P. J. Maloney, "Vacuum ultraviolet loss in magnesium fluoride films", Appl. Opt. **23**, 3644-3649 (1984)

[7.25] H. R. Philipp, "Silicon Dioxide (SIO_2) (Glas)" in **Handbook of Optical Constants of Solids,** E. D. Palik ed., (Academic Press, Inc., Orlando, 1985) pp. 749

[7.26a] M. Zukic, D.G. Torr, J.F. Spann and M. R. Torr, "VUV Thin Films, Part II: Vaccum ultraviolet all-dielectric narrowband filters", paper submited for publication in Applied Optics

[7.26b] M. Zukic, "Optical Filters in the Vacuum Ultraviolet", PhD Dissertation, University of Alabama in Huntsville 1989

[7.27] E. Spiller, "Multilayer interference coatings for the vacuum ultraviolet" in **Space Optics,** B. J. Thompson and R. R. Shannon eds. **Proceeding of the** Ninth International Commission for Optics (National Academy of Sciences, Washington, D.C., 1974)

[7.28] B. K. Flint, " Special application coatings for the vacuum ultraviolet" in **Optical Coatings-Applications and Utilization II, Proc. SPIE 140** (1978)

[7.29] Acton Research Corporation, **Optical Filters,** Catalog (1989)

[7.30] A. Malherbe, "Interference filters for the far ultraviolet", **Appl. Opt. 13,** 1275-1276 (1974)

[7.31] E. Spiler, "Interference filters for the ultraviolet and the surface plasmon of aluminium", Appl. Opt. **13**, 1209-1215 (1974)

Table 7.1 Deposition Conditions

Material	P_0 (torr)	P (torr)	D_R (nm/sec)	d (nm)
BaF_2	9.5×10^{-7}	1.5×10^{-6}	0.16	53.0
CaF_2	8.5×10^{-7}	2.5×10^{-6}	0.20	99.0
LaF_3	8.5×10^{-7}	2.0×10^{-6}	0.14	51.0
MgF_2	8.5×10^{-7}	2.5×10^{-6}	0.23	68.0
$Al_2O_3^a$	8.5×10^{-7}	1.0×10^{-4}	0.10	112.0
HfO_2	8.5×10^{-7}	1.5×10^{-4}	0.10	30.0
SiO_2	9.5×10^{-7}	1.2×10^{-4}	0.10	51.0

[a] Oxygen leaked into the chamber during the deposition of oxides.

Table 7.2 Achromatic Beamsplitter

Material	Physical Thickness [nm]	
	Initial Design	Final Design
Air		
LaF_3	24.3	23.6
MgF_2	31.5	30.6
LaF_3	24.3	24.6
MgF_2	31.5	34.7
LaF_3	24.3	13.9
MgF_2	31.5	16.8
Substrate		

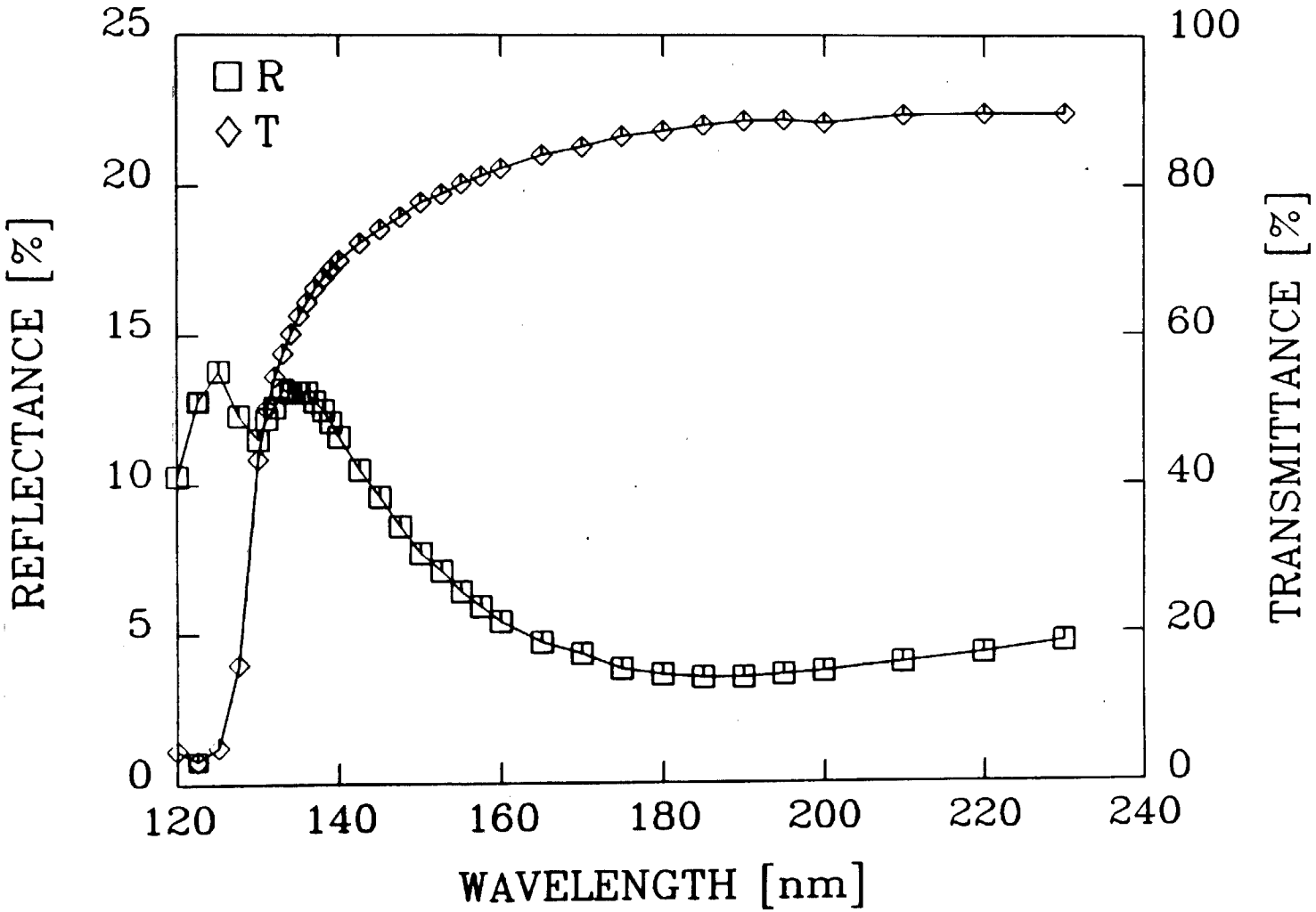

Zukic/Torr Figure 7.4a

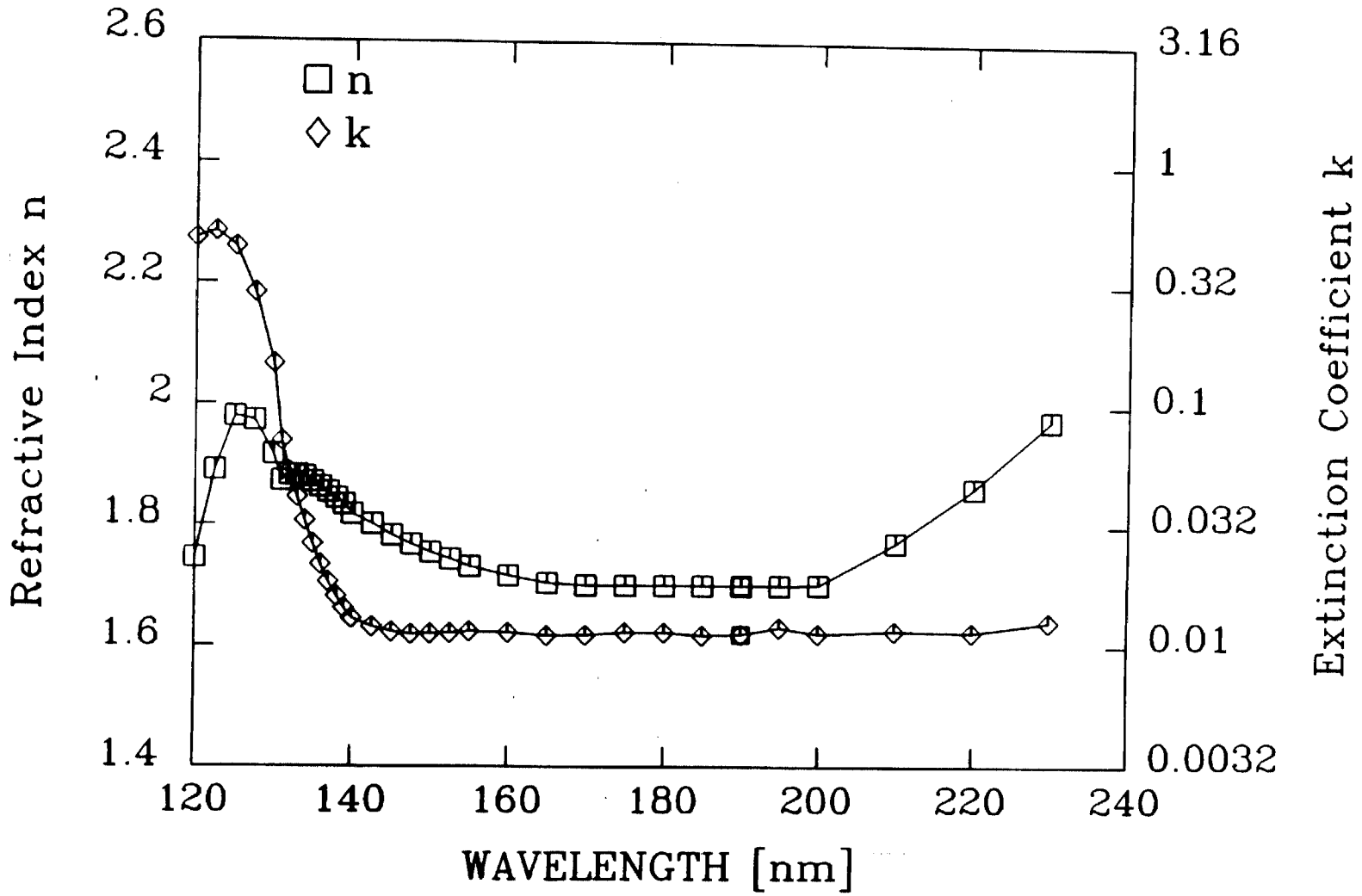

Zukic/Torr Figure 7.4b

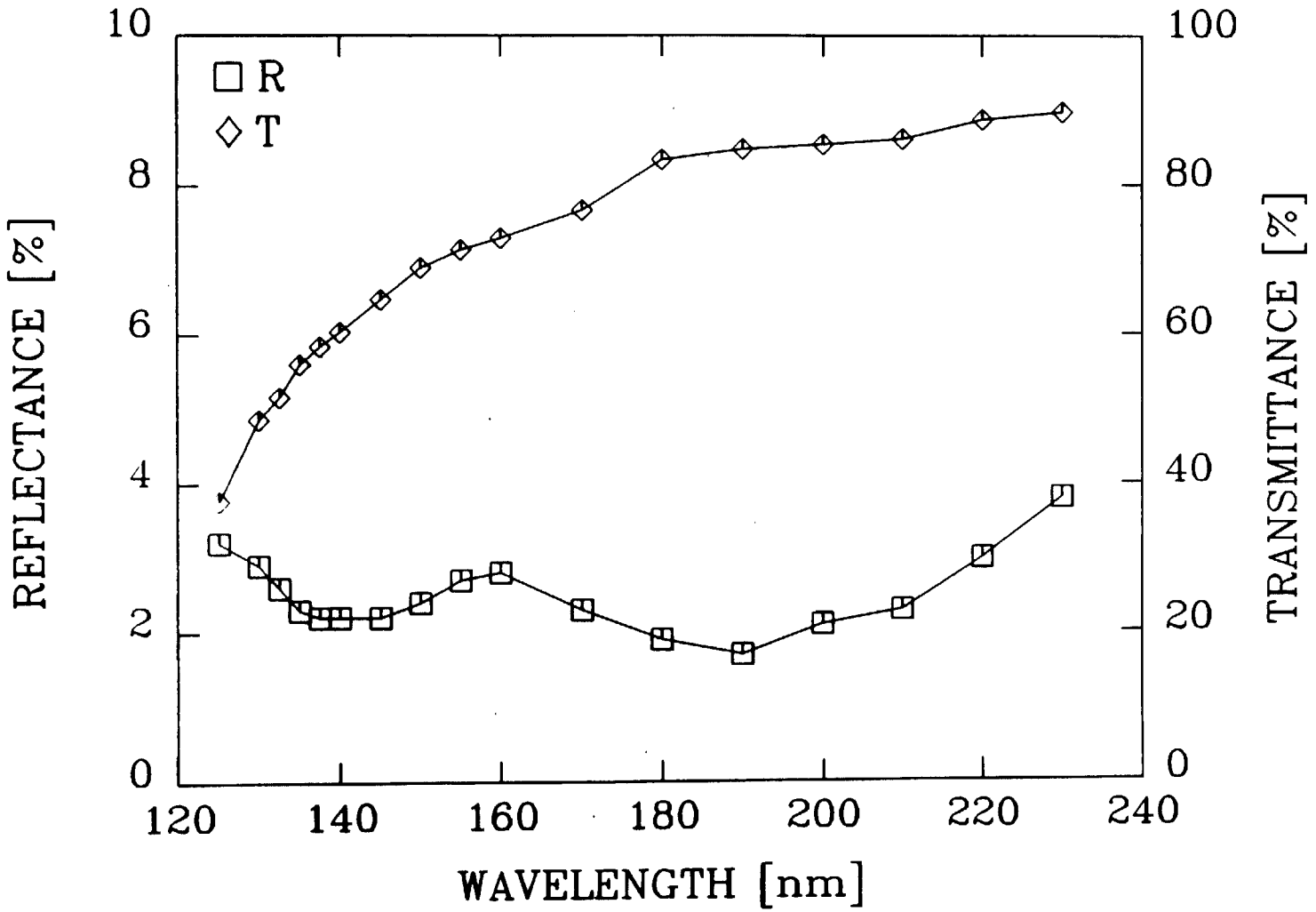

Zukic/Torr Figure 7.5a

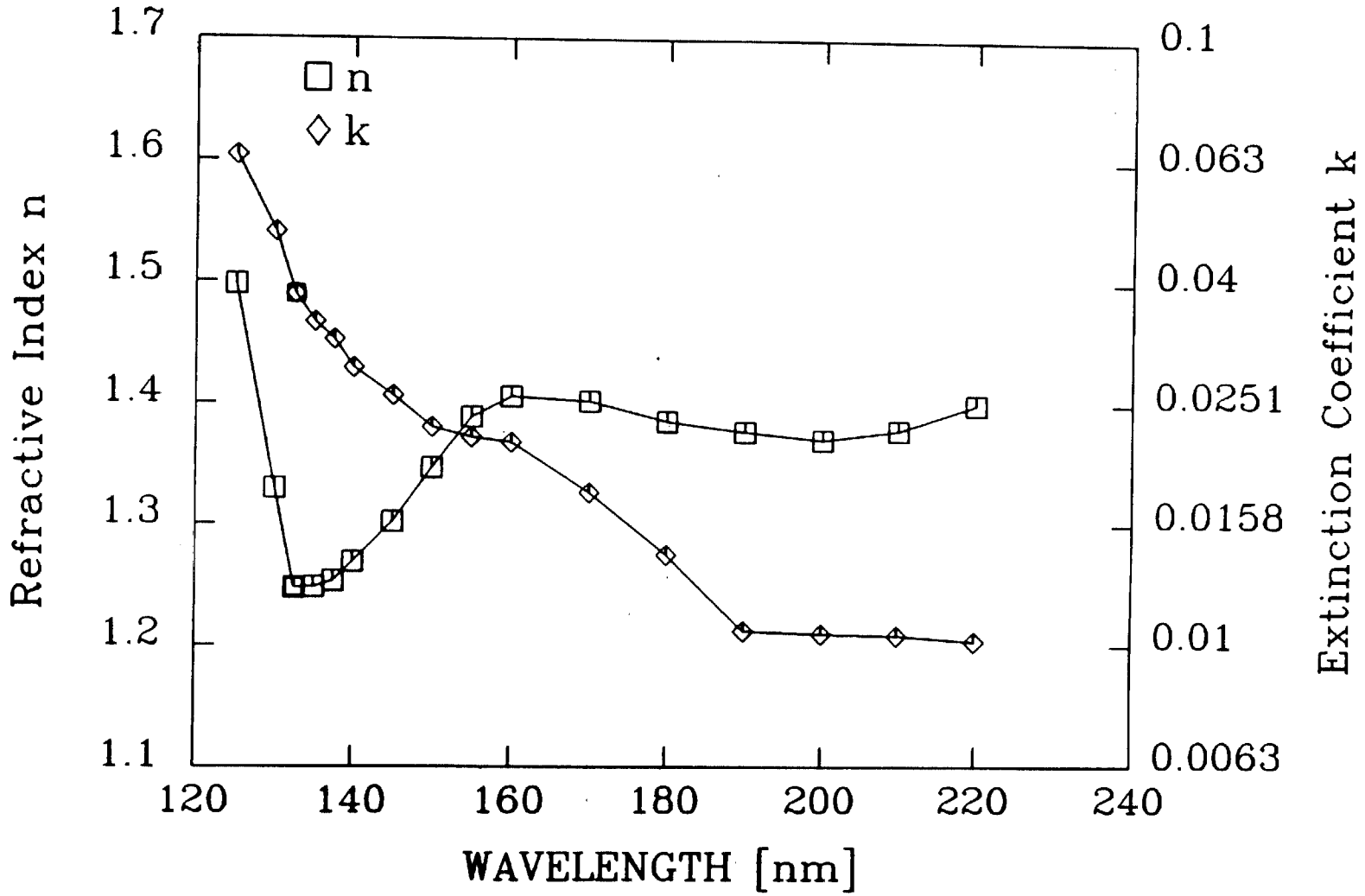

Zukic/Torr Figure 7.5b

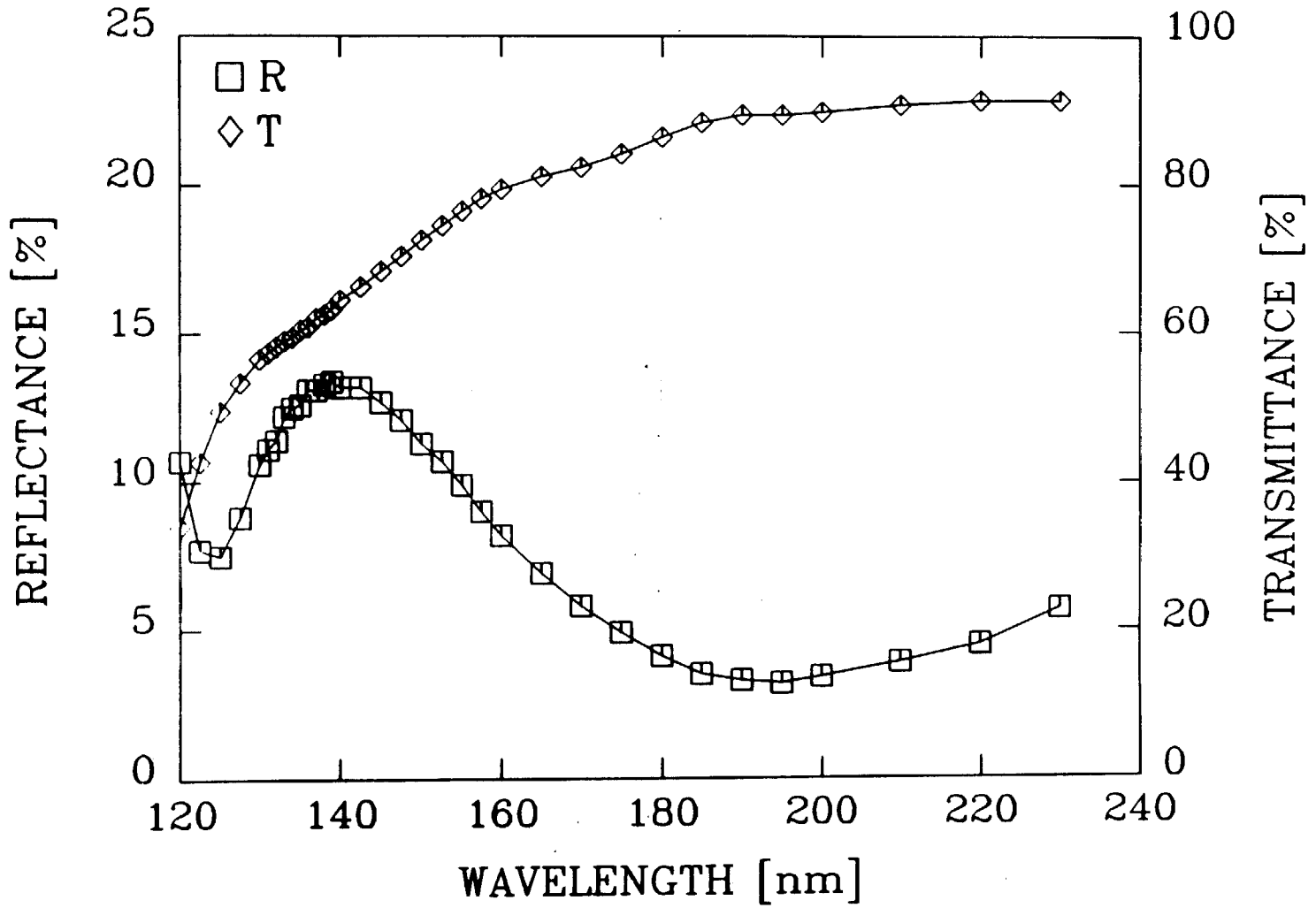
25
20
15
10
5
0
100
80
60
40
20
0
120
140
160
180
200
220
240
R
T
REFLECTANCE [%]
TRANSMITTANCE [%]
WAVELENGTH [nm]

Figure 7.6a

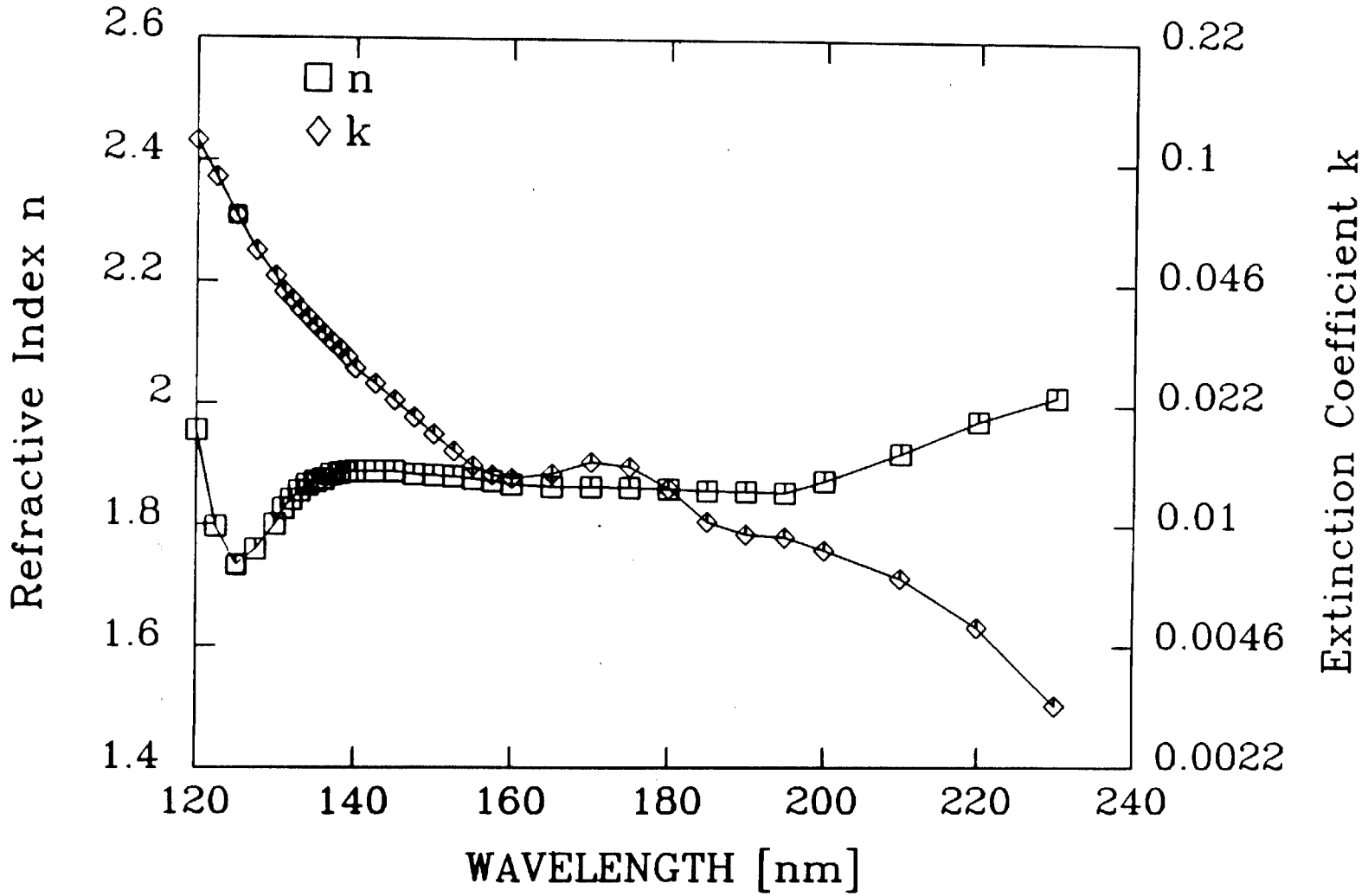

Zukic/**Torr Figure 7.6b**

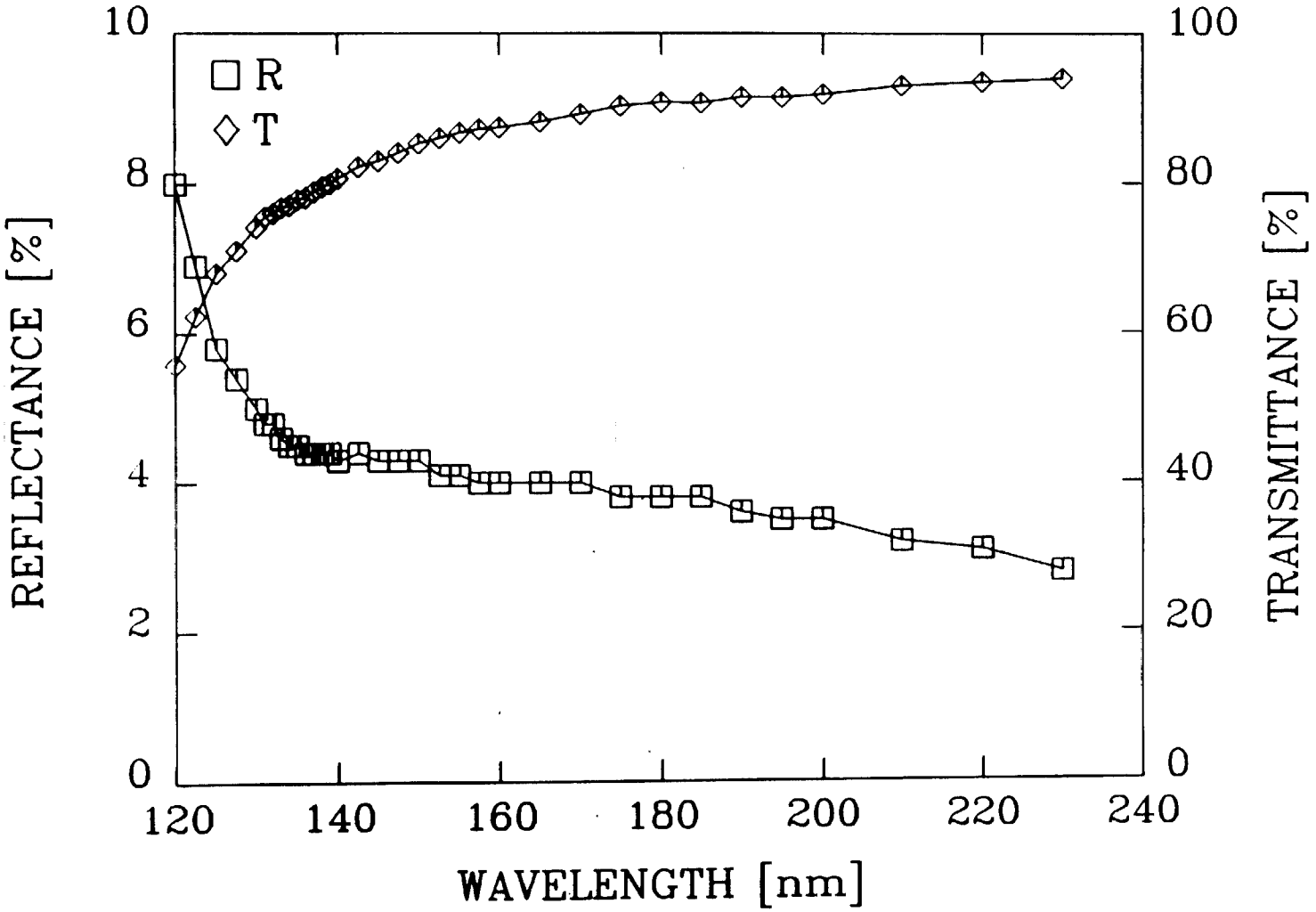

Zukic/Torr Figure 7.7a

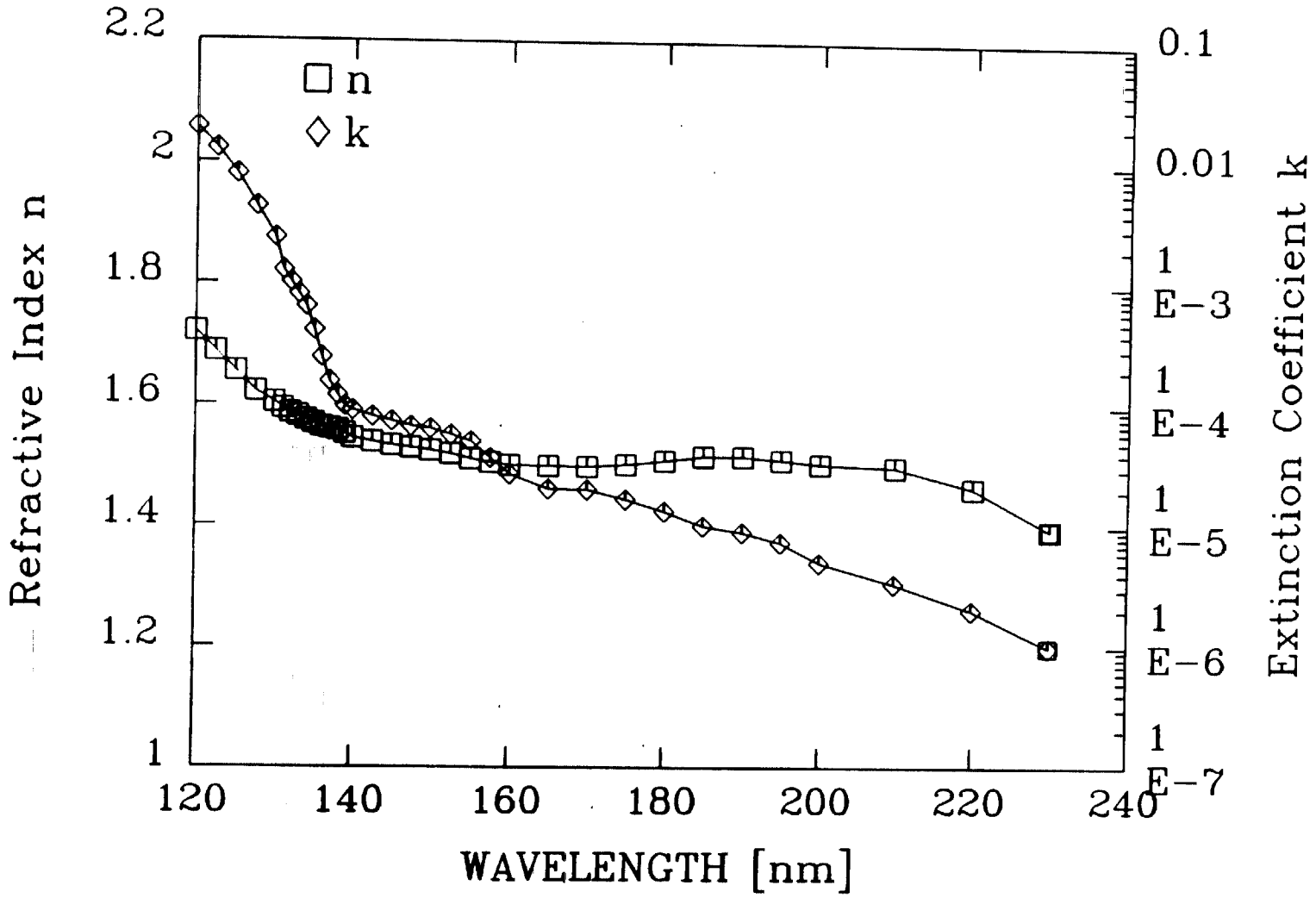

Zukic/Torr Figure 7.7b

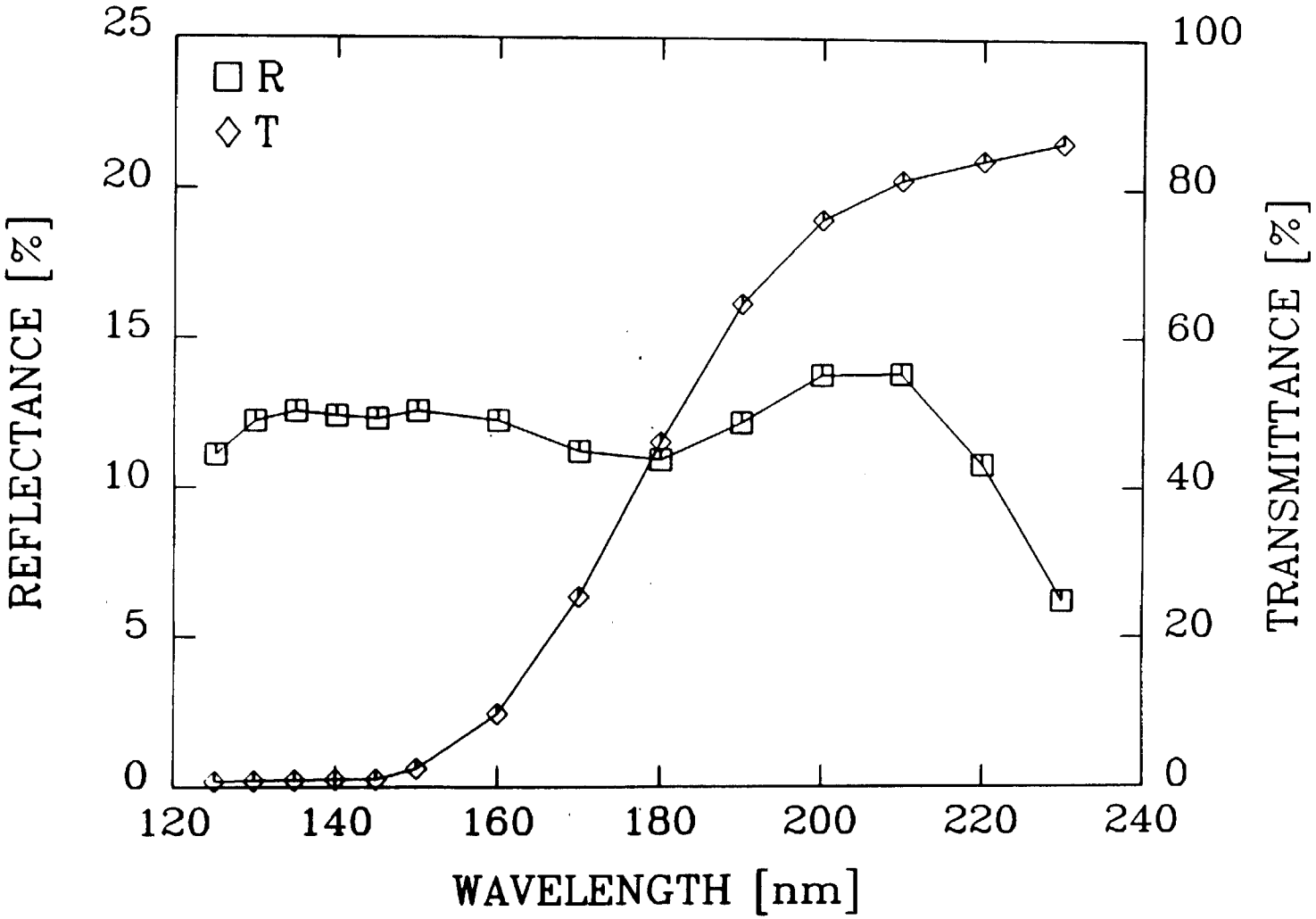

Zukic/Torr Figure 7.8a

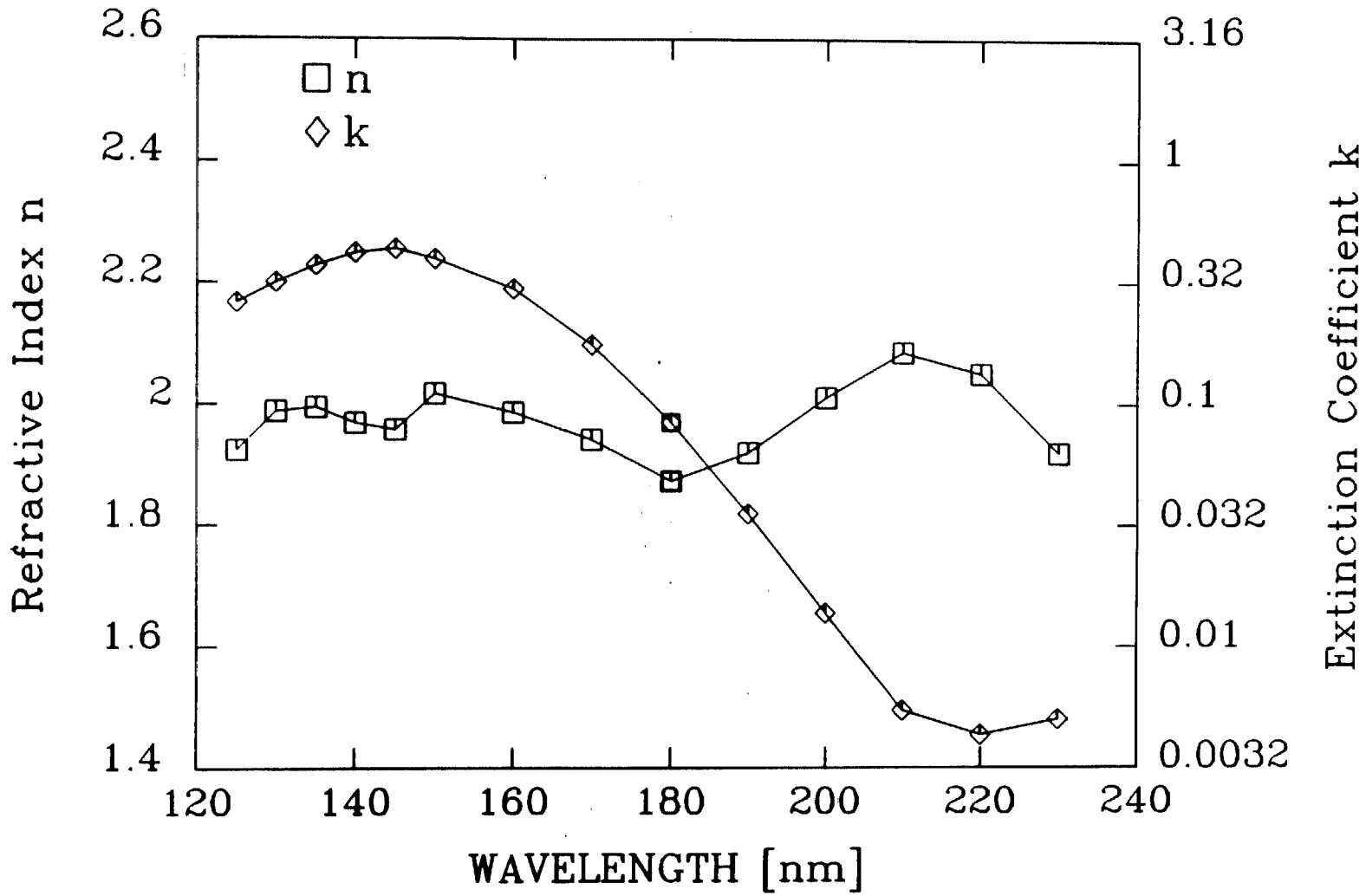

Zukic/Torr Figure 7.8b

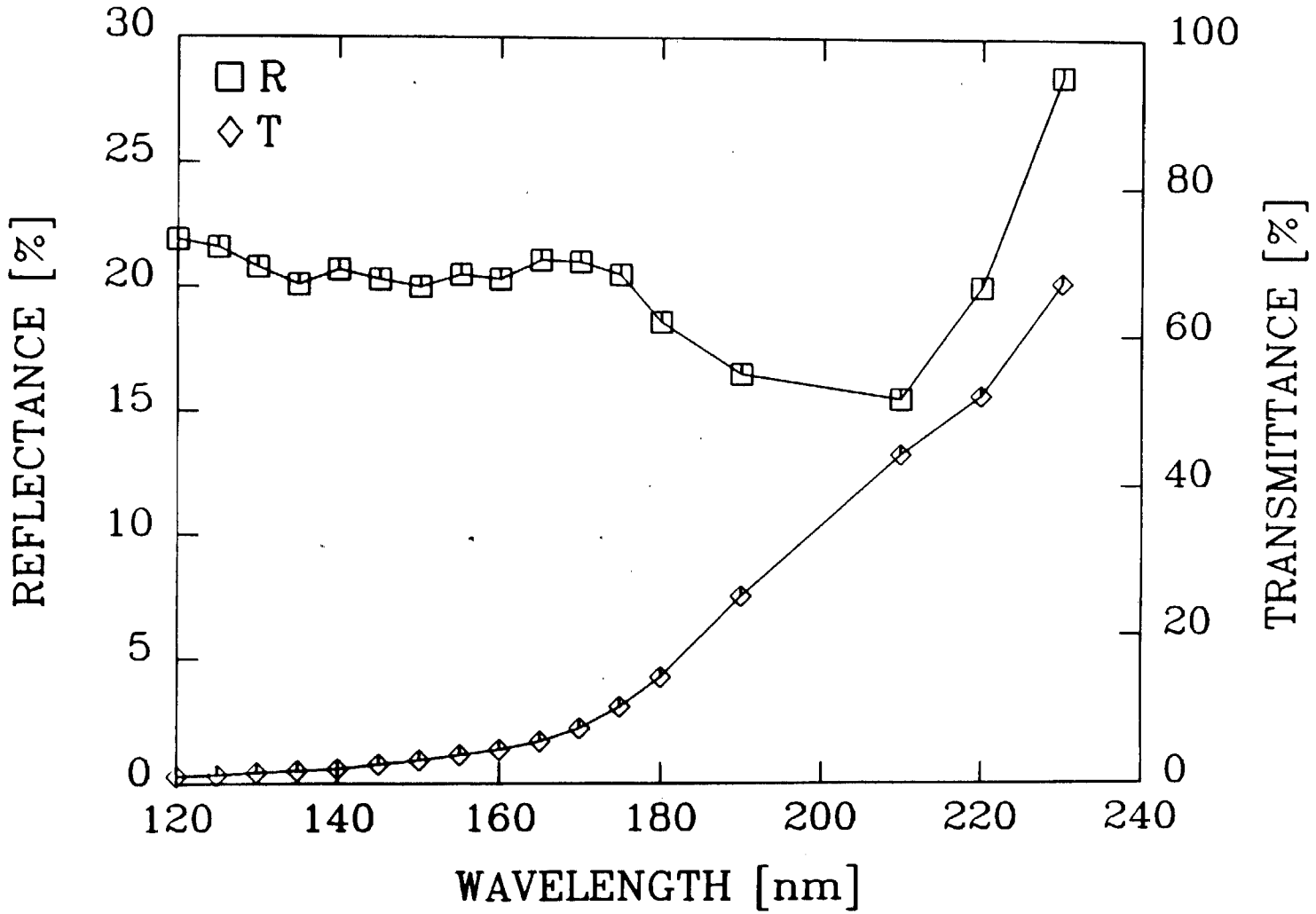

Zukic/Torr **Figure 7.9a**

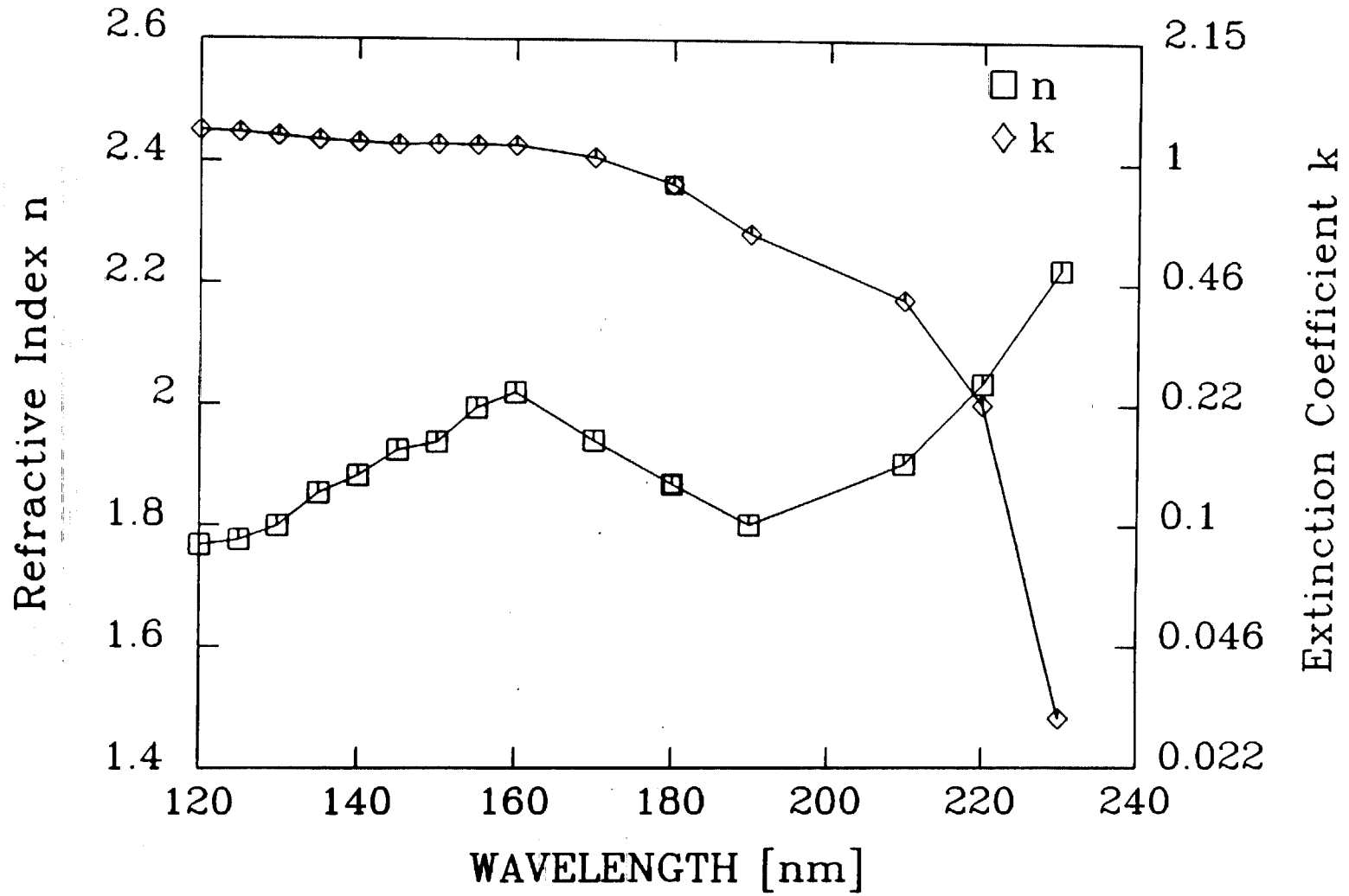

Zukic/**Torr Figure 7.9b**

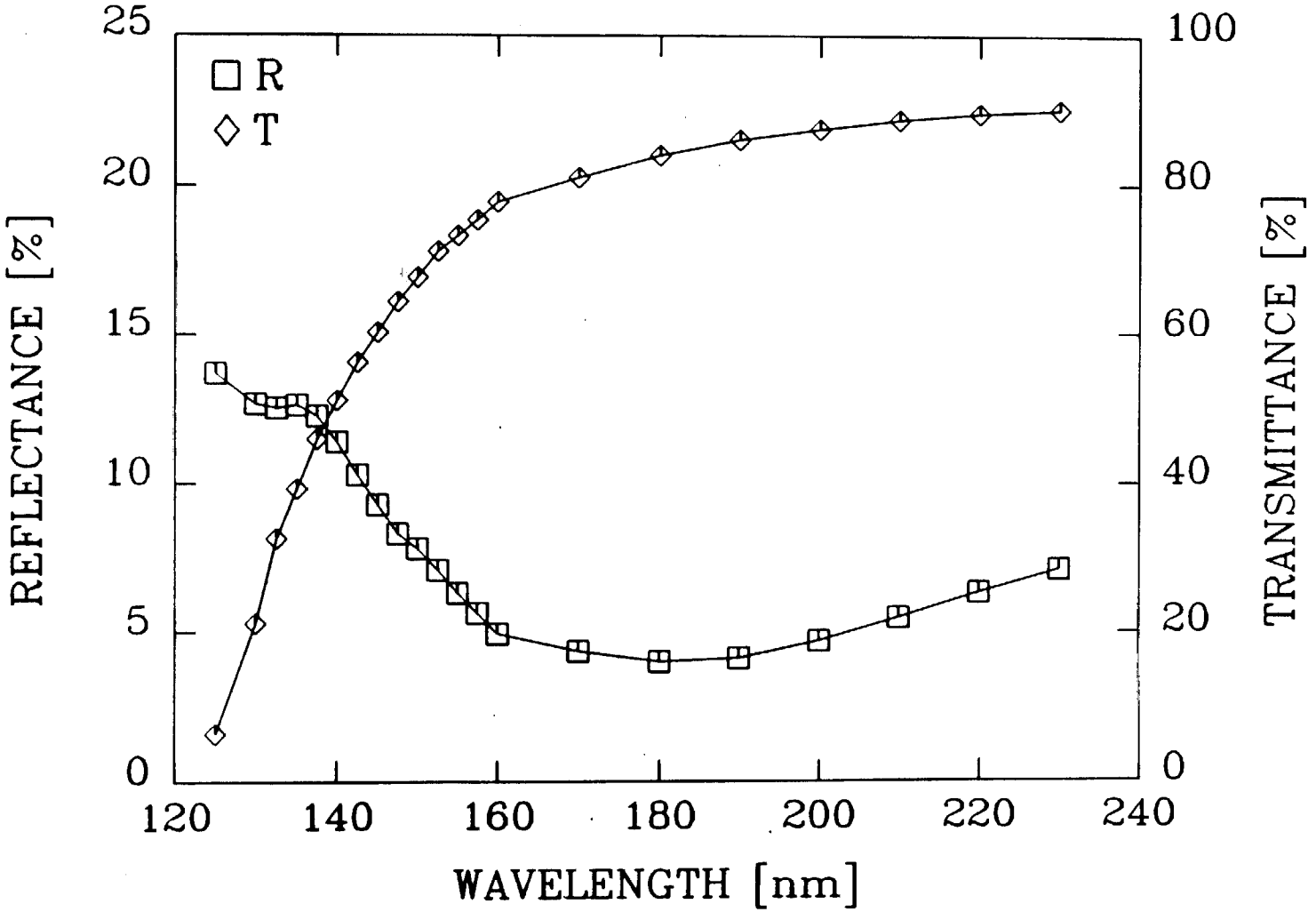

Zukic/**Torr Figure 7.10a**

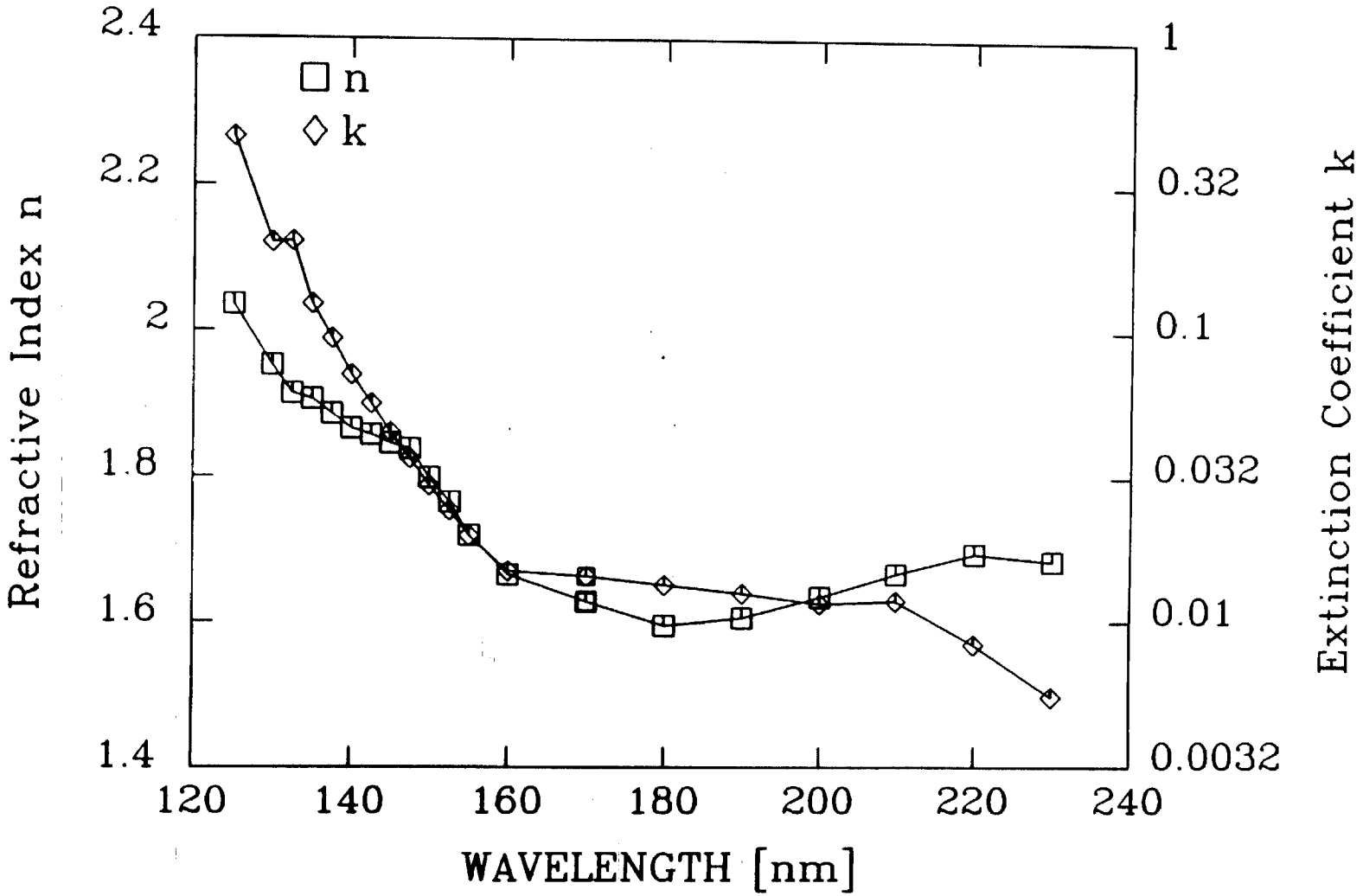

Zukic/Torr Figure 7.10b

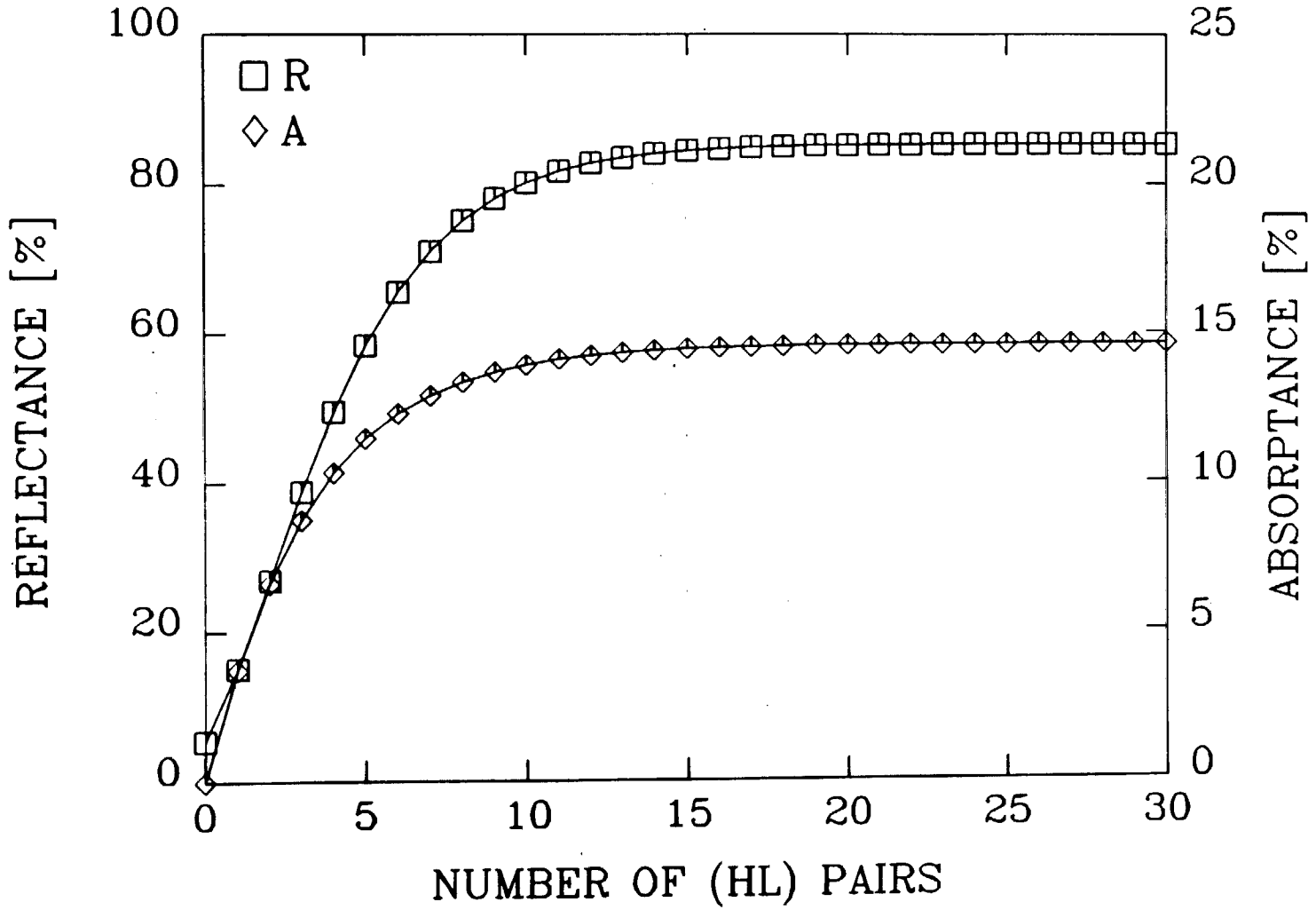

Zukic/Torr Figure 7.11a

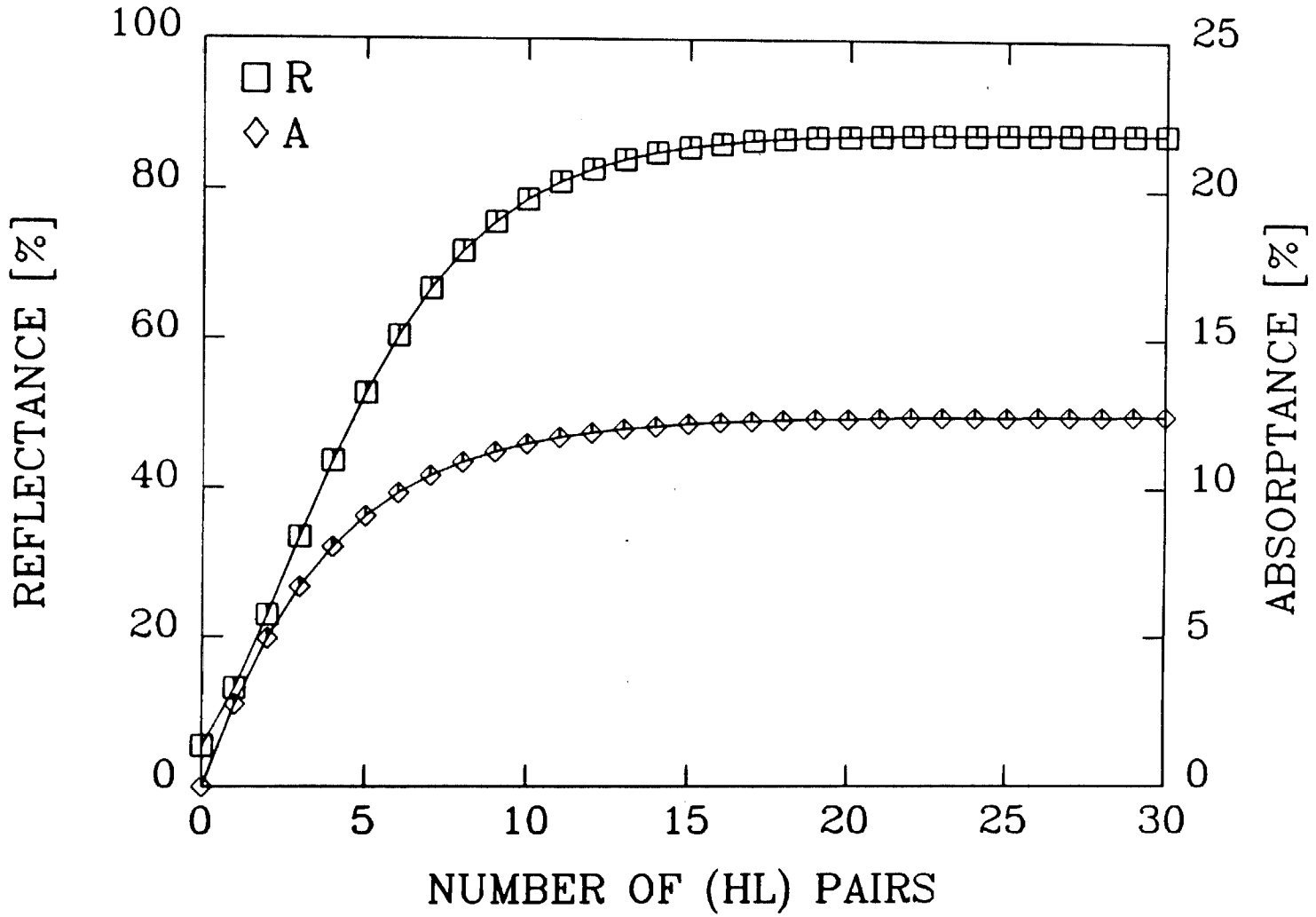

Zukic/Torr Figure 7.11b

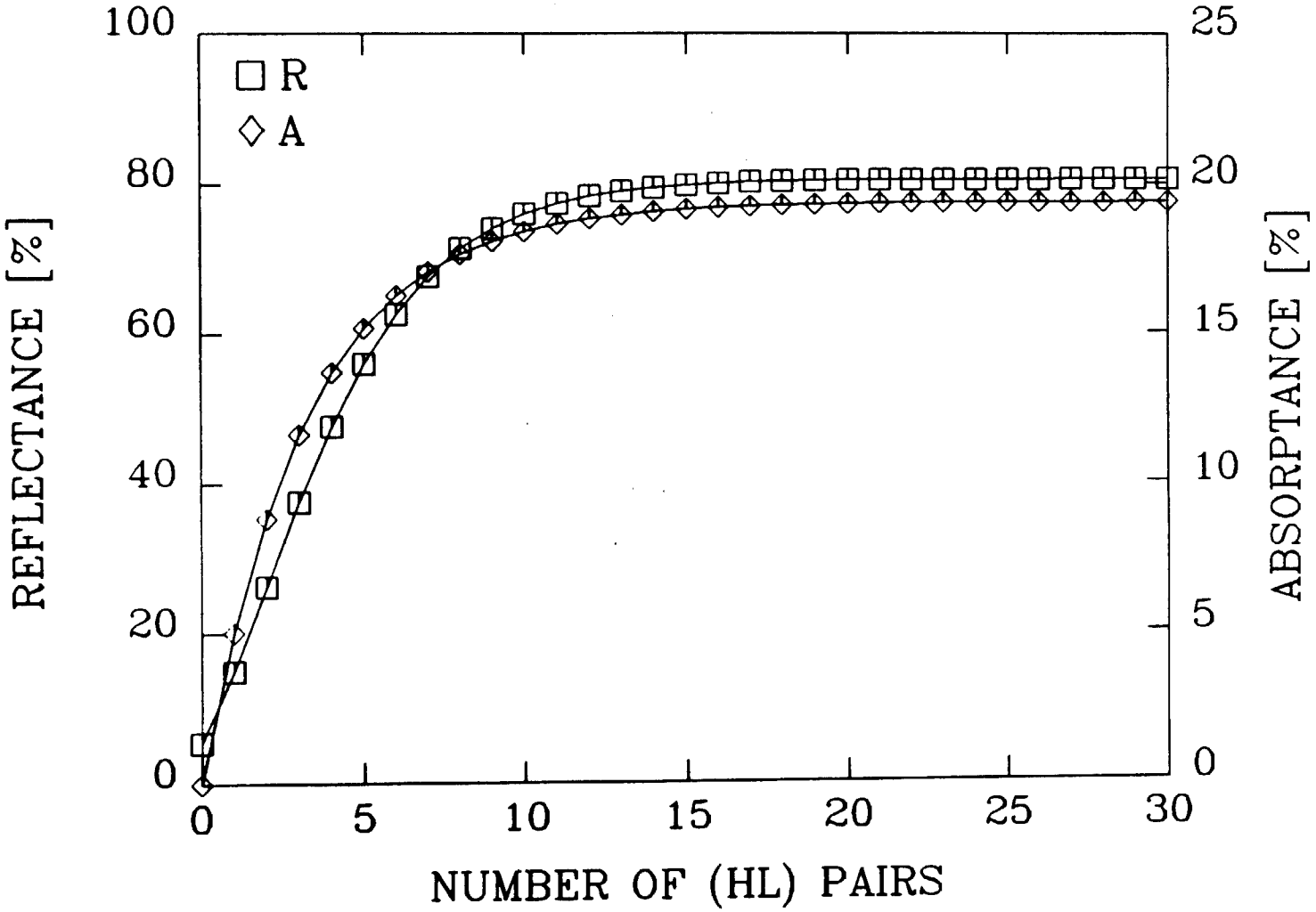

Zukic/Torr Figure 7.12a

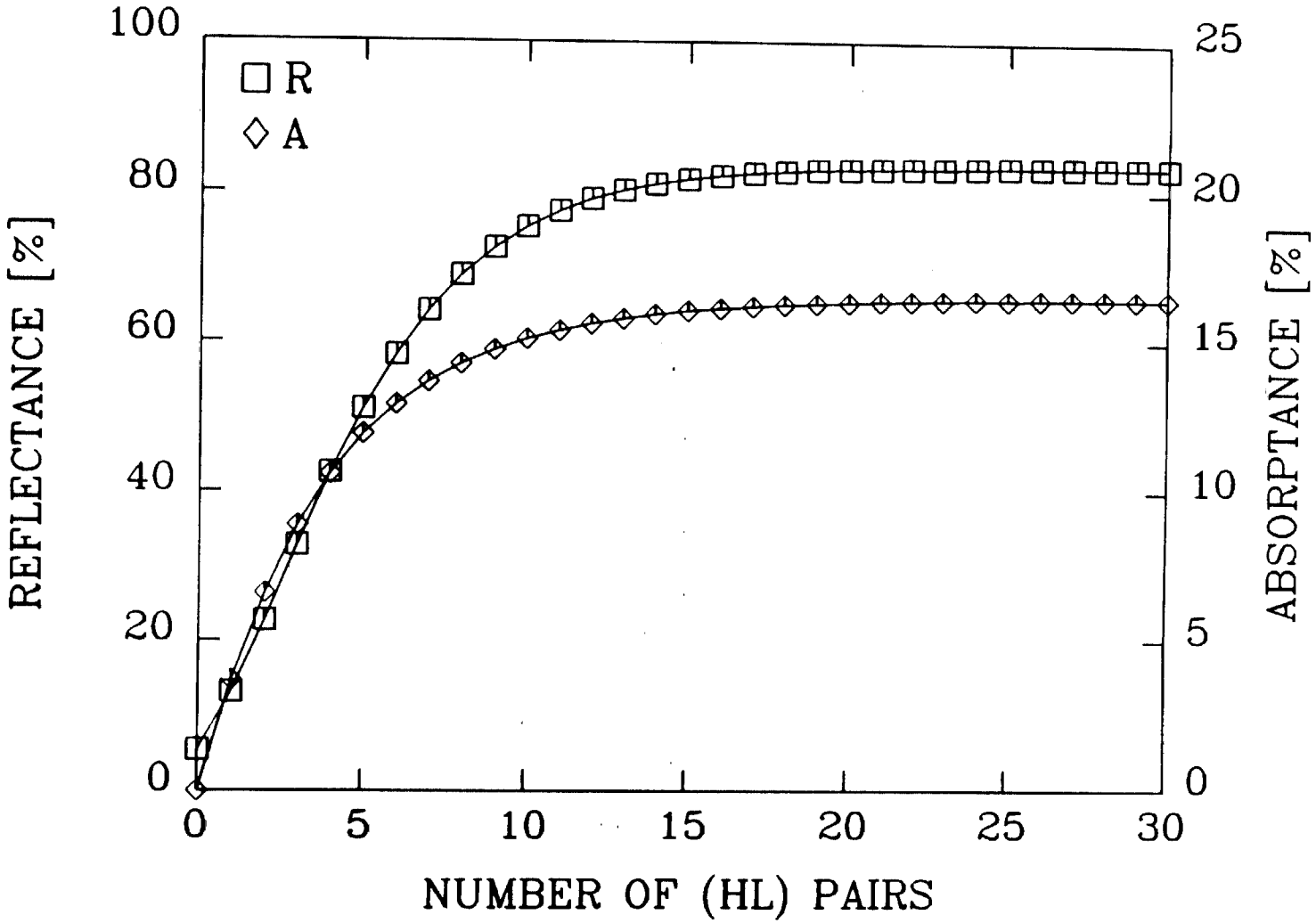

Zukic/Torr Figure 7.12b

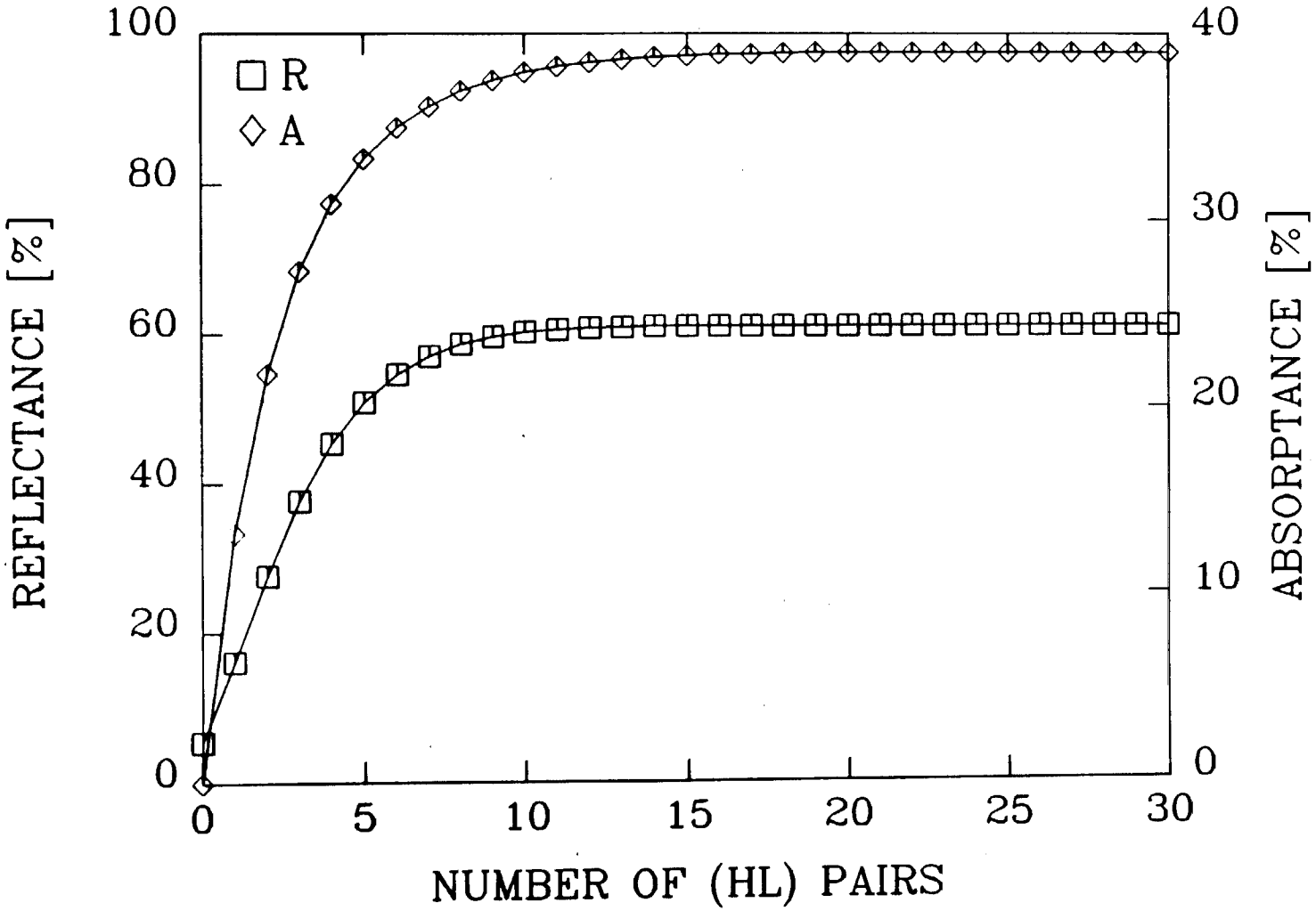

Zukic/Torr Figure 7.13a

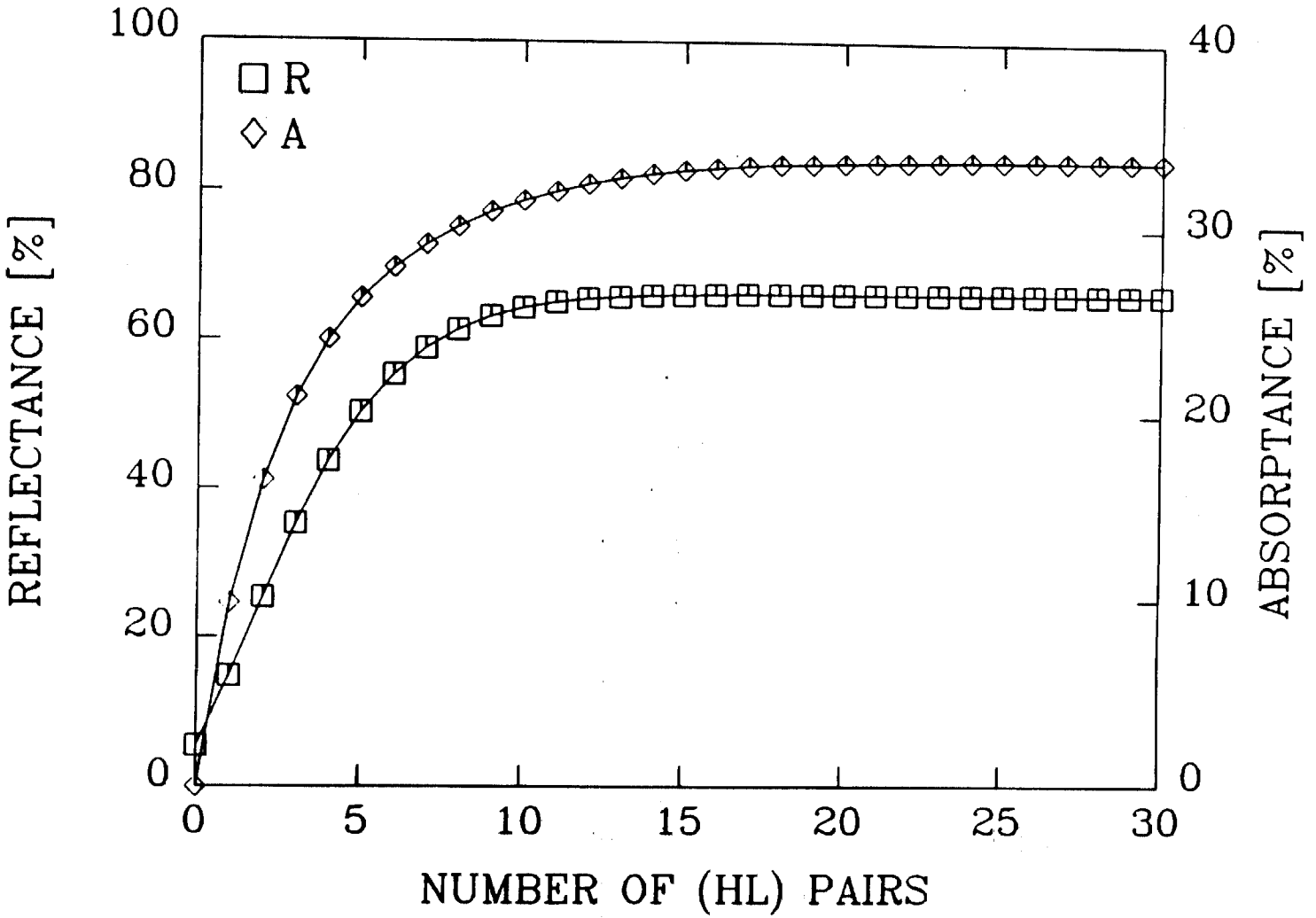

Zukic/Torr Figure 7.13b

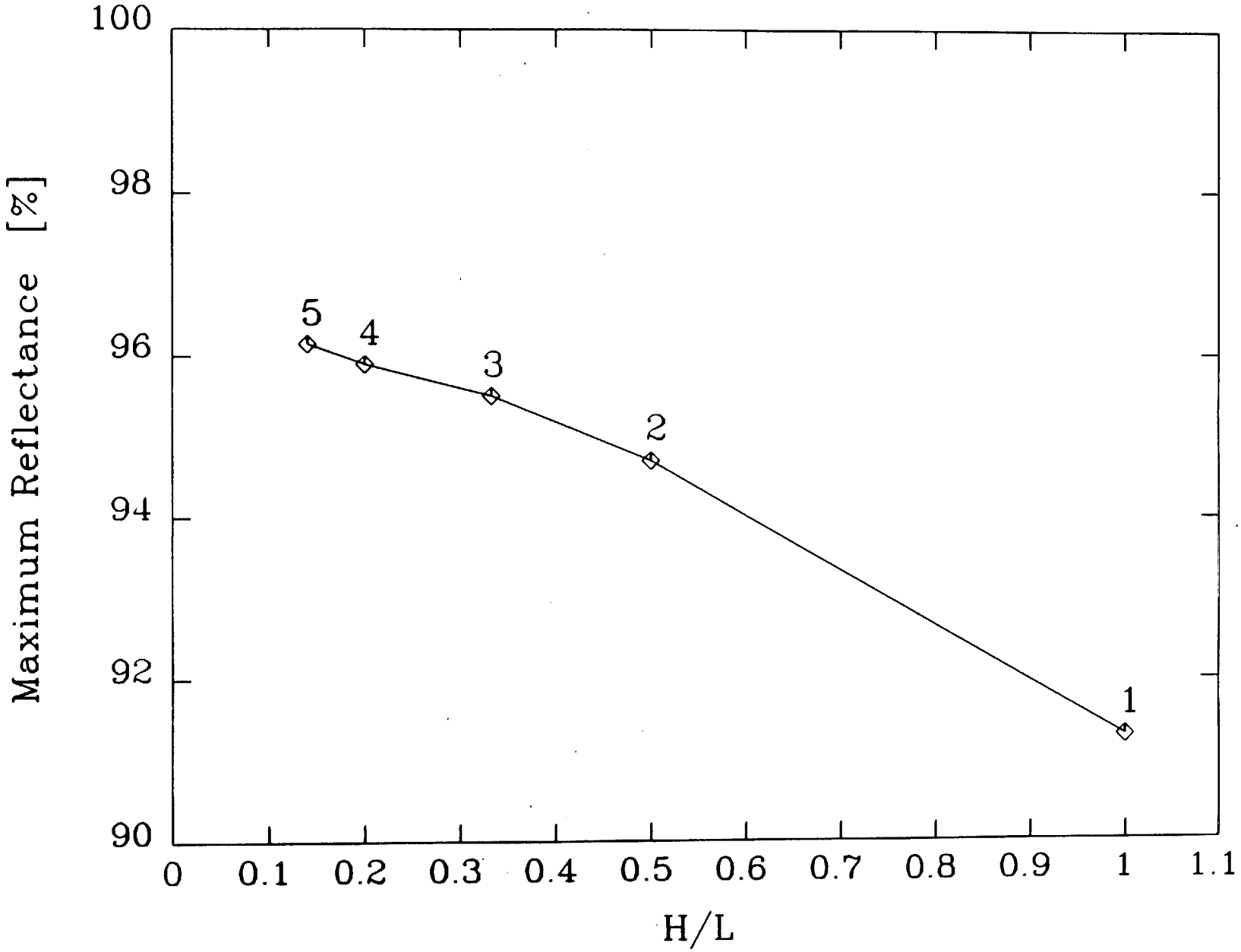

Zukic/Torr Figure 7.14

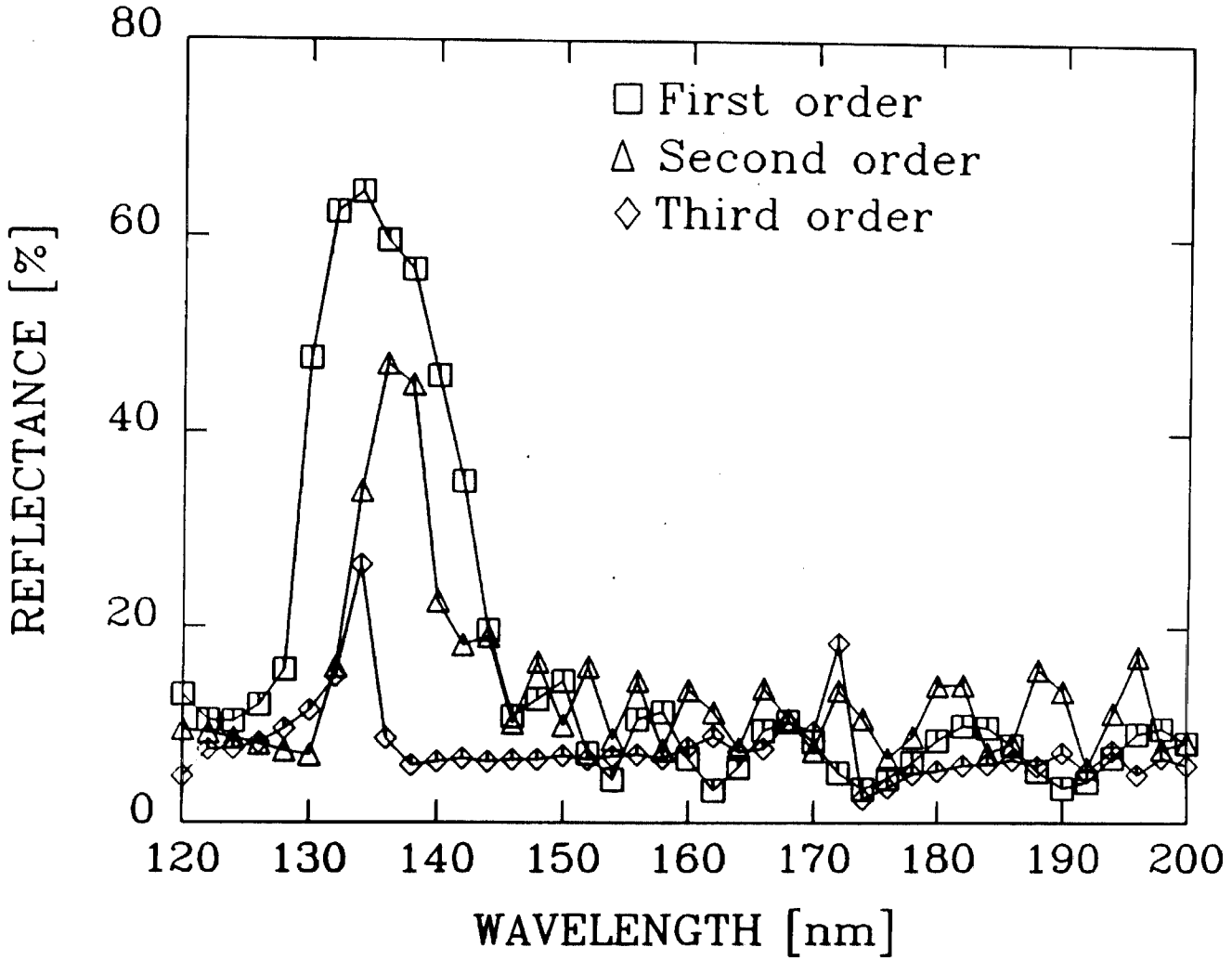

Zukic/Torr Figure 7.15

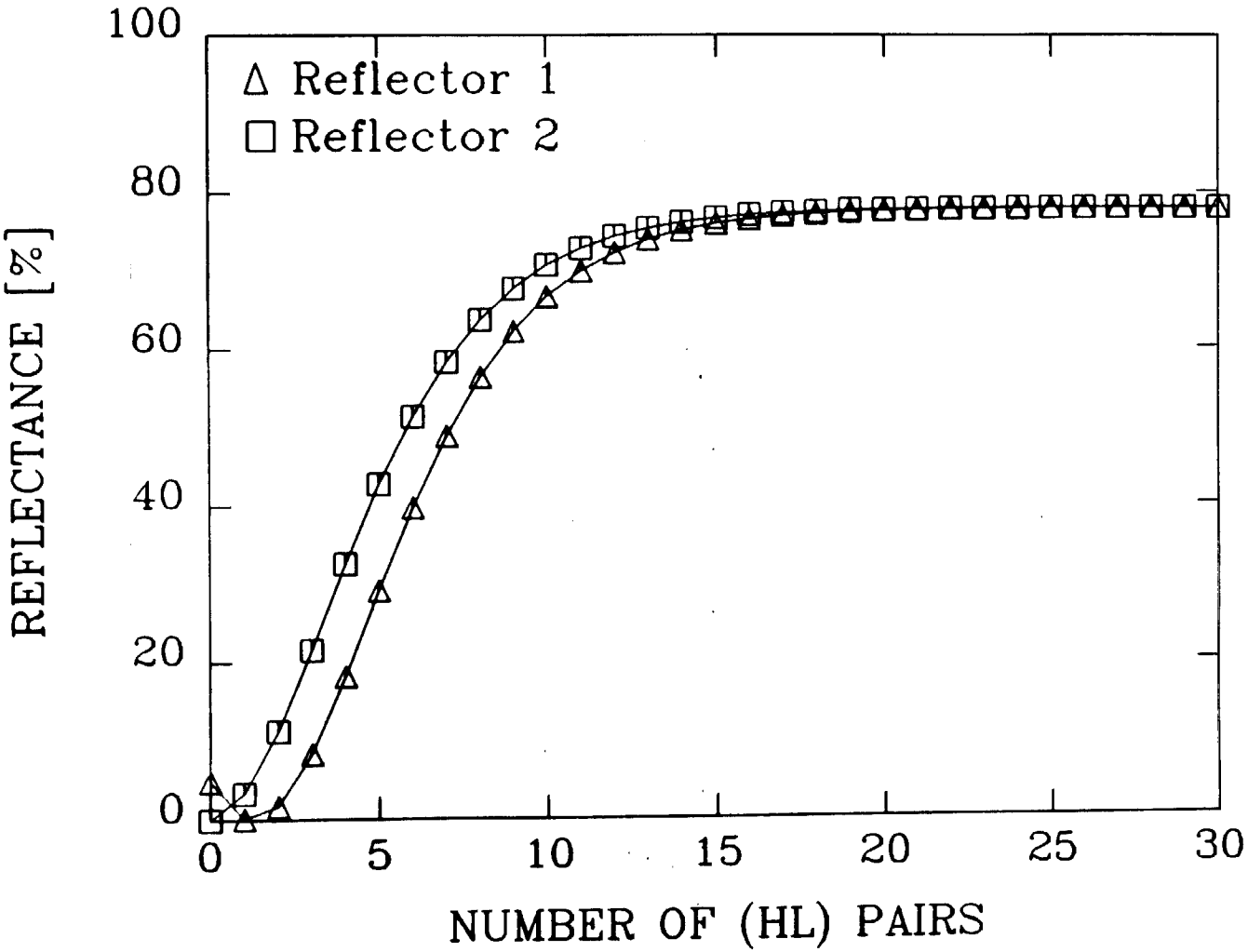

Zukic/Torr Figure 7.16a

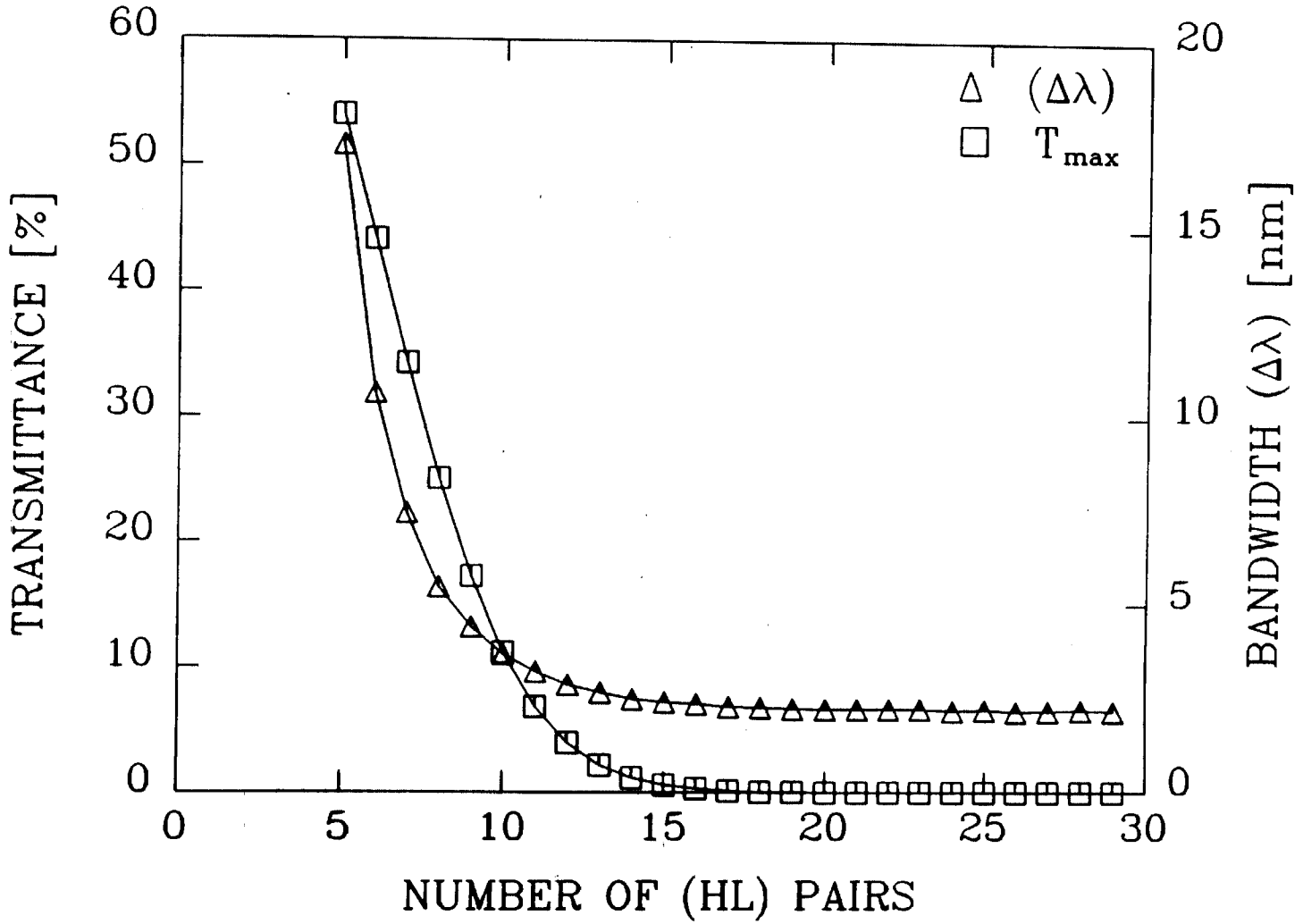

Zukic/Torr Figure 7.16b

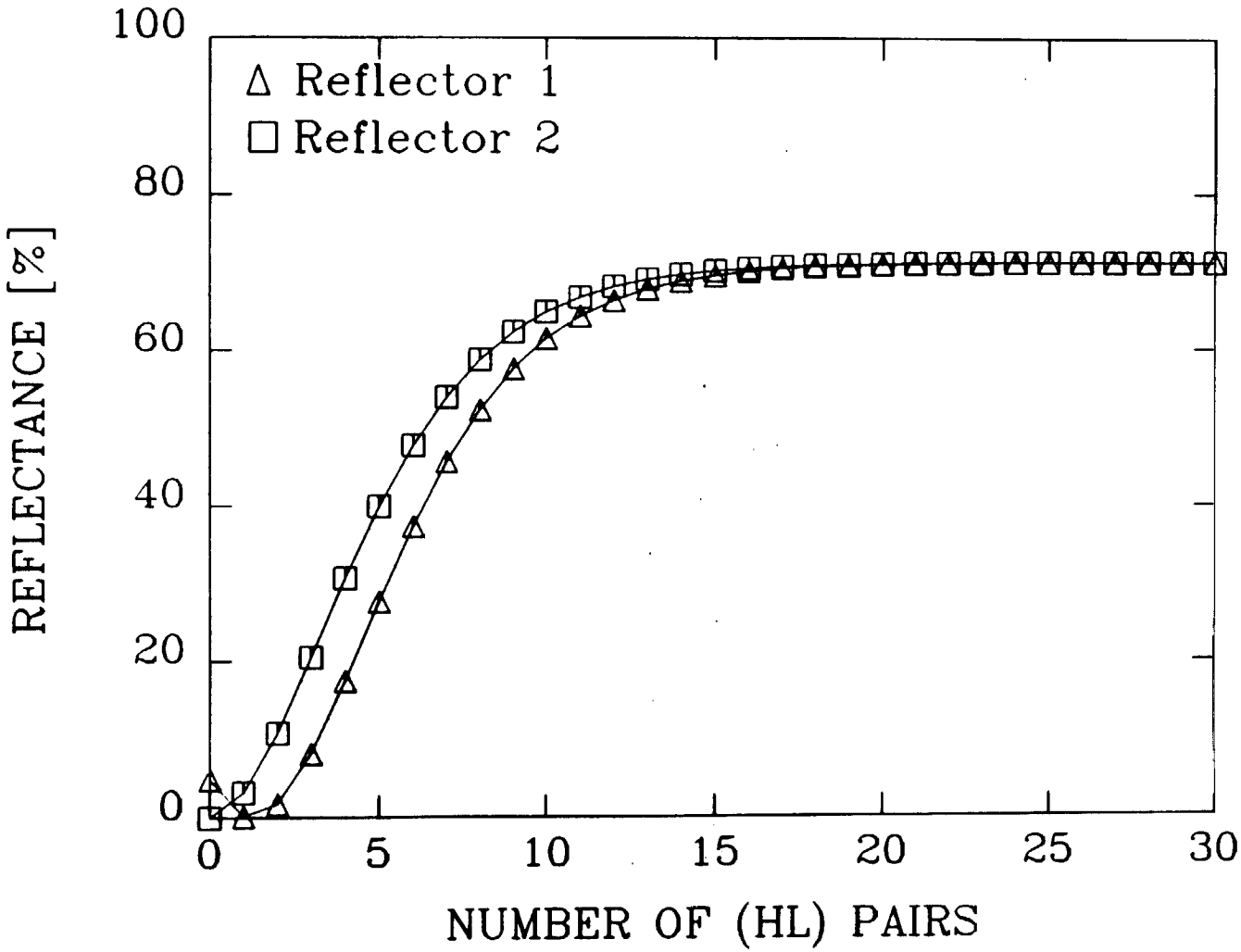

Zukic/Torr Figure 7.17a

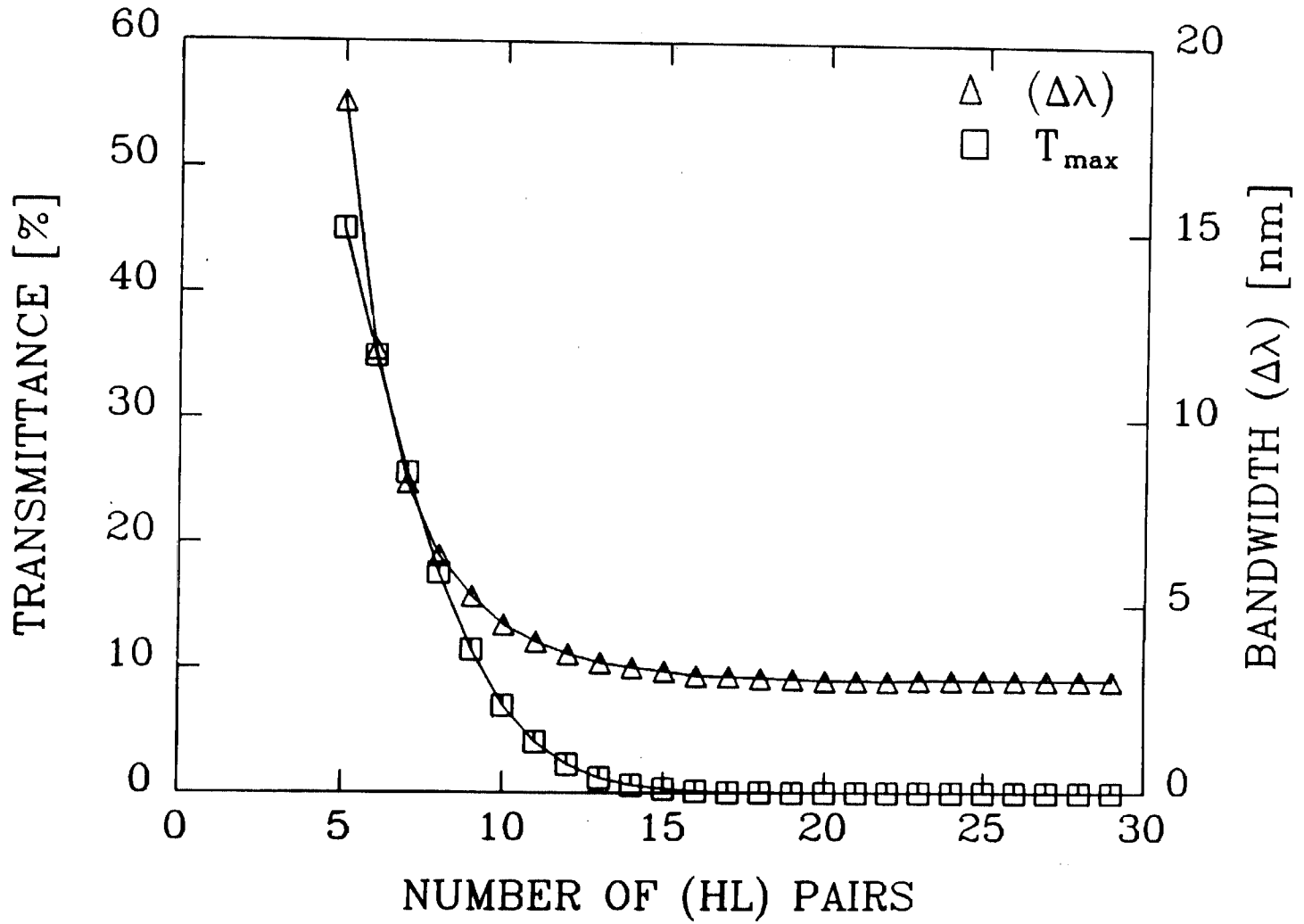

Zukic/Torr Figure 7.17b

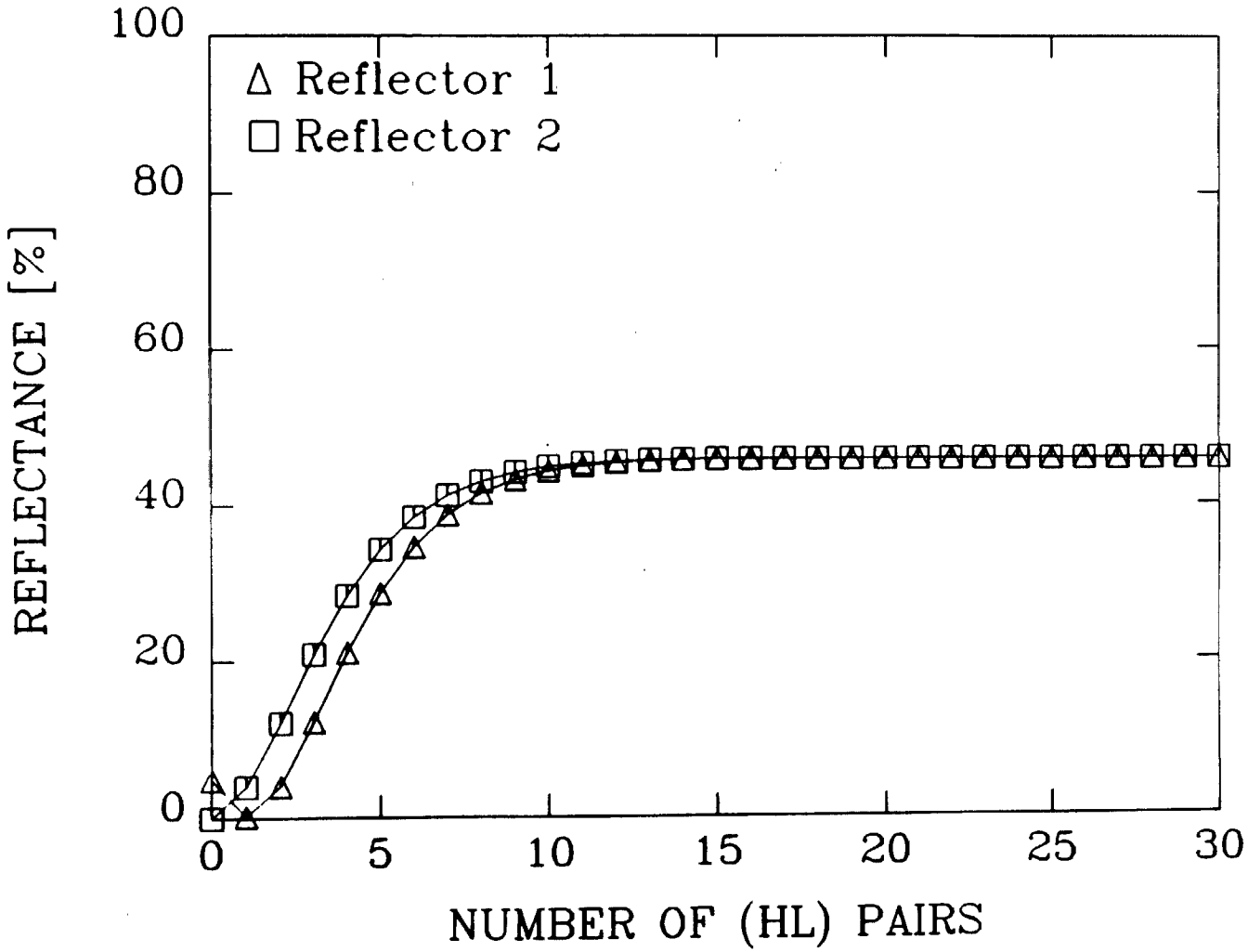

Zukic/Torr Figure 7.18a

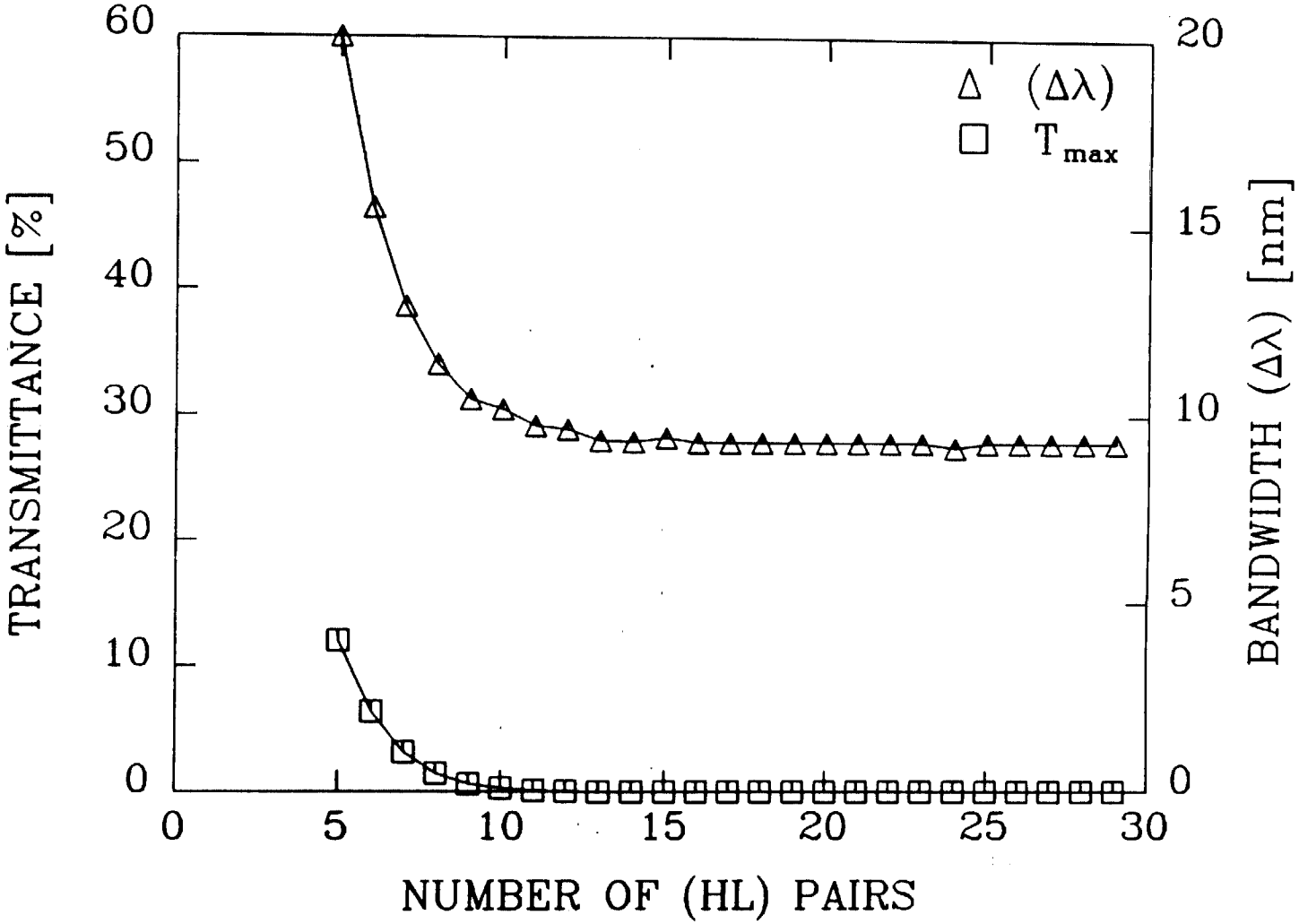

Zukic/Torr **Figure 7.18b**

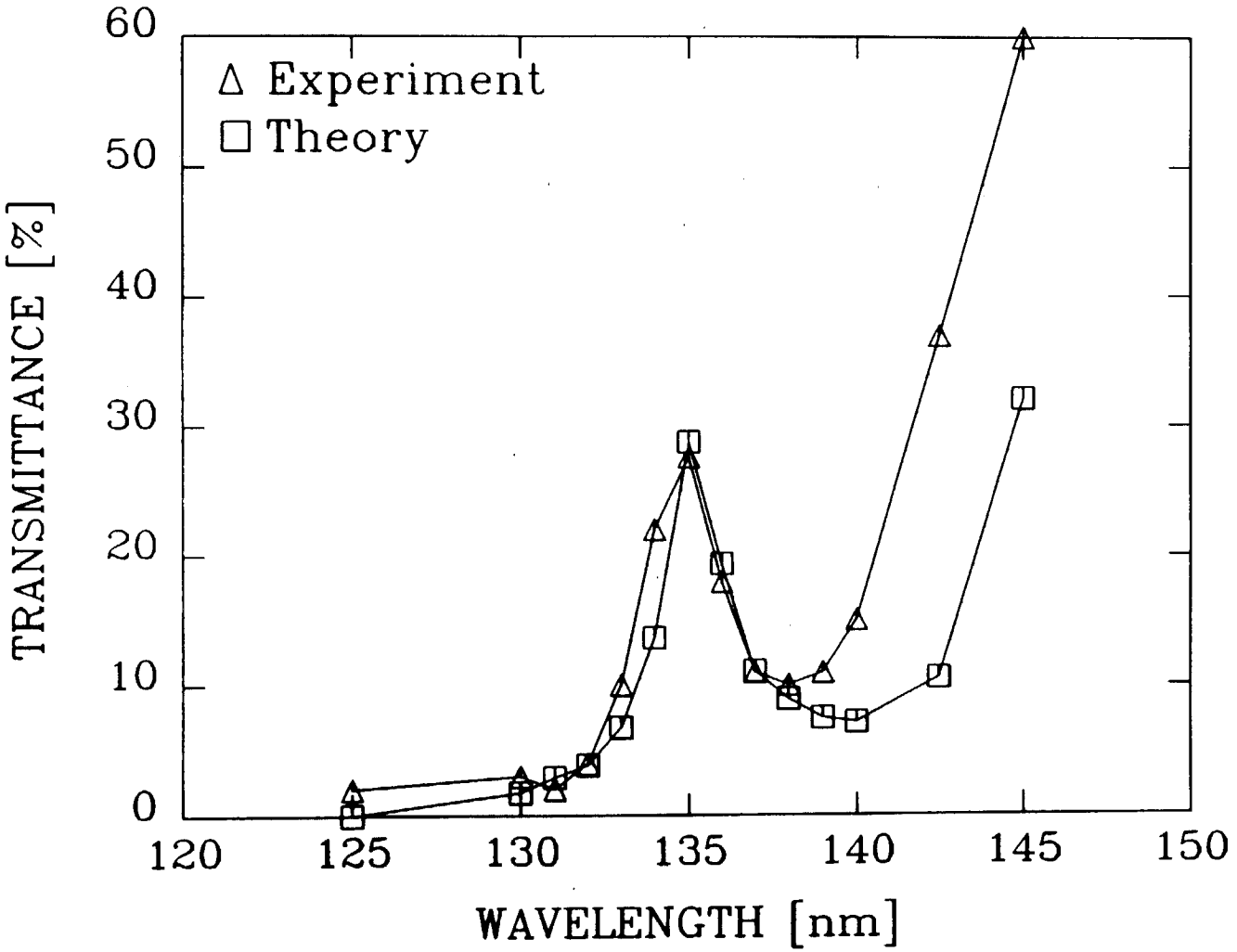

Zukic/**Torr Figure 7.19**

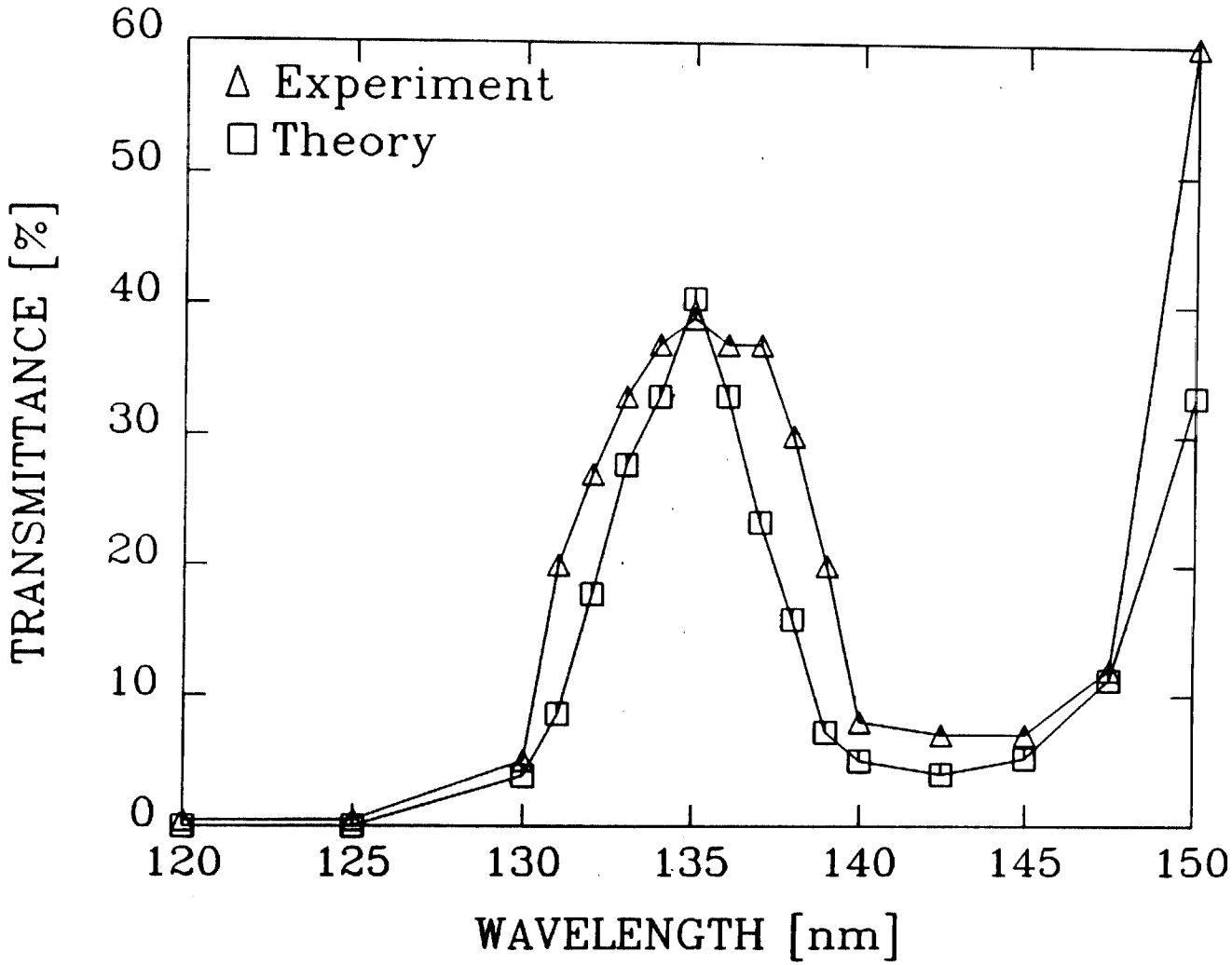

Zukic/**Torr Figure** 7.20

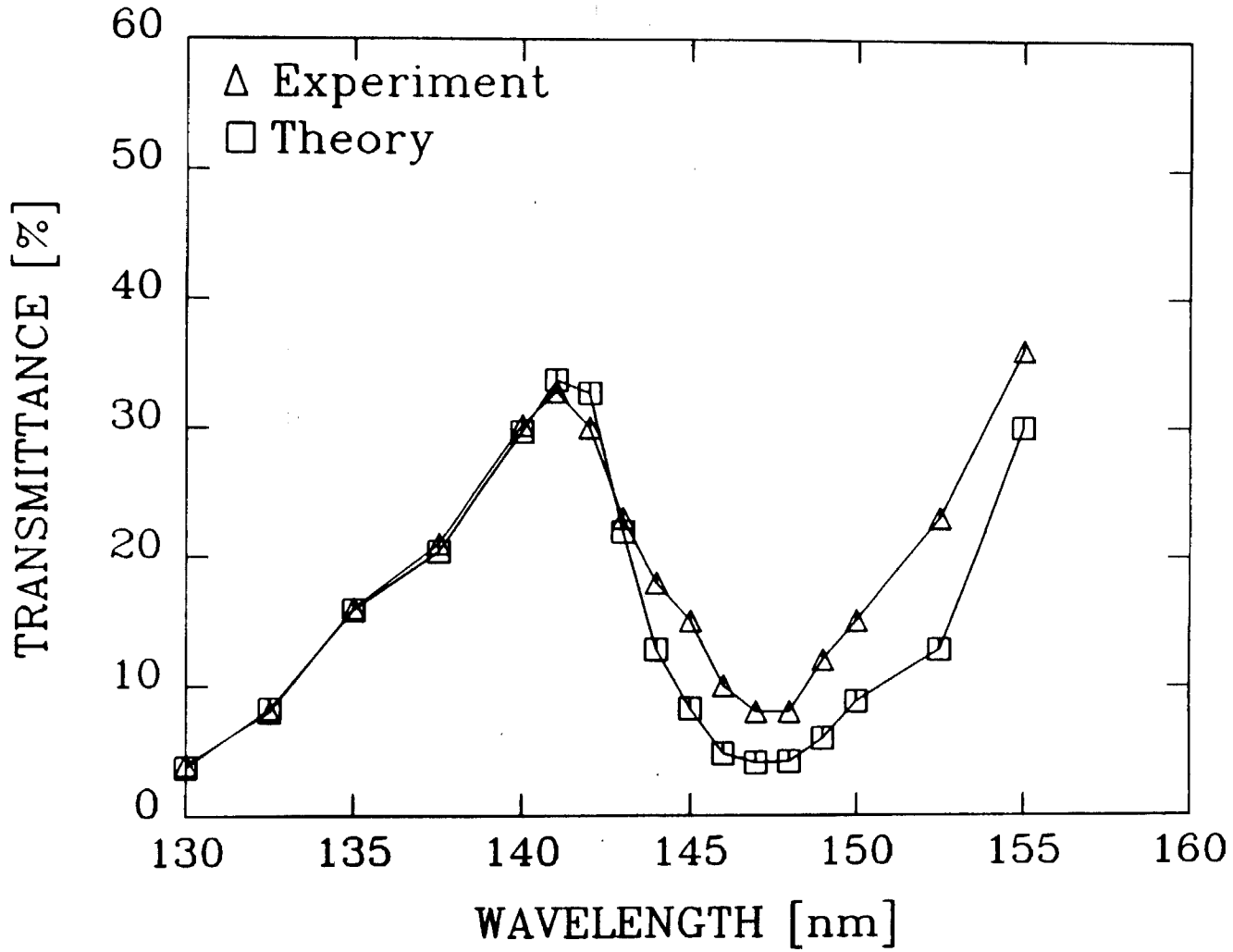

Zukic/**Torr Figure** 7.21

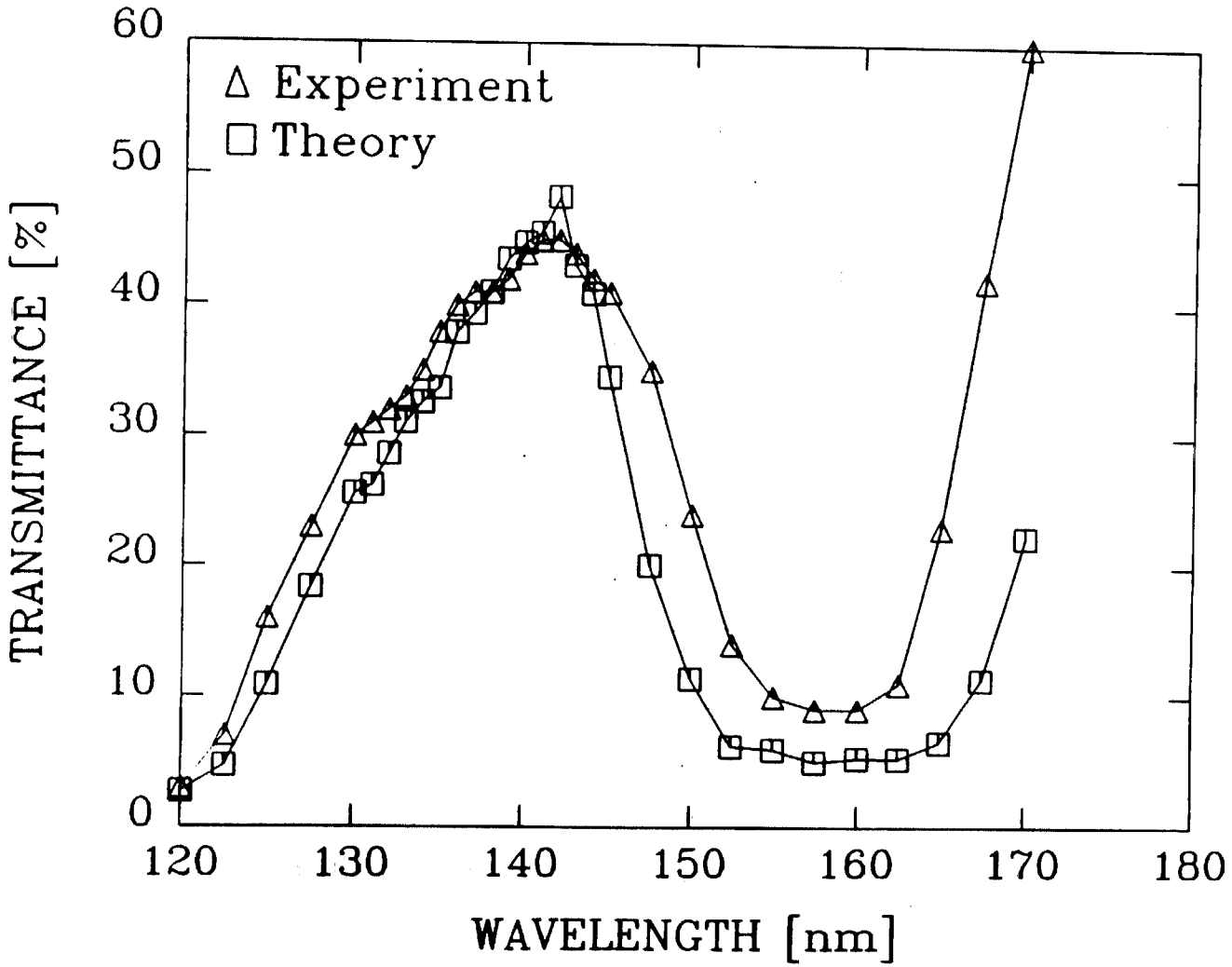

Zukic/**Torr Figure 7.22**

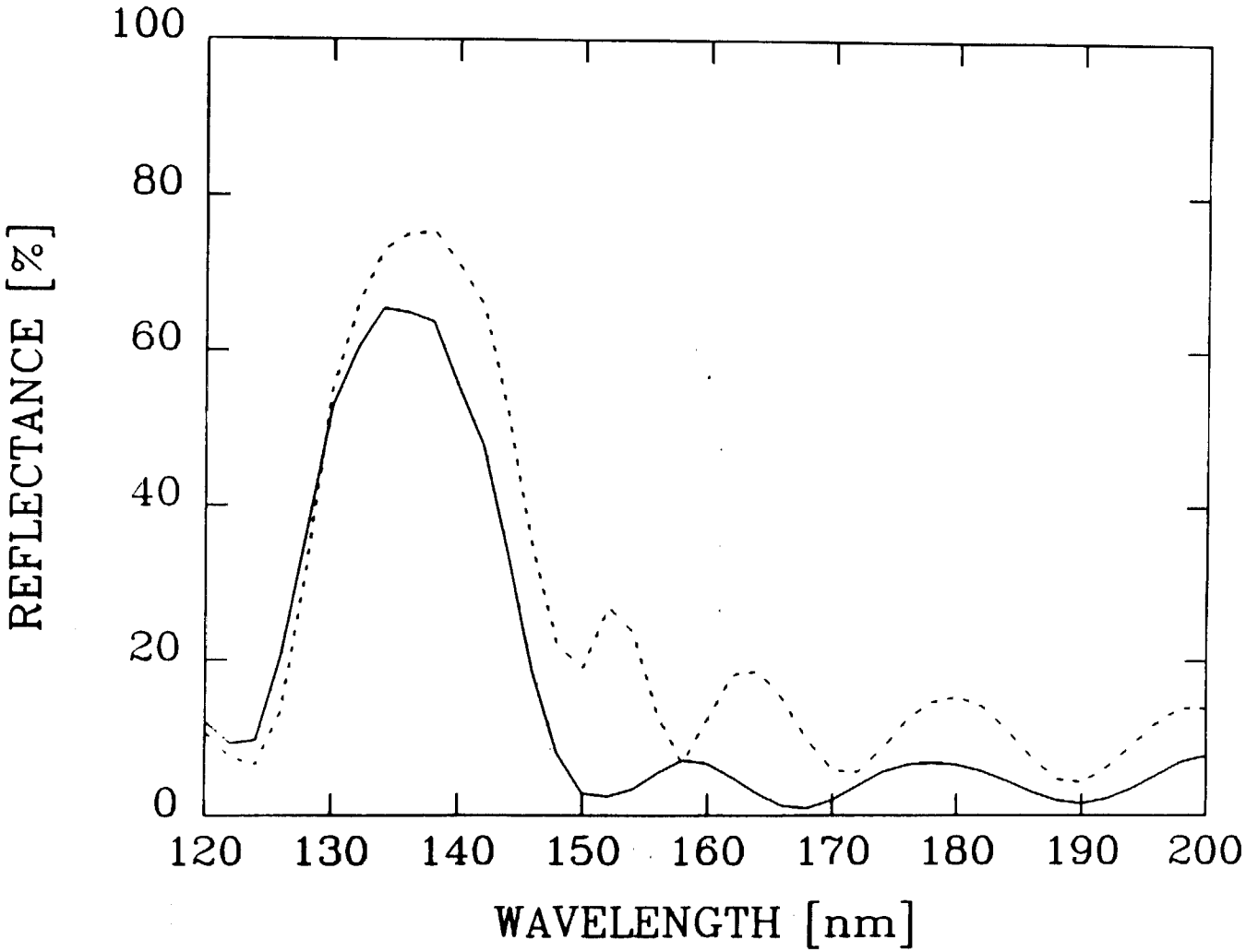

Zukic/**Torr Figure** 7.23

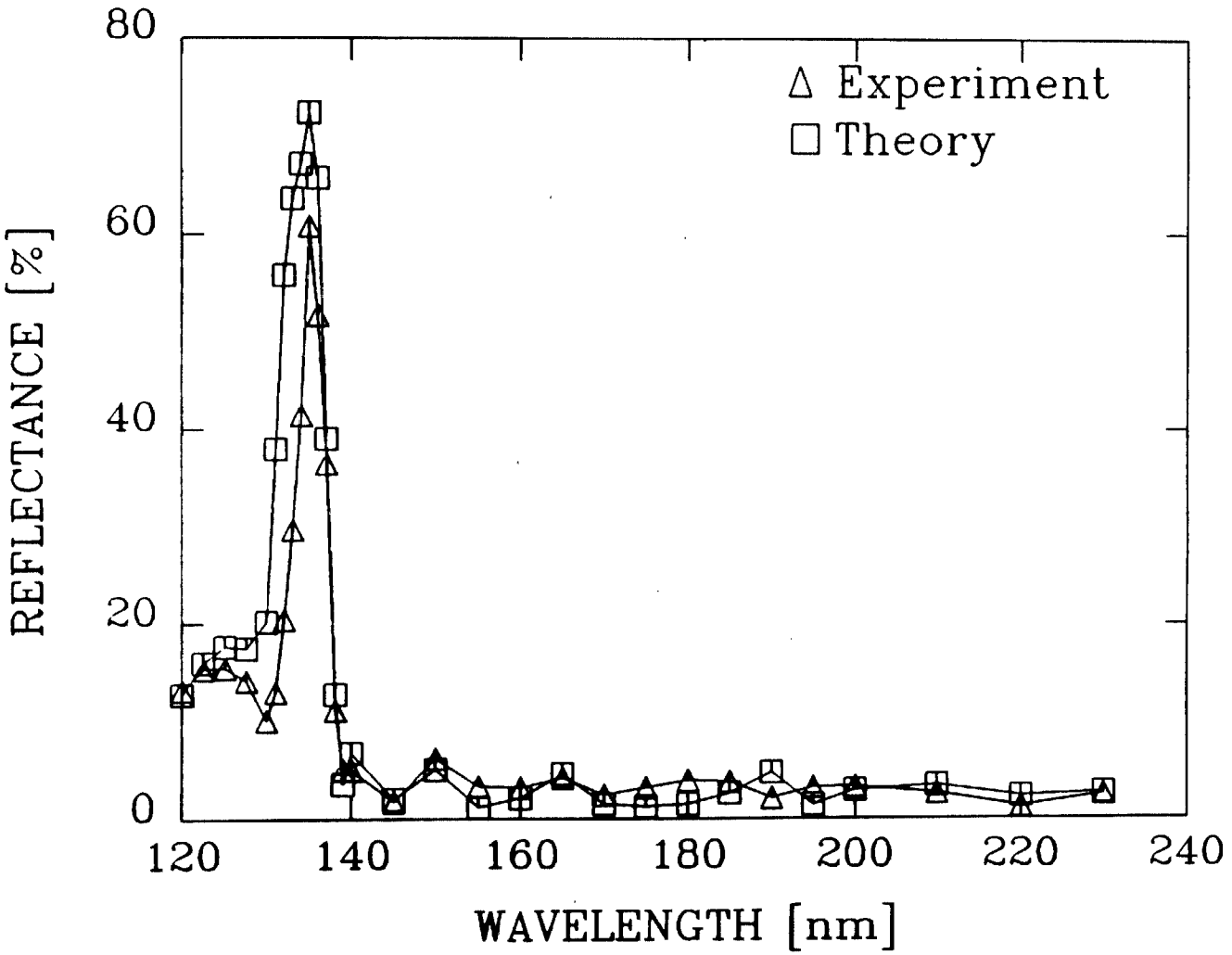

Zukic/**Torr Figure 7.24**

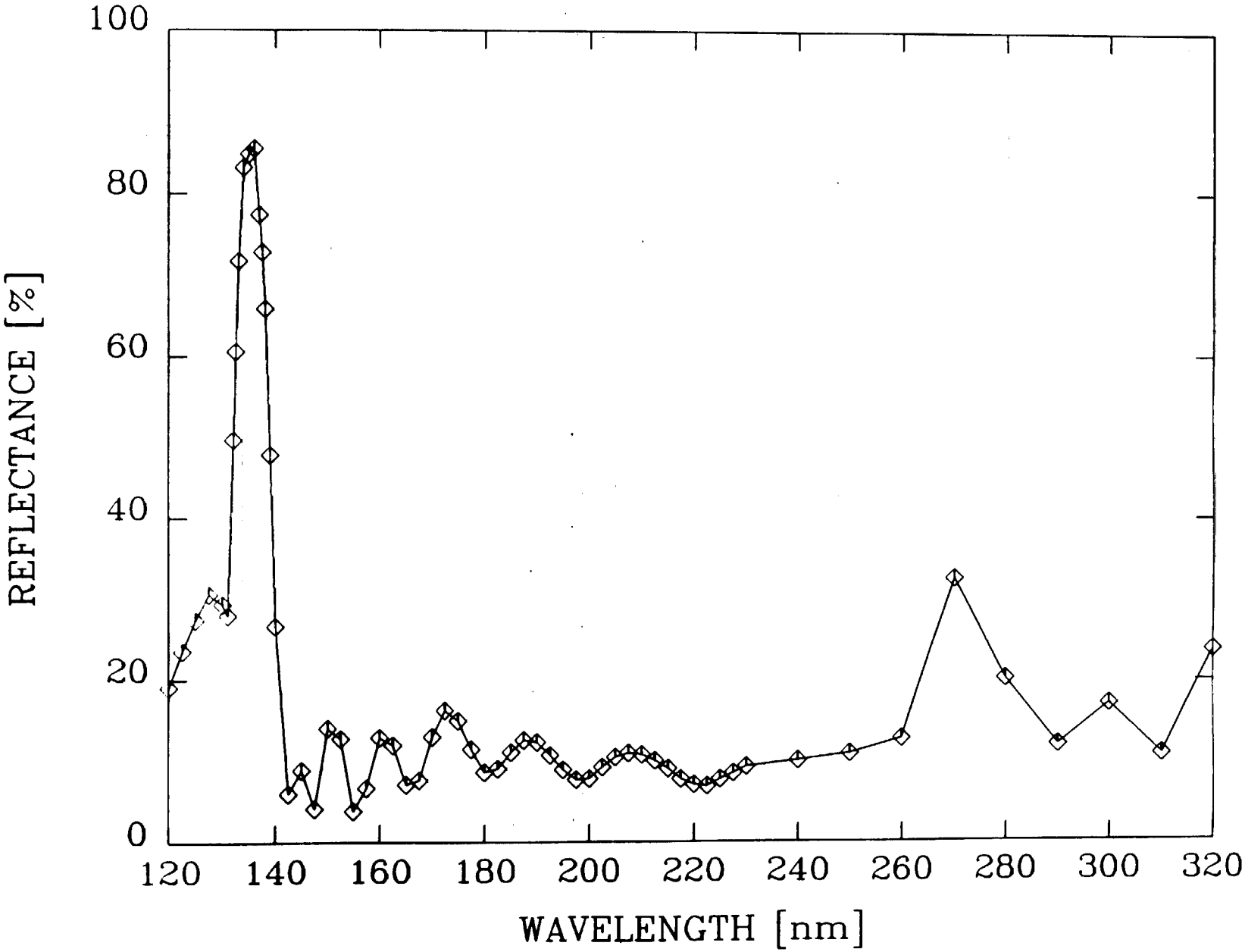

Zukic/Torr Figure 7.25

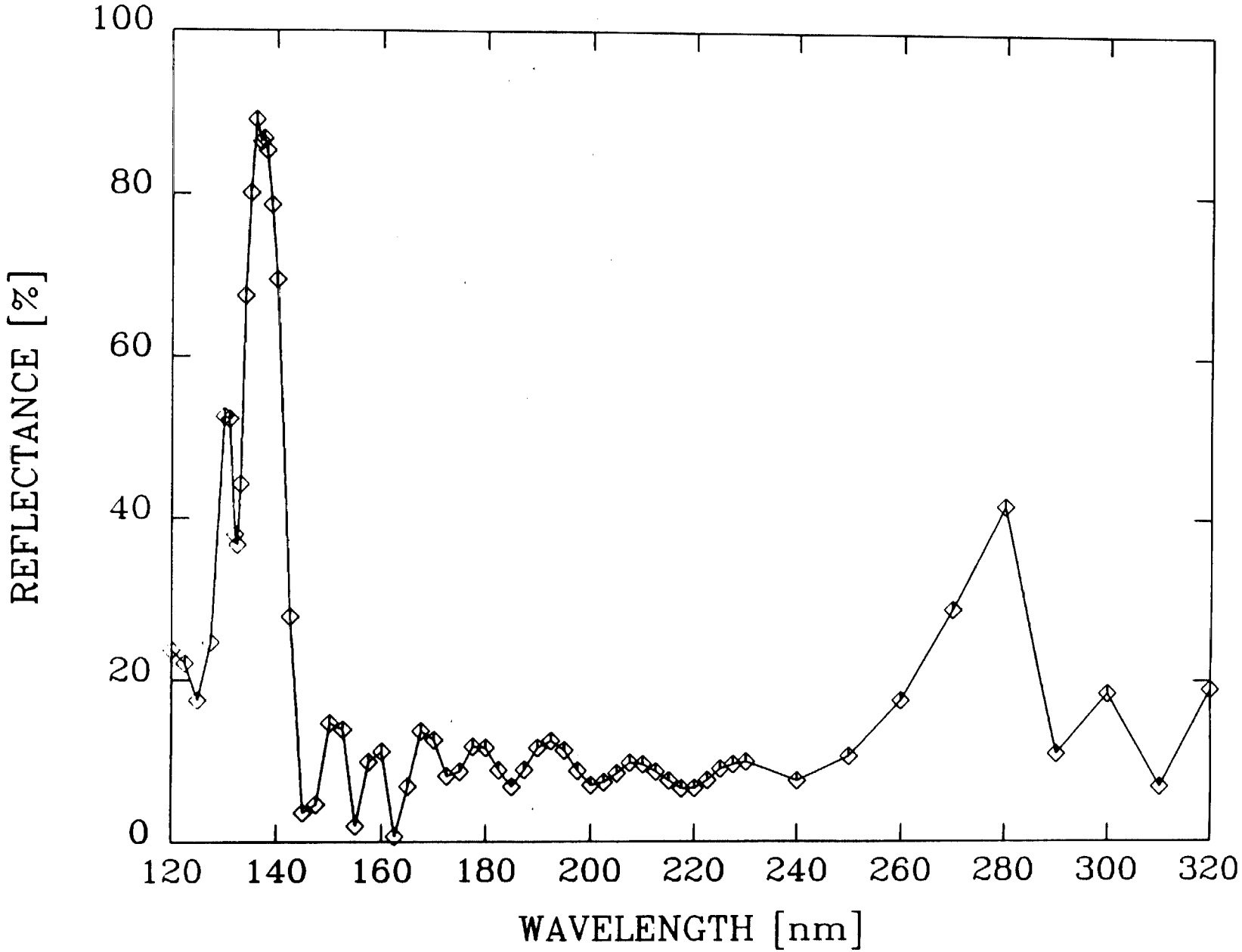

Zukic/Torr Figure 7.26

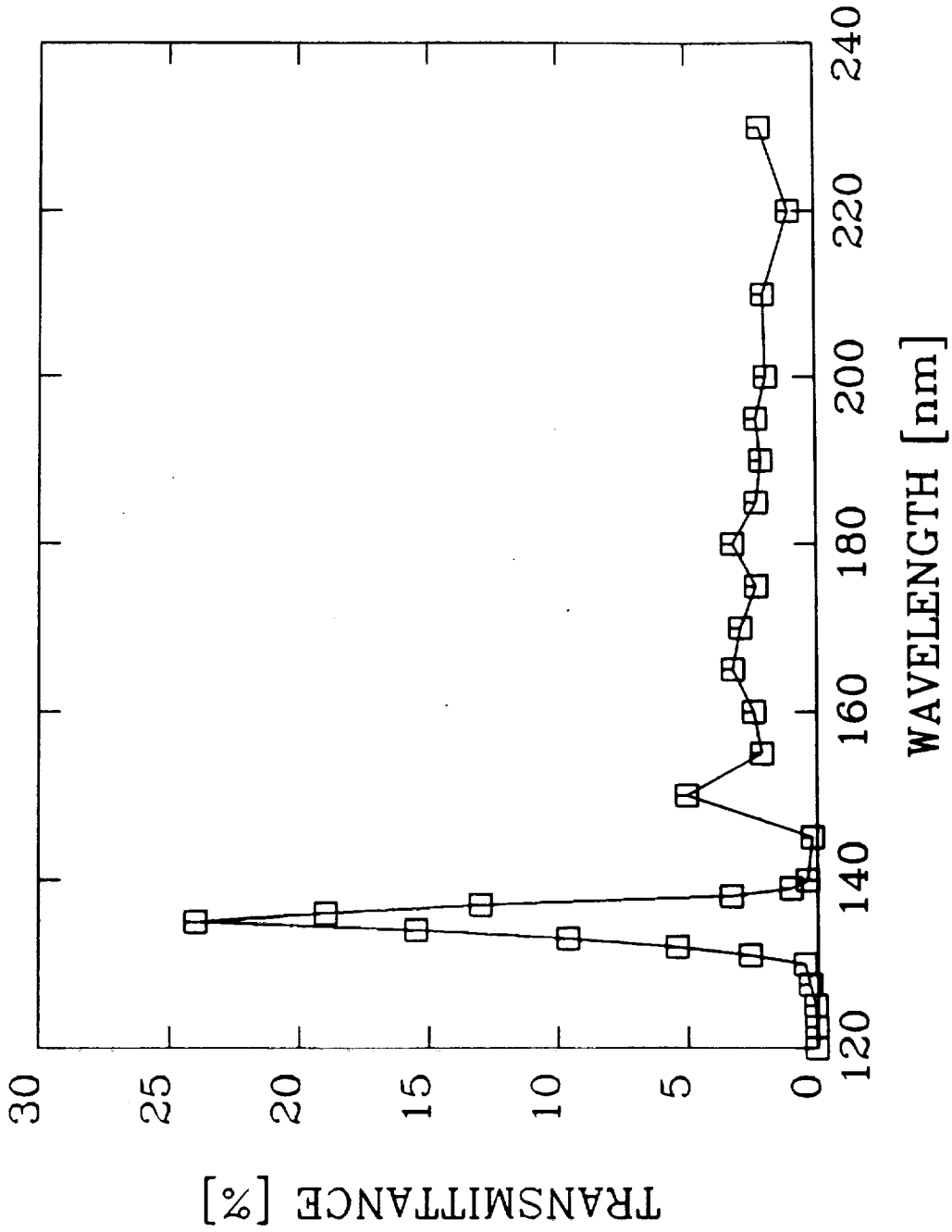

Zukic/Torr Figure 7.27

C-2

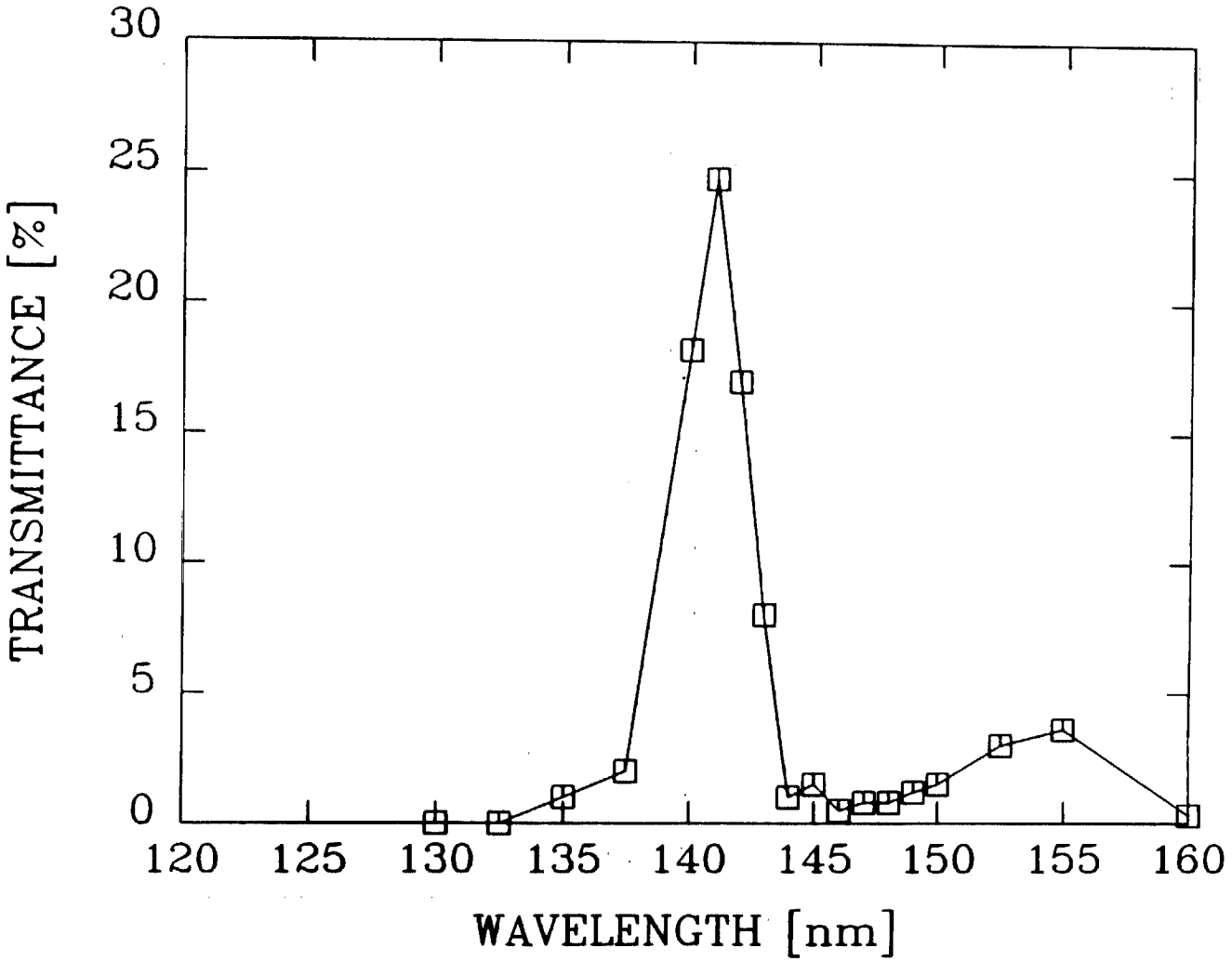

Zukic/**Torr Figure 7.28**

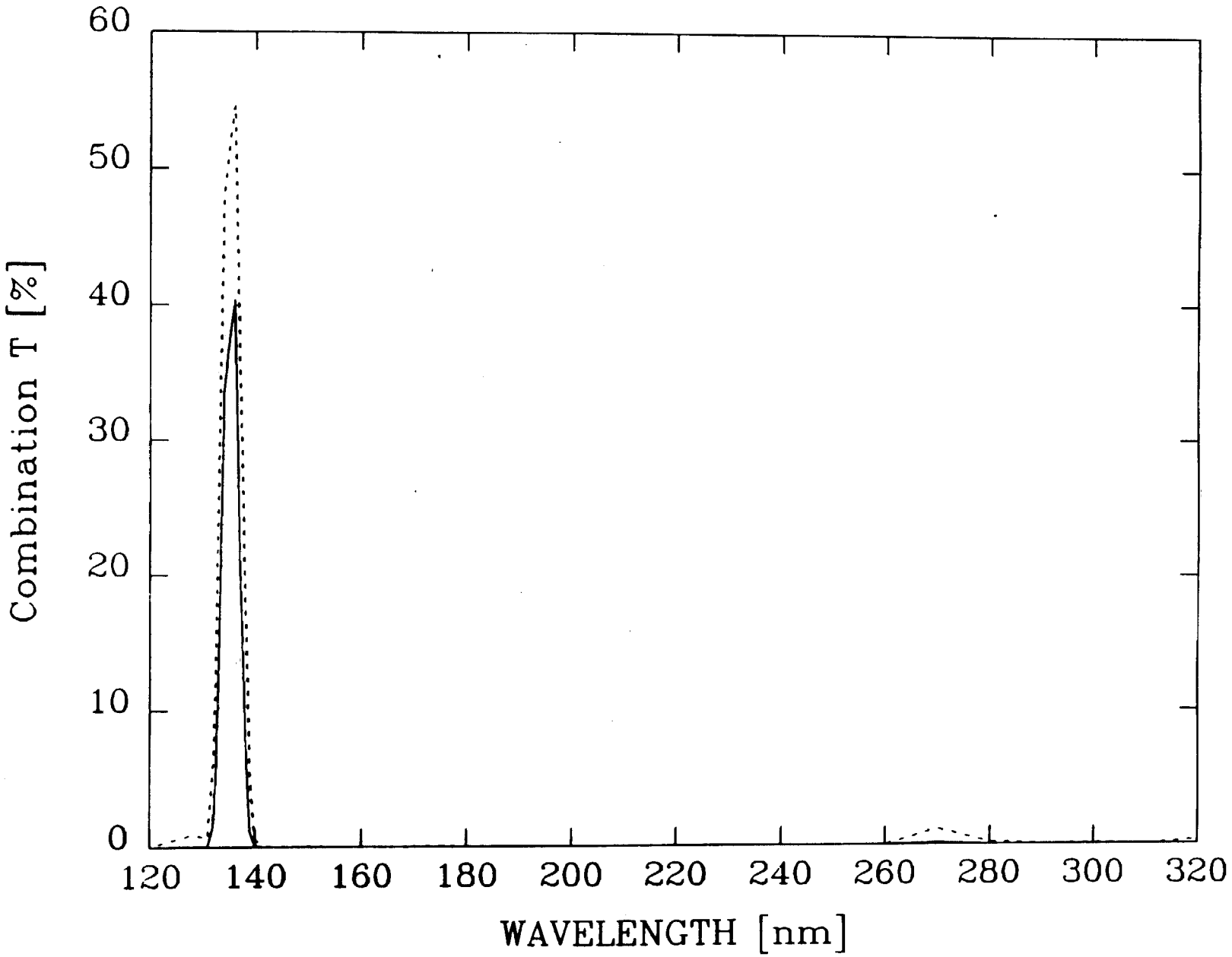

Zukic/Torr Figure 7.29

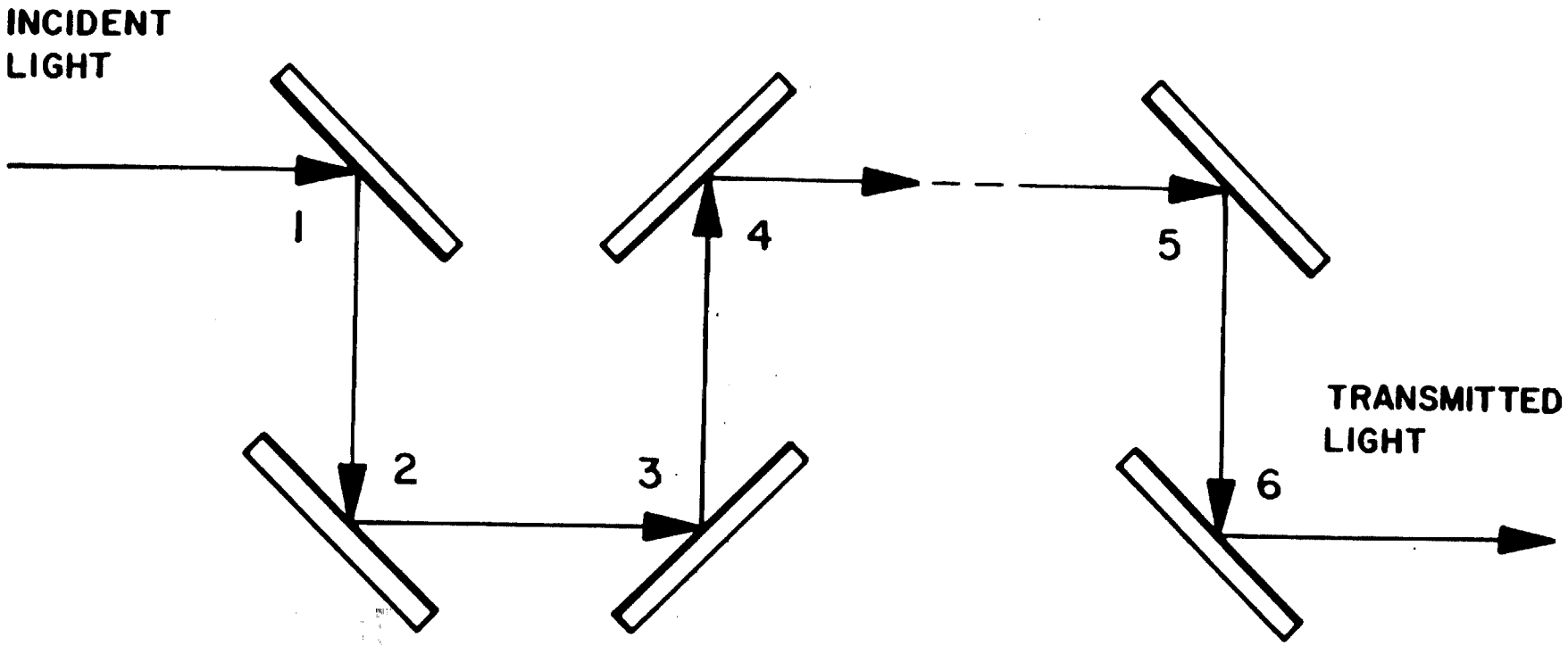

Zukic/Torr Figure 7.30

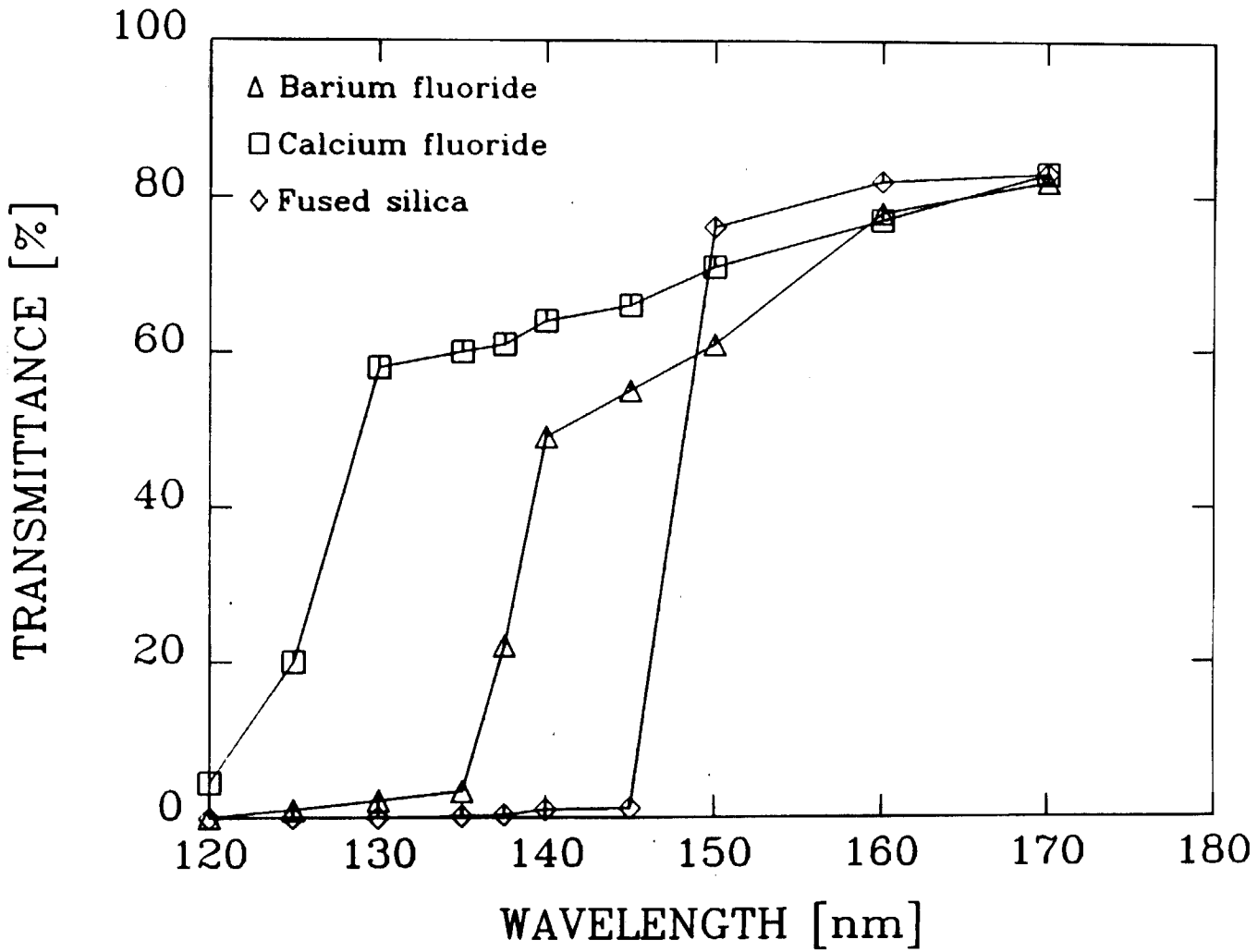

Zukic/Torr **Figure** 7.31

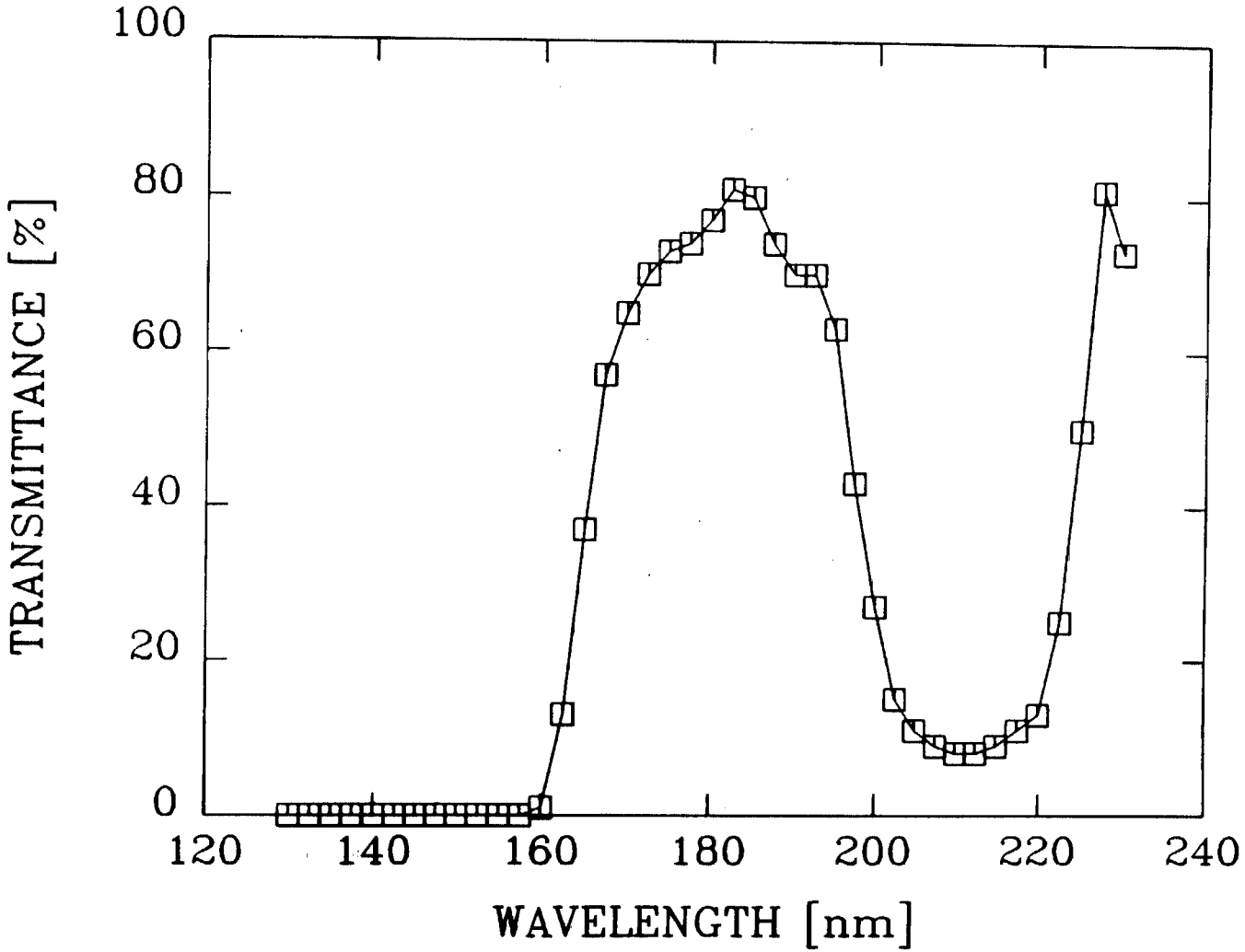

Zukic/**Torr Figure 7.32**

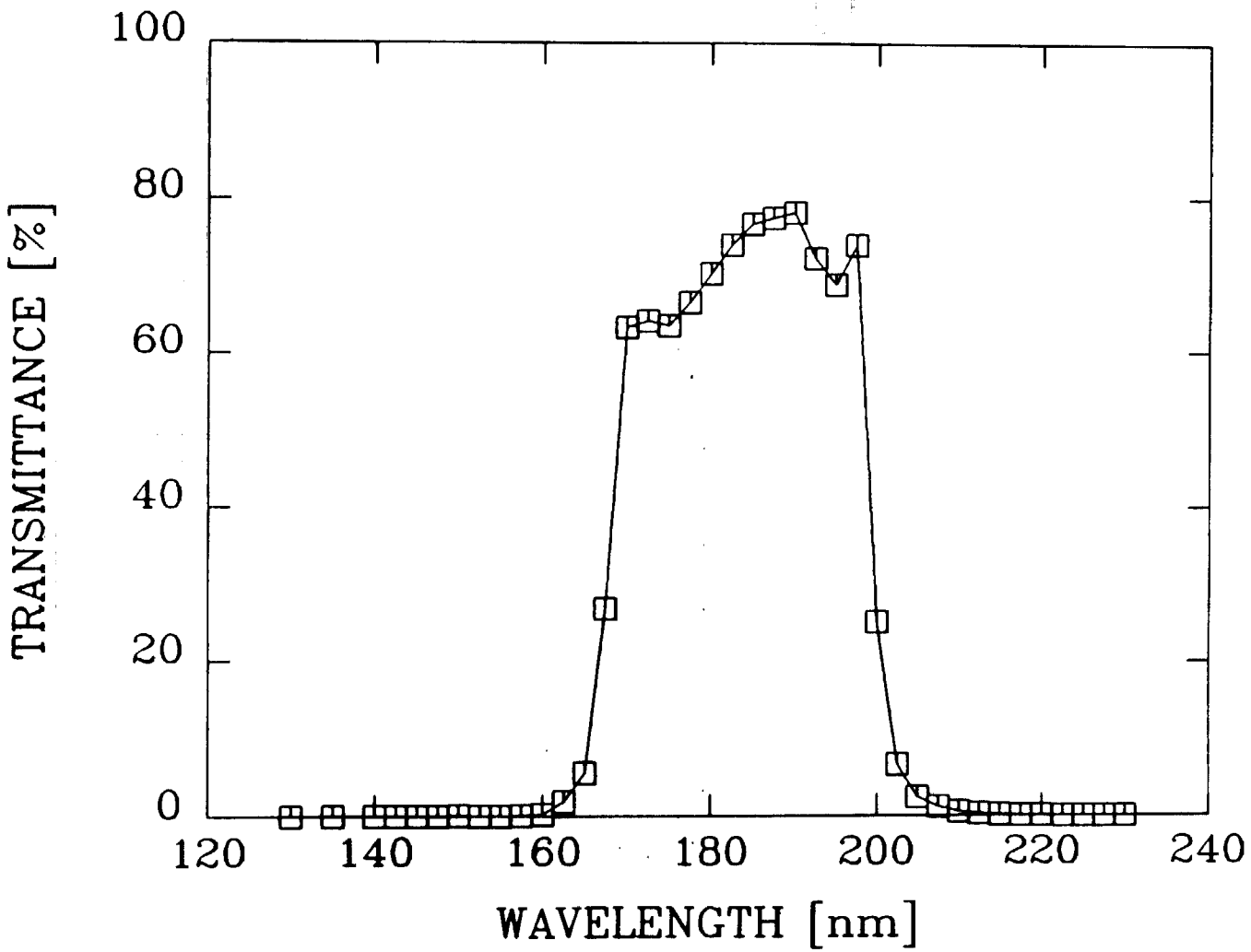

Zukic/**Torr Figure** 7.33

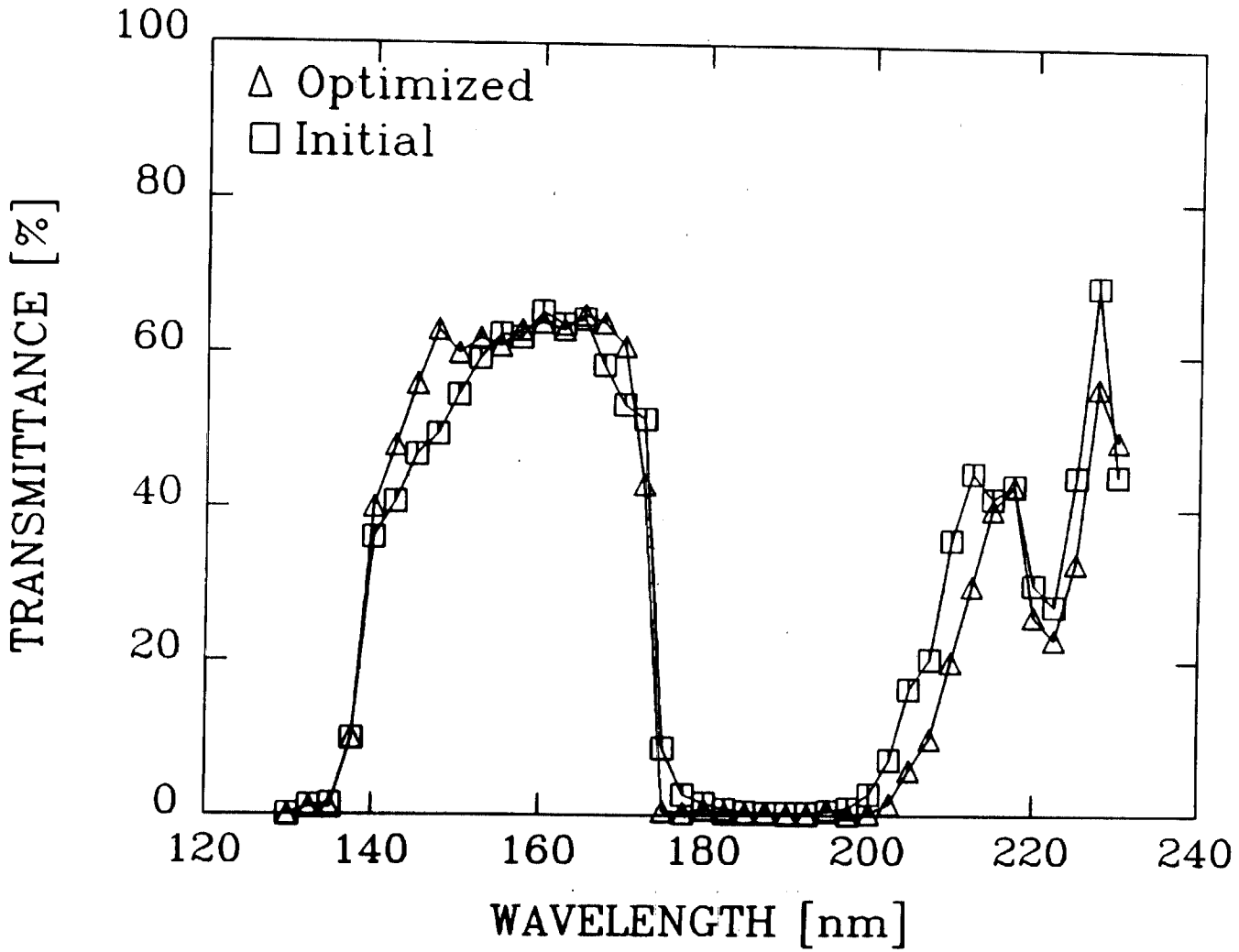

Zukic/**Torr Figure 7.34**

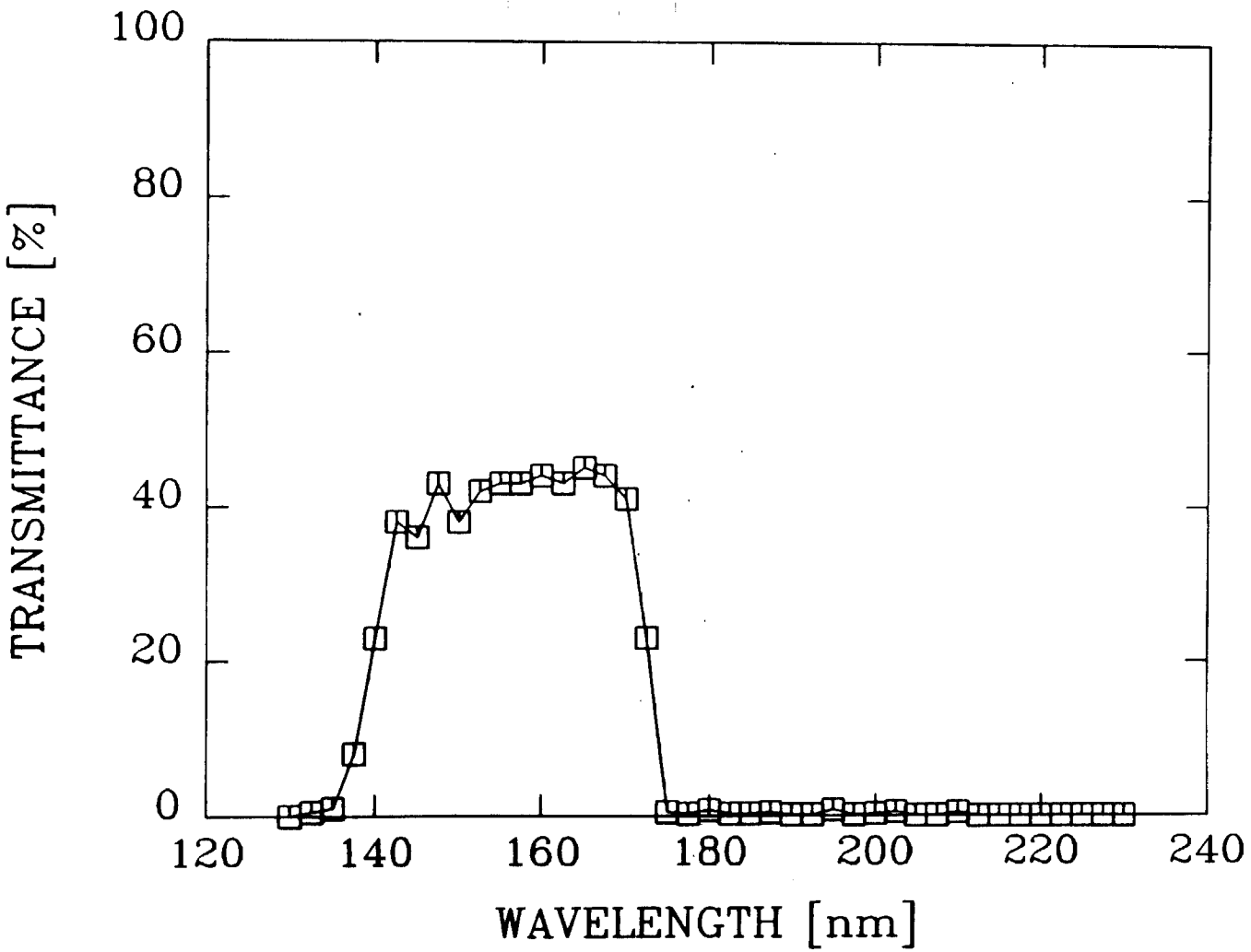

Zukic/**Torr Figure 7.35**

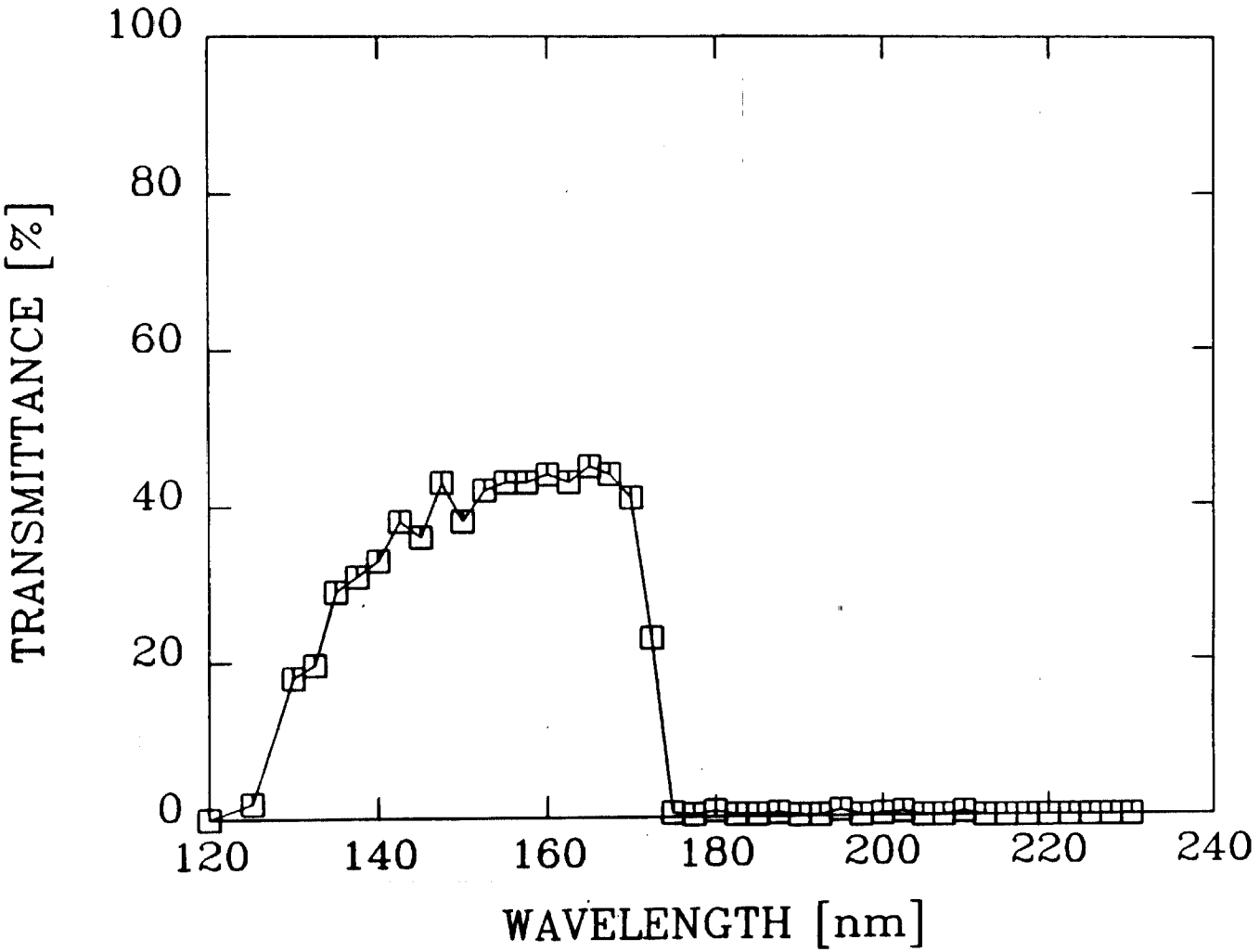

Zukic/Torr Figure 7.36

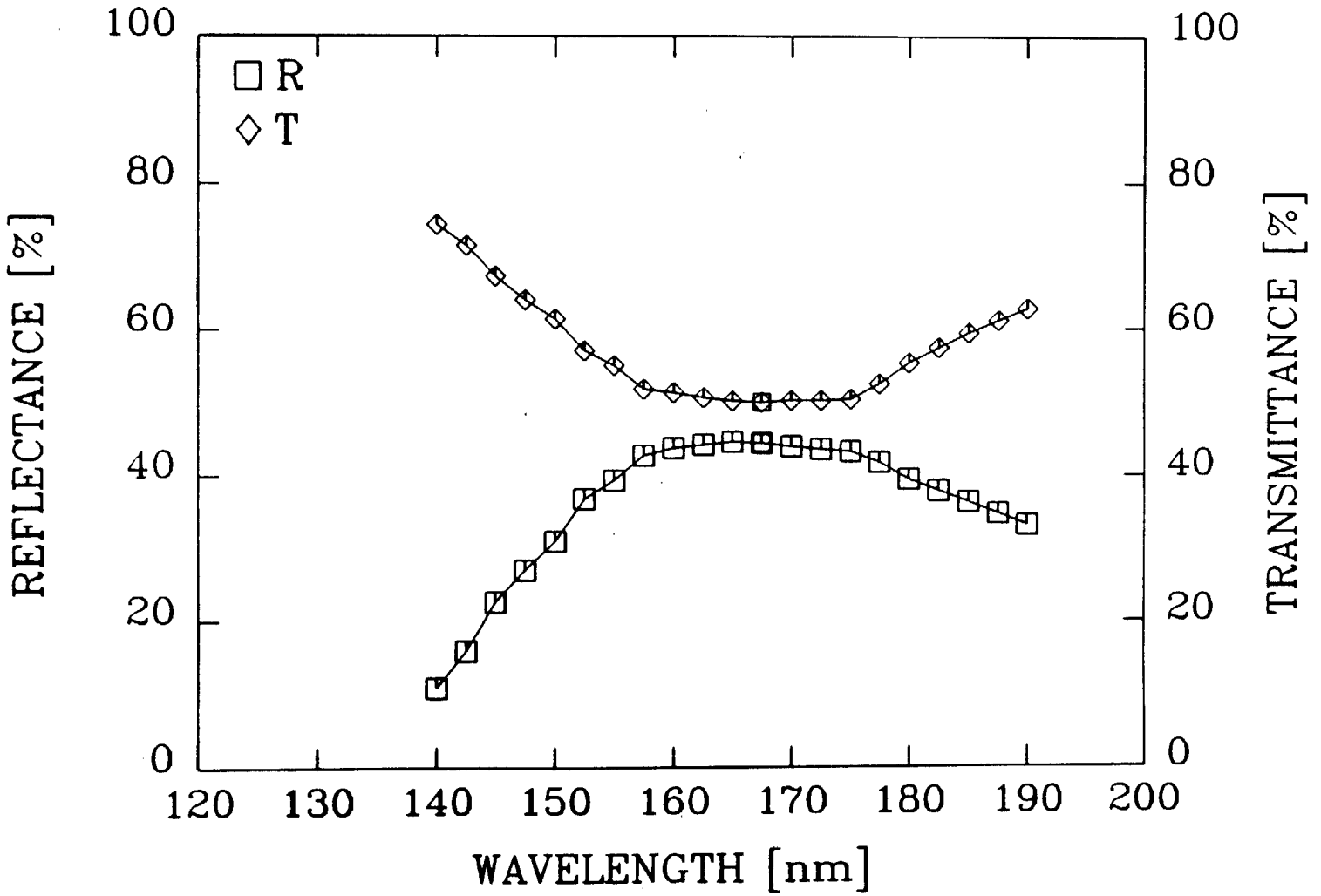

Zukic/Torr Figure 7.37

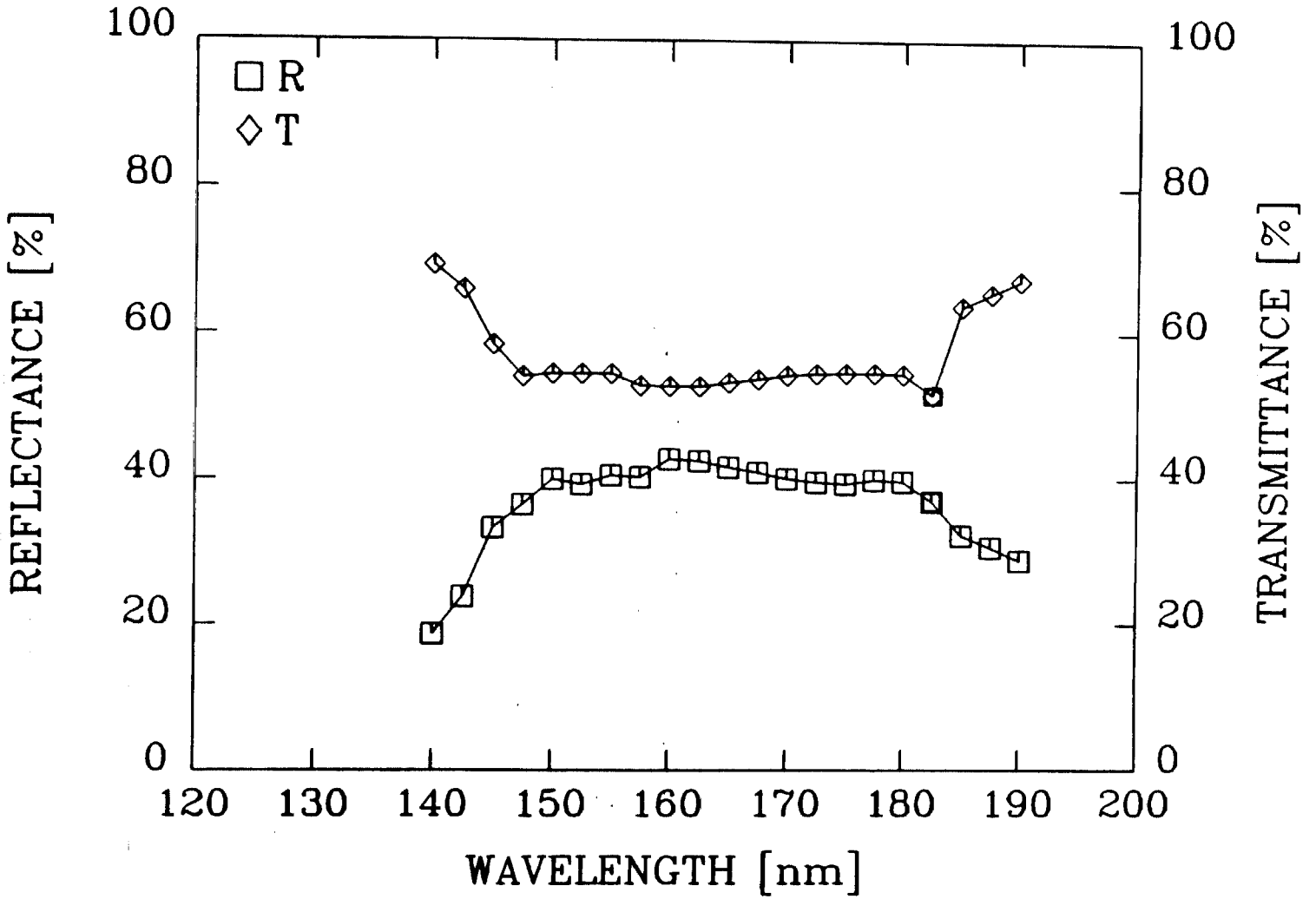

Zukic/**Torr Figure 7.38**

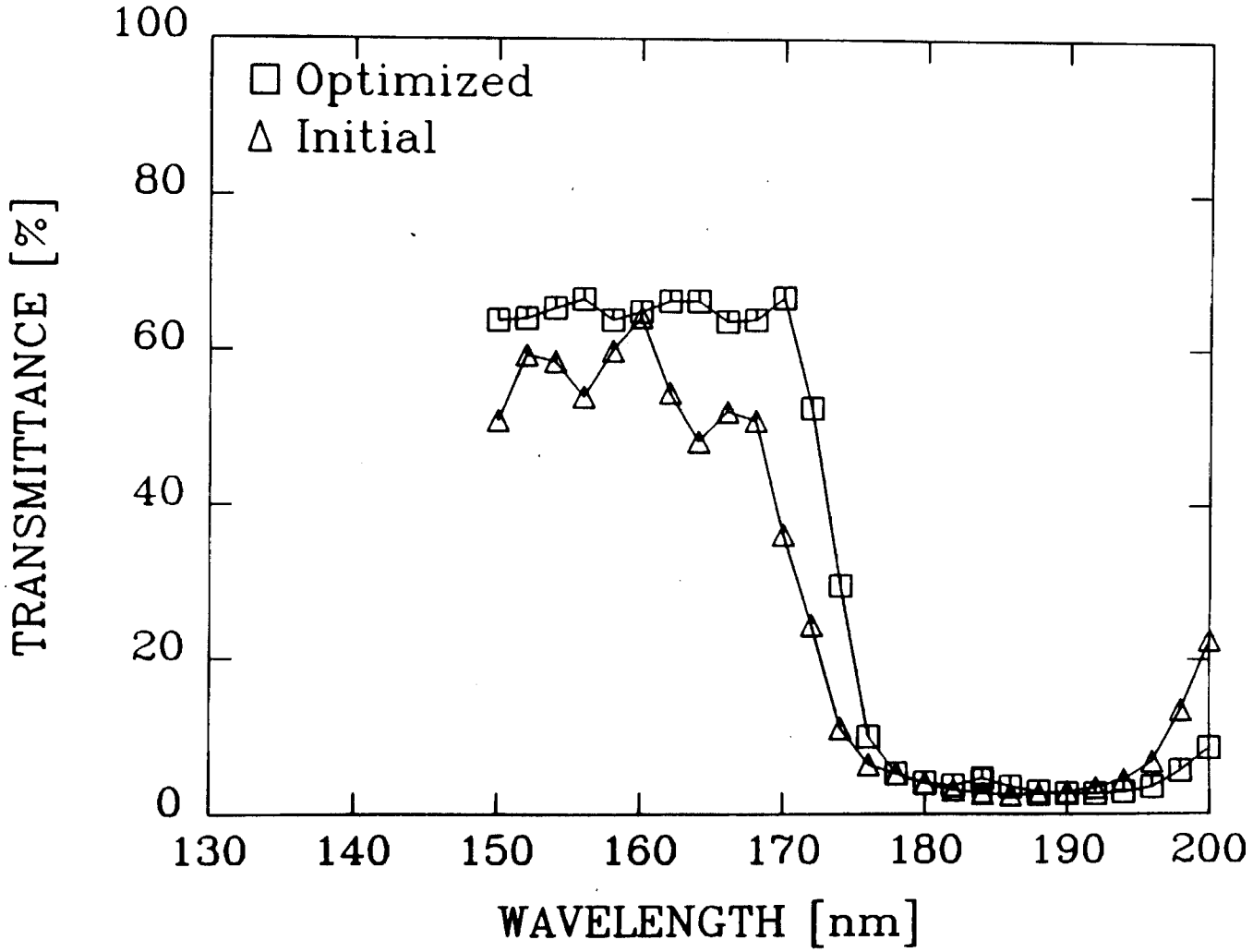

Zukic/Torr Figure 7.39

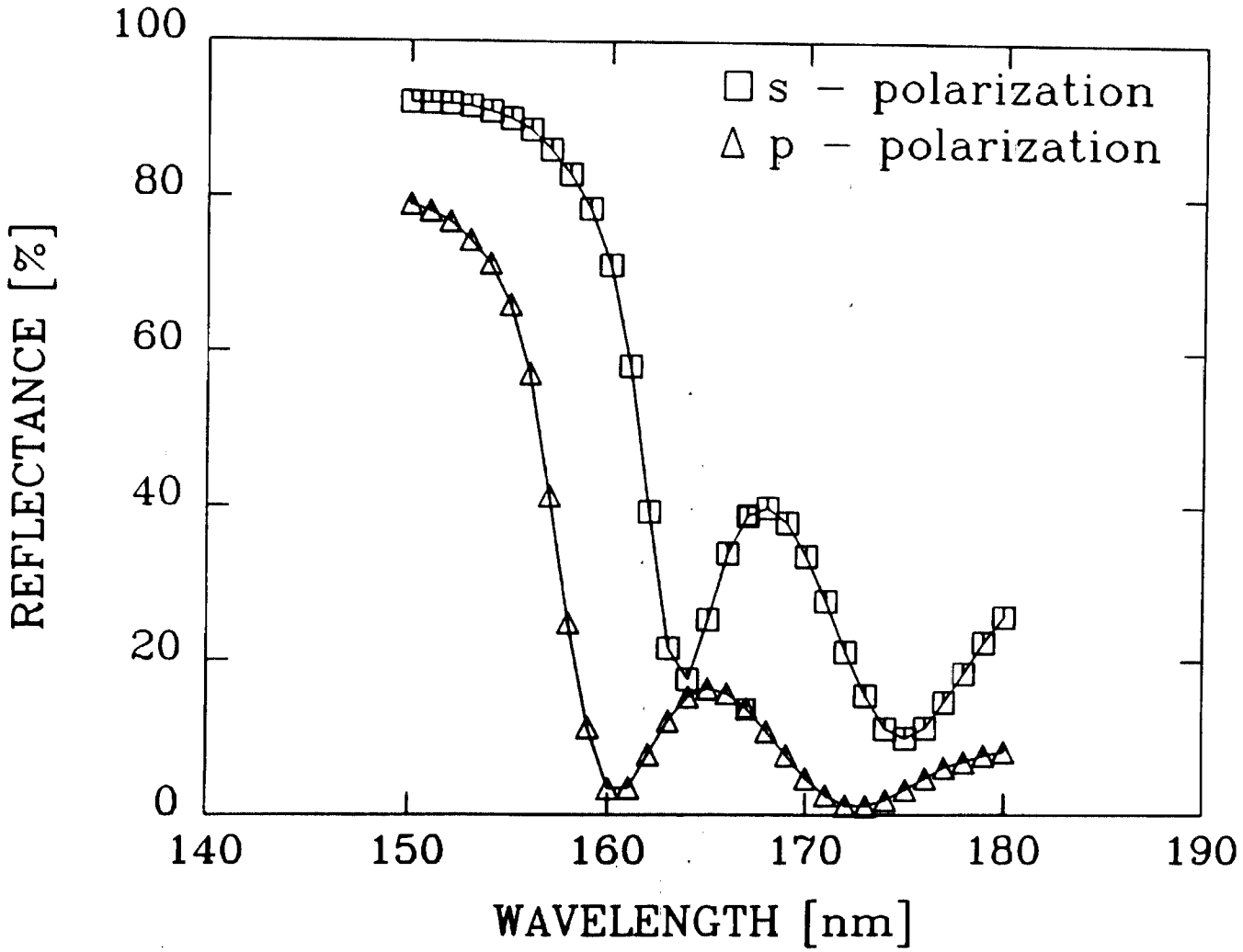

Zukic/**Torr Figure 7.40**

Table 7.3 Dichroic Beamsplitter

	Physical Thickness [nm]	
Material	Initial Design	Final Design
Air		
LaF_3	27.0	27.4
MgF_2	35.0	34.8
LaF_3	27.0	27.4
MgF_2	35.0	34.6
LaF_3	27.0	27.9
MgF_2	35.0	35.1
LaF_3	27.0	29.3
MgF_2	35.0	36.0
LaF_3	27.0	28.7
MgF_2	35.0	34.9
LaF_3	27.0	27.4
MgF_2	35.0	34.4
LaF_3	27.0	27.2
MgF_2	35.0	34.6
LaF_3	27.0	27.7
MgF_2	35.0	35.5
LaF_3	27.0	28.1
MgF_2	35.0	35.3
LaF_3	27.0	27.5
MgF_2	35.0	34.2
LaF_3	27.0	27.3
MgF_2	35.0	35.2
LaF_3	27.0	31.3
MgF_2	35.0	38.4
LaF_3	27.0	28.9
Substrate		

Figure Captions

Figure 7.1a Beam diagram for the theoretical derivation of the transmittance of a non-absorbing thick slab

Figure 7.1b Beam diagram for the theoretical derivation of the transmittance T_0^F of a single film deposited on a non-absorbing substrate

Figure 7.2 Schematic diagram of the single beam VUV spectrophotometer

Figure 7.3a The reflectance R_1 and transmittance T_M measurements on a MgF_2 wedged and a 2 mm thick parallel substrates, respectively

Figure 7.3b Optical constants of a MgF_2 substrate

Figure 7.4a The reflectance R_1^F and transmittance T_M^F of a 53 nm thick BaF_2 film deposited on a MgF_2 substrate

Figure 7.4b Optical constants of BaF_2 determined from R and T measurements of 53 nm, 45 nm, and 94.5 nm thick films deposited on MgF_2 substrates

Figure 7.5a The reflectance R_1^F and transmittance T_M^F of a 99 nm thick CaF_2 film deposited on a MgF_2 substrate

Figure 7.5b Optical constants of CaF_2 determined from R and T measurements of 99 nm, and 54.5 nm thick films deposited on MgF_2 substrates

Figure 7.6a The reflectance R_1^F and transmittance T_M^F of a 51 nm thick LaF_3 film deposited on a MgF_2 substrate

Figure 7.6b Optical constants of LaF_3 determined from R and T measurements of 51 nm, 68 nm, and 83 nm thick films deposited on MgF_2 substrates

Figure 7.7a The reflectance R_1^F and transmittance T_M^F of a 68 nm thick MgF_2 film deposited on a MgF_2 substrate

Figure 7.7b Optical constants of MgF_2 determined from R and T measurements of 68 nm, and 109 nm thick films deposited on MgF_2 substrates

Figure 7.15 The calculated reflectances for first, second, and third order TW multilayer stacks

Figure 7.16a The reflectances of the partial reflectors of the Fabry-Perot-type filter as functions of the number of (HL) pairs. H = Barium fluoride and L = Magnesium fluoride

Figure 7.16b The maximum transmittance and bandwidth of the Fabry-Perot type filter calculated using Equations (7.86, 91), respectively. H = Barium fluoride and L = Magnesium fluoride

Figure 7.17a The reflectances of the partial reflectors of the Fabry-Perot-type filter as functions of the number of (HL) pairs. H = Lanthanum fluoride and L = Magnesium fluoride

Figure 7.17b The maximum transmittance and bandwidth of the Fabry-Perot type filter calculated using Equations (7.86, 91), respectively. H = Lanthanum fluoride and L = Magnesium fluoride

Figure 7.18a The reflectances of the partial reflectors of the Fabry-Perot-type filter as functions of the number of (HL) pairs. H = Silicon dioxide and L = Magnesium fluoride

Figure 7.18b The maximum transmittance and bandwidth of the Fabry-Perot-type filter calculated using Equations (7.86, 91), respectively. H = Silicon dioxide and L = Magnesium fluoride

Figure 7.19 The 25-layer Fabry-Perot-type filter with H = Barium fluoride and L = Magnesium fluoride

Figure 7.20 The 25-layer QW tuned filter with the high reflectance zone centered at 140 nm. H = Barium fluoride and L = Magnesium fluoride

Figure 7.21 The 25-layer TW tuned filter with the high reflectance zone centered at 147.5 nm. H = Silicon dioxide and L = Magnesium fluoride

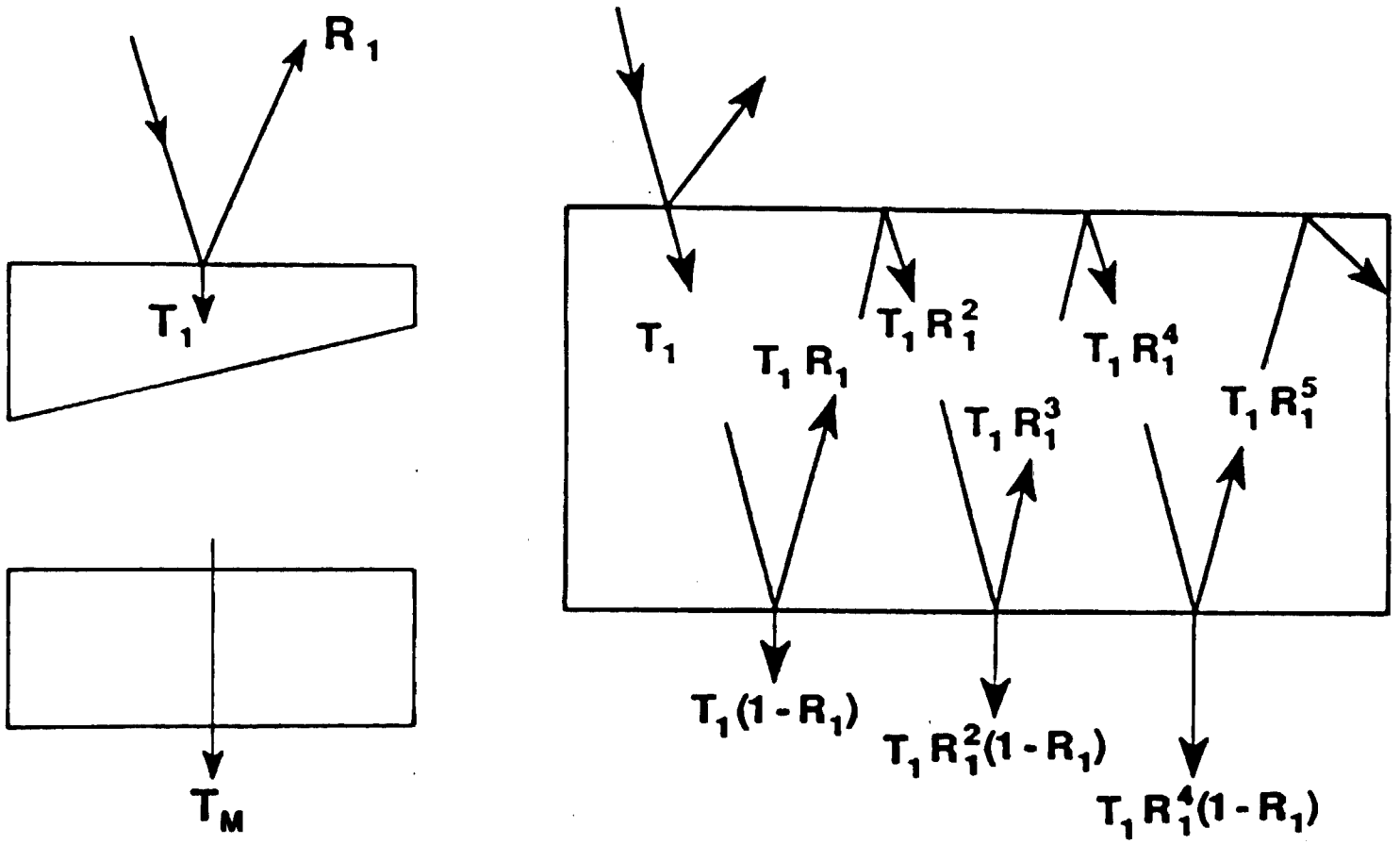

Zukic/Torr Figure 7.1a

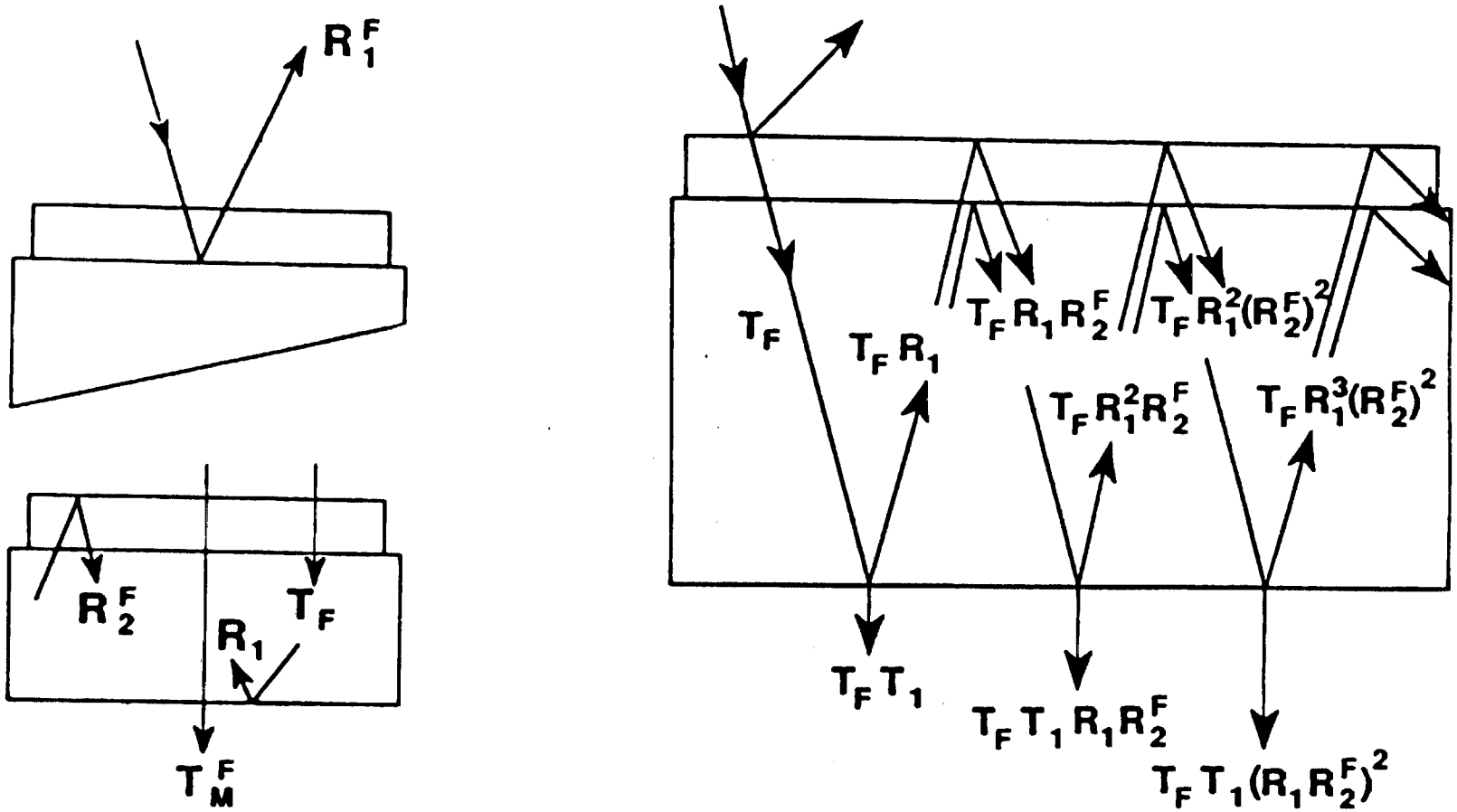

Zukic/Torr Figure 7.1b

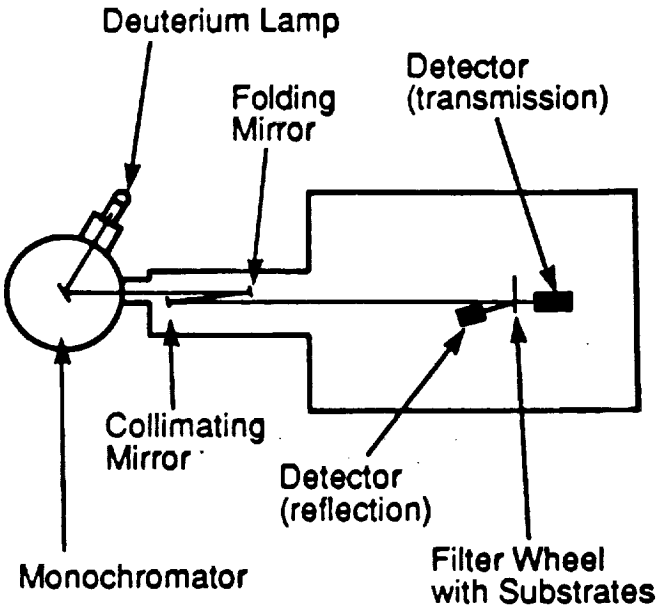

Zukic/Torr Figure 7.2

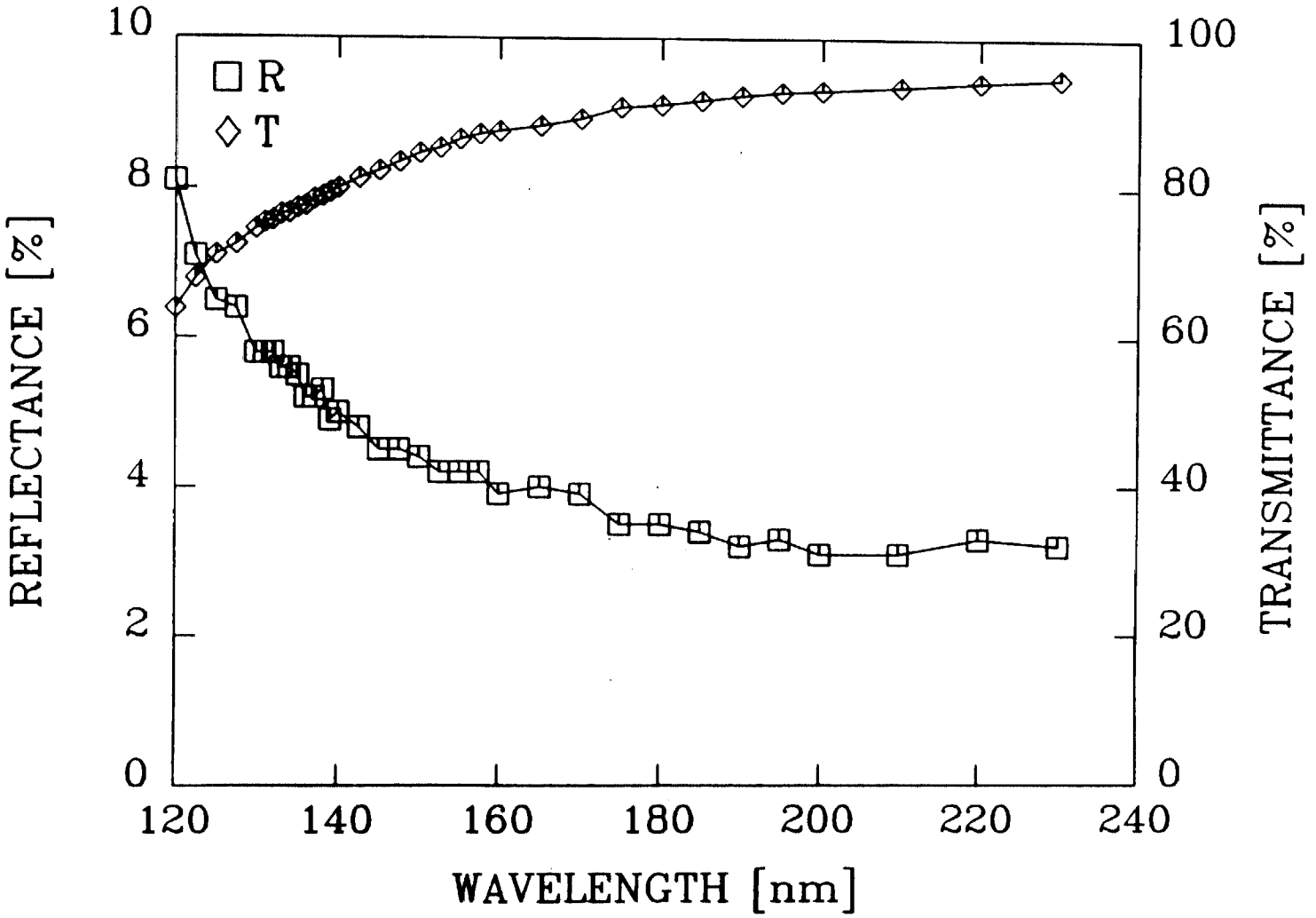

Zukic/Torr Figure 7.3a

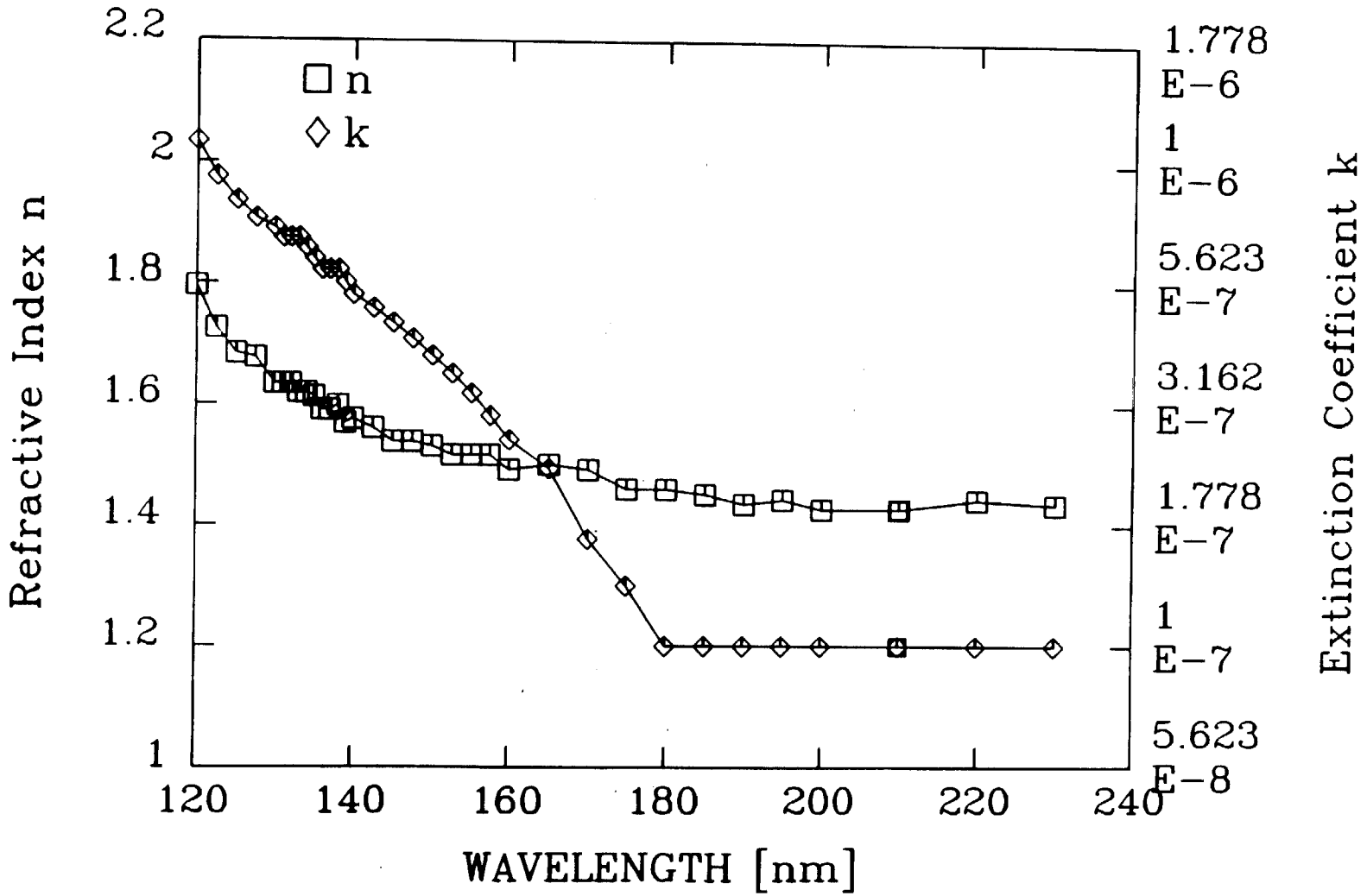

Zukic/Torr Figure 7.3b